Politecnico di Torino

Politecnico di Torino

MASTER OF SCIENCE IN CIVIL ENGINEERING
Academic Year 2022/2023

Performance assessment of waste-plastic modified asphalt mixtures for road pavements

Supervisors:
Prof. Davide Dalmazzo
Prof. Pier Paolo Riviera
Prof. Ezio Santagata

Candidate:
Majd Salhab

ACKNOWLEDGEMENTS

This journey did not come without challenges and difficult times, especially being far away from home and the retreat of social life during the Covid-19 pandemic. At times, the finish-line seemed unthinkably distant. I ever so gratefully appreciate the full and unconditional support, patience, and encouragement I received from my loving parents, siblings, uncles, family, and my precious ones. I love you. Without you it wouldn't have been possible. I am grateful to life and its interminable blessings, the blessings we see and the ones only felt.

I am short for words to express my gratitude for my supervisors Prof. Davide Dalmazzo and Prof. Pier Paolo Riviera, who have shown me unwavering support and guidance throughout my work at DIATI. I am very lucky to have had the honour of working under your supervision, and for receiving the knowledge you generously shared. Thank you for all the questions answered, all the advice and time you dedicated for my work, and above all for the kindness you have shown towards me.

I must express my gratitude to Joseph La Macchia, my laboratory mentor who most graciously shared with me his knowledge and valuable skills, but also for providing motivation in tough moments. It was a pleasure to learn and work with you, and I will not forget the brainstorming and research sittings we did together. I also thank all my laboratory colleagues. I won't forget the help you offered, the good times, and the laughs we shared together. I sincerely wish every single one of you all the best in your lives.

Last but not least, I remain indebted to my friends who were my support system during stressful times, without whom this may not have been possible. A heartfelt thanks to Ward, Masha, Beatrice, Fouad, Adam, Lu, Mattia, and Raso. Endless thanks to Vale the Pear of the island; words are not enough. I won't forget the unrelenting encouragement you provided me to reach the finish-line; all of you.

I thank Politecnico di Torino for the friendships woven in its hallways, and the city of Torino for its ceaseless charm and inspiration.

Thanks to my daily muses, my piano, the music, the films, the books, the camera and photos. This work is dedicated to every child deprived of the right to study, safety, healthcare, and a home. To every child devastated by war and violence. Anywhere on this planet. May peace lead humanity onward.

~

I did my work slowly, drop by drop. I tore it out of me by pieces. ~ Maurice Ravel

كُلَّما اتّسَعَت الرؤيَة ضاقَت العِبارَة ~ النفري

The broader the vision, the narrower the expression. ~ Al-Niffari

The real voyage of discovery consists not in seeking new landscapes, but in having new eyes. ~ Marcel Proust

For small creatures, such as we, the vastness is bearable only through love. ~ Carl Sagan

~

Torino,
30 November 2023

ABSTRACT

In line with the global pursuit of rendering construction materials reusable and more sustainable, the study of waste-plastic modified asphalt represents an innovative research field. In addition to the use of reclaimed asphalt pavements to produce new roads, asphalt modifiers such as waste-plastic provide the possibility to recycle and reuse materials which are otherwise not biodegradable. Moreover, the introduction of plastics in hot mix asphalt mixtures has shown improved mechanical properties of pavements, particularly for what concerns stiffness and resistance to cracking. From the economical point of view, the addition of plastics reduces in turn the bitumen content in asphalt mixtures, thus decreasing the total cost of mixture materials as bitumen comes with an elevated price tag.

This study deals with the reuse of recycled polymers obtained from the processing of plastic waste in asphalt mixtures for road paving. Originating from common household plastic waste collected from the metropolitan city of Turin (Italy), plastic shreds were added to the asphalt mixtures by means of the dry method. The mixtures under scrutiny in this study were produced on real scale in a production plant, then collected during paving operations of a road section in Brandizzo (Piedmont), Italy. Three different asphalt mixtures for wearing course were produced with 24% reclaimed asphalt pavement (RAP), and varying dosages of waste plastic shreds: 0%, 0.5%, and 1%. The experimental laboratory activities serve to characterise and compare the various bituminous mixtures by investigating the compositional (volumetric & granulometric) and mechanical properties. In particular, stiffness modulus (IT-CY), fatigue performance (CIT-CY), and indirect tensile strength (ITS wet & dry) as per European standards EN 12697-23, EN 12697-24, and EN 12697-26, for both short- & long-term aged samples were investigated. The results allowed the evaluation of the effects of plastic content based on the mechanical properties obtained from the tests described above. Experimental assessment found that mixtures containing plastic shreds possess significantly higher air void contents at N_{100}, with identical particle size distribution and binder content similar to the control mixture. The mixtures modified with plastics showed equivalent fatigue resistance results to the control mixture, displaying the advantageous impact of plastics in maintaining stiffness with increasing air void content, both in short- and long-term aged conditions. The increase in plastic shred content is not directly associated with an increase in the stiffness modulus of the mixtures. However, the mixtures exhibit stiffening behaviour with long-term ageing as was confirmed by the increasing stiffness moduli, at various test temperatures. The results suggest no water susceptibility for all three blends and no significant impact of plastics on the ITS, while confirming geometrical expansive behaviour of specimens with increasing plastic content.

Furthermore, the research highlights the possible future benefits as well as the operational difficulties and environmental concerns surrounding the adoption of waste plastic modified mixtures in modern transportation infrastructures.

Keywords: Asphalt, Wearing course, Waste plastic, Recycled plastic, Dry method, Modified bituminous mixtures, Long-term ageing, Stiffness modulus, Fatigue, Indirect tensile strength, IT-CY, CIT-CY, ITSM, ITS, ITSR, Sustainability, RAP, EN 12697-23, EN 12697-24, EN 12697-26.

INDEX

LIST OF FIGURES

LIST OF TABLES

A. ABBREVIATIONS, SYMBOLS, & UNITS

A.1 Abbreviations

AASHTO	**American association of highway and transportation officials**
BS EN	**British standard European norm**
CIT-CY	**Cyclic indirect tensile test on cylindrical shaped specimens**
DIATI	**Department of environment, land, and Infrastructure engineering**
HMA	**Hot-mix asphalt**
IT-CY	**Indirect tensile test on cylindrical shaped specimens**
ITS_d	**Indirect tensile strength test, dry**
ITS_w	**Indirect tensile strength test, wet**
ITSM	**Indirect tensile stiffness modulus**
ITSR	**Indirect tensile strength ratio**
LTA	**Long-term aged**
LDPE	**Low density polyethylene**
HDPE	**High density polyethylene**
NMAS	**Nominal maximum aggregate size**
RAP	**Reclaimed asphalt pavement**
SSD	**Saturated surface dry**
STA	**Short-term Aged**
TMD	**Theoretical maximum density**
UR24	**Usura (Wearing course) RAP 24 %**
UR24PS0,5	**Usura (Wearing course) RAP 24 % with 0,5% plastic shreds**
UR24PS1	**Usura (Wearing course) RAP 24 % with 1 % plastic shreds**
UTM-30	**Universal testing machine – 30 kN**

A.2 Symbols

N_{100}	**Final number of compaction gyrations = 100**
N_{200}	**Final number of compaction gyrations = 200**
u_a	**Horizontal displacement amplitude (mm)**
N_f	**Number of load cycles until fracture life according to energy criterion**
ε_a	**Maximum horizontal strain amplitude in the middle of the specimen (m/m)**
$\Delta\varepsilon$	**Maximum strain difference in the middle of the specimen (mm/m)**
ER(n)	**Energy ratio for load interval represented by load cycle number n (-)**
ε6	**Critical strain equivalent to 10^6 load cycles**
ν	**Poisson ratio (-)**
$S_{mix,n}$	**Stiffness modulus as calculated for the load interval n (MPa)**
σ_a	**Amplitude of horizontal tensile stress in the middle of the specimen (MPa)**
k_ε	**Material constant of the fatigue function (-)**
n_ε	**Material constant of the fatigue function (-)**
ρ_{SSD}	**Bulk density obtained by SSD test**
v_{real}	**Real void content (%)**
v_{geom}	**Theoretical geometrical void content (%)**
C_x	**Real degree of compaction considering wall effect (%)**
C_{ux}	**Theoretical degree of compaction without considering wall effect (%)**

C_1	**Self-compaction of the mixture**
k	**Workability of the mixture**

A.3 Units

mm	**Millimetres**
%	**Percent**
‰	**Per mille**
g	**Grams**
kg	**Kilograms**
kN	**Kilonewtons**
kPa	**Kilopascals**
Mpa	**Megapascals**
˚C	**Degrees Celsius**
Mg/m^3	**Megagrams per cubic metres**
Hz	**Hertz**
µm	**Micro metres**

All other abbreviations, symbols, and units are explained in context.

B. NORMS & STANDARDS

Laboratory activity	Standard followed
Material sampling	*BS EN 12697-28:2020*
Theoretical maximum density	*BS EN 12697-5:2018*
Binder content by ignition	*BS EN 12697-39:2020*
Particle size distribution (sieve analysis)	*BS EN 933-1:2012*
Specimen preparation by gyratory compaction	*BS EN 12697-31:2019; BS EN 12697-29:2020*
Bulk density of specimens	*BS EN 12697-6:2020*
Short- & long-term ageing of specimens	*AASHTO R 30-02 (2015)*
Indirect tension stiffness modulus (ITSM IT-CY)	*BS EN 12697-26:2018 - Annex C*
Resistance to fatigue (CIT-CY)	*BS EN 12697 24:2018 - Annex F*
Indirect tensile strength (ITS dry & wet)	*BS EN 12697-23:2017; BS EN 12697-12:2018; AASHTO T 283*

Table 1. Norms & implemented standards

C. RESEARCH OBJECTIVES

This study aims to assess and compare three plant-produced wearing course HMA mixtures modified with recycled waste-plastics. The mixtures were assessed for granulometric, volumetric, and mechanical characteristics. In this context, the following experiments were applied chronologically:

1) Mixture division into reduced quantities for sampling
2) Assessment of the plastic shred quality
3) Assessment of the binder content by ignition
4) Assessment of the theoretical maximum density (TMD)
5) Assessment of the particle size distribution by sieve analysis
6) Specimen preparation by gyratory shear compaction
7) Assessment of specimen dimensions
8) Assessment of the bulk density of specimens by SSD test
9) Long-term ageing of specimens (for step 15)
10) Assessment of specimen dimensions following long-term ageing (for step 15)
11) Indirect tension stiffness modulus (ITSM IT-CY) tests at 10, 20, 25, and 30 °C
12) Indirect tensile strength (ITS) dry tests at 25 °C
13) Conditioning of specimens for Indirect tensile strength (ITS) wet tests
14) Indirect tensile strength (ITS) wet tests at 25 °C
15) Resistance to fatigue (CIT-CY) tests at 20 °C for short- & long-term aged specimens

Key parameters of the above scheme have been summarized below in Table 2 & Figure 1:

Test type	**Temperature [°C]**	**Specimen condition**
Mixture division	110 ± 5	Loose HMA; STA
Plastic shred assessment	160 ± 5	Loose HMA; STA
Ignition	540	Loose HMA; STA
TMD	Room temperature	Loose HMA; STA
Sieve Analysis	Room temperature	Loose aggregates; STA
Gyratory shear compaction	160 ± 2	Loose HMA; STA
Bulk density	Room temperature	Compacted cylindrical specimens; STA
Long-term ageing	85 ± 3	Compacted cylindrical specimens; STA
ITSM IT-CY	10, 20, 25, 30 ± 0,5	Compacted cylindrical specimens, STA & LTA
ITS dry	25 ± 0,5	Compacted cylindrical specimens; STA
Wet conditioning for ITS	25 ± 2	Compacted cylindrical specimens; STA; Water bath
ITS wet	25 ± 0,5	Compacted cylindrical specimens; STA
CIT-CY	20 ± 0,5	Compacted cylindrical specimens; STA & LTA

Table 2. Laboratory experimental regime parameters

All laboratory activities have been conducted in line with the safety practice regulations of personnel, following comprehensive safety training. Suitable personal protective equipment was provided for the above-mentioned activities.

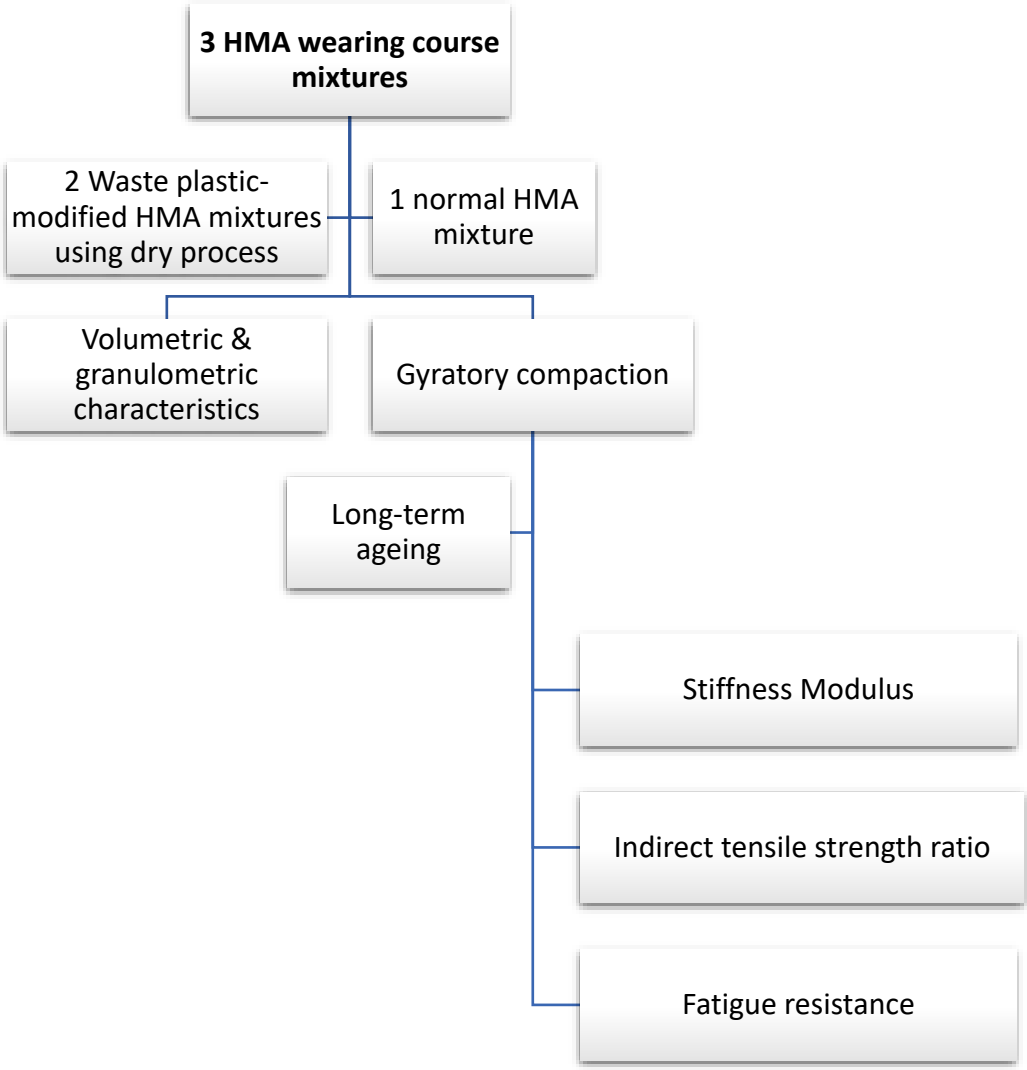

Figure 1. Laboratory experimental assessment regime

D. THEORETICAL FRAMEWORK AND LITERATURE

D.1 Waste Plastic Modified HMA

D.1.1 Introduction

This research aims to evaluate whether the introduction of waste plastics as modifier of HMA would lead to the improvement of the road stiffness, resistance to fatigue cracking, and water susceptibility compared to ordinary pavements. This will be assessed by means of the fatigue performance of both short- and long-term aged HMA specimens, as well as the ITSR and the stiffness modulus at various temperatures.

The purpose of the introduction of waste plastics is to improve the performance of pavements undergoing various service conditions, as well as reducing the material cost of HMA production. The modification of HMA using waste plastics can occur in wearing, binder, or base courses of pavement layers, depending on the desired pavement characteristics.

Transportation infrastructure pavements are commonly designated as flexible or rigid (Aziz et al., 2015). Flexible pavements are made using bituminous and aggregate mixtures, while rigid ones are bound with Portland cement (Aziz et al., 2015; Rahman et al., 2020). Globally, 95 % of highways are constructed as flexible pavements (Aziz et al., 2015; Rahman et al., 2020), containing by weight around 90 % to 95 % aggregates and around 5 % bitumen binder (World Bank et al., 2023). Typically, in the modification of flexible pavement mixtures, less than 10% of bitumen replacement is achieved by the addition of plastic wastes (Aziz et al., 2015; Nizamuddin et al., 2020).

Plastic-roads are described by 'the use of plastic waste as a bitumen modifier in road construction' (World Bank et al., 2023). The source of plastic wastes is distinguished into two sets: post-consumer plastic waste & post-industrial plastic waste. The first is gathered from municipal solid waste, open dumps, and households, while the latter from manufacturer's plastic waste (Kaza et al., 2018; Willis et al., 2020). The plastic waste is introduced as a partial substitute of aggregates or bitumen, ranging from 6 to 8 % by weight of bitumen (World Bank et al., 2023).

D.1.2 Historical recap and regulatory framework

Since the arrival of plastic as a synthetic product in the early 1900s (World Bank et al., 2023), it has become an essential part of production chains and the global economy. The world bank reports that in 1974, the first patent was filed for the use of plastic waste in road pavements (World Bank et al., 2023). Today, about 100.000 kilometres of plastic roads have been constructed in India (World Bank et al., 2023). In particular, more than 2500 kilometres of pavements in India have been fabricated using plastic waste, reporting road conditions without potholes and rutting after about ten years of service (Indian Roads Congress IRC:SP:98, 2013; Vasudevan et al., 2010). Furthermore, in 2013 the Indian ministry of road transport and highways published guidelines on the use of waste plastic asphalt for roads using dry process (Indian Roads Congress IRC:SP:98, 2013), thus further establishing this technology.

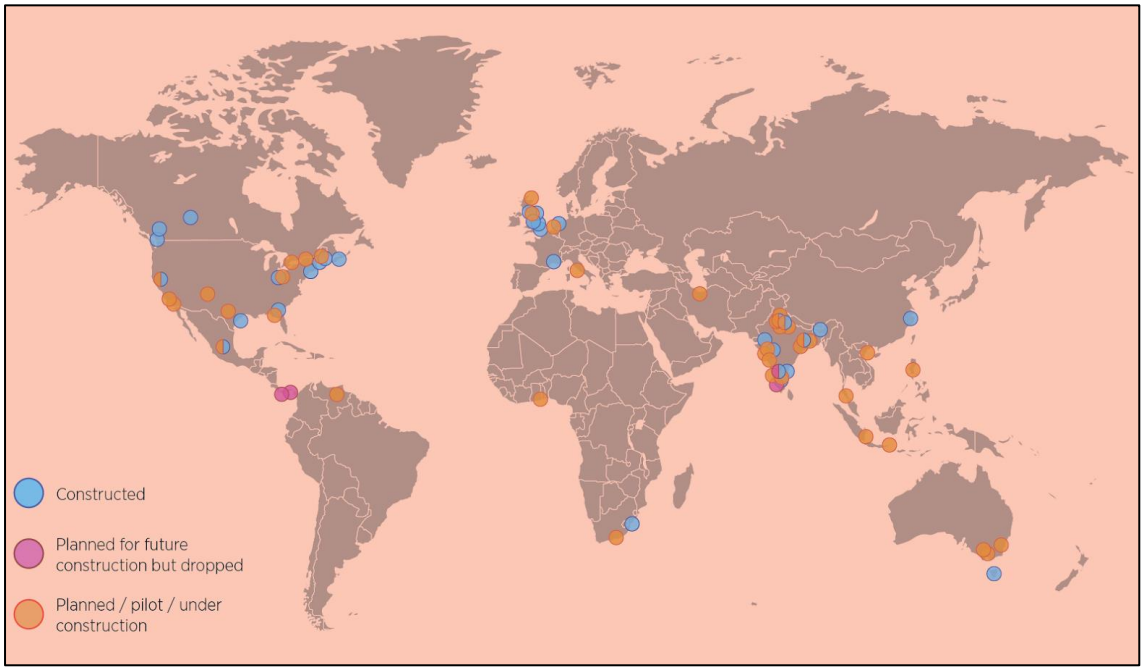

Figure 2. Map of plastic roads (World Bank et al., 2023)

In terms of regulatory framework, in 2019 the UK has inducted a guide on the use of plastic waste in road construction (Sasidharan et al., 2019), and public offices declared a 23-million-pound investment fund for pilot studies using waste plastic in roads (Sasidharan et al., 2019; World Bank et al., 2023).

Currently, regulations in the EU and Italy provide guidelines and specifications for the use of RAP in new roads, without any direct reference to waste plastics, as specifications for the inclusion of recycled waste plastic in HMA is lacking on the standard level (Willis et al., 2020; World Bank et al., 2023). The EU nonetheless has employed policies regarding waste management and sustainable infrastructures, which may support the call for use of waste plastics in road pavements.

The world bank has reported 76 patent requests and invention publications for plastic or crumb rubber waste incorporation in roads for the period between 1935 and 2021, originating from post-consumer and post-industrial waste (World Bank et al., 2023). Moreover, 27 copyrights were filed for post-consumer and post-industrial plastic waste use in asphalt mixtures (World Bank et al., 2023).

D.1.3 Waste plastic classification

Plastics originating from waste come in diverse chemical compositions, shapes, and properties. Depending on their polymeric structure, they are generally classified in seven resin identification codes (RIC) (World Bank et al., 2023). The figures below differentiate between the RICs as well as their origin and recyclability. These plastics come with different melting points, thus being different in behaviour when added to HMA mixtures (Figure 4). Melted plastics may dissolve in the binder and coat aggregates, as would bitumen do (Vasudevan et al., 2012), while intact plastics will behave as aggregates.

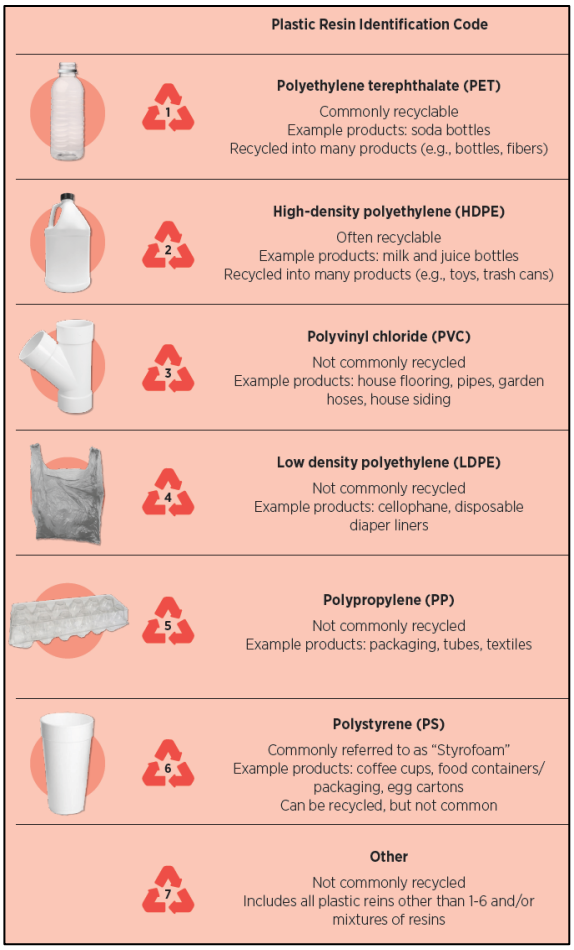

Figure 3. Plastic resin identification codes, their origin and recyclability (World Bank et al., 2023)

Recycling category	Plastics type	Application/Uses	Melting Point (°C) [1]
1	Polyethylene Terephalate (PET)	Bottles for water and soda, food packaging, food containers	>250
2	High Density Polyethylene (HDPE)	Plastic mailing envelopes, flexible pipes, plastic chairs/stools, toys and playground equipment, plastic bags shampoo bottles	130 but can vary in grade
3	Polyvinyl Chloride (PVC)	Pipes, electric cables, construction material, sign boards, vinyl flooring	100–260
4	Low Density Polyethylene (LDPE)	Trays and containers, plastic wraps, plastic bags, juice, and milk containers	110–120
5	Polypropylene (PP)	Plastic hinges, piping system, plastic chairs, reusable plastic containers, plastic moldings	160–165
6	Polystyrene (PS)	Food packaging, CD and DVD casing, disposable utensils, license plate frames, foam beverage cups	Glass transition at 100
7	Other[2]	Baby bottles, car parts, water cooler bottles, food containers	Based on grade and plastic type

Figure 4. Plastic recycling categories (Willis et al., 2020; World Bank et al., 2023)

D.1.4 Mixing processes for waste plastic HMA

To produce plastic-roads, three methods exist to mix plastics with bituminous mixtures, namely the wet and dry process, or a combination of both (Lu et al., 2023). They differ not only in the mixing methodology, but also in the resulting nature and role of the plastics inside the final HMA mixture (Figure 5).

D.1.4.1 Dry Process

In the dry process, shredded plastic waste is mixed with preheated aggregates prior to adding bitumen at 160 degrees Celsius (World Bank et al., 2023). It is noticed that in the dry process, LDPE coats the aggregate surface partially, and the remainder rests in the asphalt binder phase (Willis et al., 2020). Generally, the dosage of plastic waste in the dry process ranges from 0,2 to 1 % by weight of aggregates (Willis et al., 2020). In this process, the plastics are incorporated directly into the mixture as aggregate substitute, mixture modifier, binder modifier, or a combination. This procedure commonly uses recycled plastics with high melting points, where their shape remains intact after mixing (Lu et al., 2023; Willis et al., 2020).

D.1.4.2 Wet Process

In the wet process, recycled plastics (usually in powder form) with low melting point (such as LLDPE, LDPE, HDPE) are introduced to the asphalt binder as modifiers, with a measure ranging from 2 to 8 % by weight of the binder (Willis et al., 2020). The plastics are melted and fuse with the bitumen and are then added to hot aggregates to obtain HMA. The plastics behave as binder modifier in this case.

D.1.4.3 Benefits and obstacles

The dry process is simple, economical and environmentally friendly, while the wet process requires more machinery investment (B. Mishra & M.K. Gupta, 2018). One limitation for the dry process is that studies have yet to confirm if the plastic wastes are uniformly scattered in the HMA mixture (Willis et al., 2020).

Although more than 60% of literature reported the use of wet process to incorporate plastics in asphalt (Willis et al., 2020), the wet process is associated with the risk of phase separation between the binder and plastics due to thermodynamics and insolubility parameters (Vasudevan et al., 2012; Willis et al., 2020). This however can be mitigated using agitated storage tanks at the production plant to prevent separation (Willis et al., 2020).

Unlike the wet process, the dry process can cover more amount of plastic-road in tons/kilometres. This advantage however comes with an elevated risk of fire in the production plant as well as the release of hazardous gases (Willis et al., 2020; World Bank et al., 2023).

Regarding mechanical properties, the dry process mixing shows improved rutting resistance, stiffer binder, while the fatigue and cracking resistance is not always improved, and no or little effect on moisture resistance is noticed (Willis et al., 2020). Whereas when plastics are added by the wet process, the mixtures show increased stiffness and rutting resistance (Willis et al., 2020).

Finally, a logistic constraint is the inability of current asphalt production plants to accommodate the use of plastics in their set-up (World Bank et al., 2023), which comes with a higher risk as gasses must be held at temperatures up to 760 °C in the dry process, the release of hazardous gaseous contaminants (Willis et al., 2020), and contamination of the production plant components with plastic residues.

Method of incorporating plastic	Description of method	Role of plastic	Plastic types	Plastic (tons) per 1 km of road[8]
Wet process	Recycled plastics in the form of powder are added to bitumen, heated at 160–170°C, mechanically mixed, and then aggregate added	Polymer modifiers, asphalt replacement	Linear low density polyethylene (LLDPE), LDPE, HDPE[9]	0.48–1.9
Dry process	Plastic waste is shredded and mixed with preheated aggregates prior to adding bitumen at 160°C	Binder modifier, mixture modifier, aggregate replacement or a combination	**Aggregate replacement**: PP, PET, PS, PC[10] **Mixture modifier**: any plastic type other than PVC[11] in most cases	0.95–4.52

Figure 5. Wet and dry process of plastic road construction (World Bank et al., 2023)

Below is an organizational scheme of the plant-mixing procedure usable for both wet and dry process (Brasileiro et al., 2019). When applying the dry process for mixing, the waste plastic shreds are added to the hot aggregates (in Figure 6: lines a, b, and d are open, c and e closed). While in the wet process, the plastics are introduced to the hot binder (in Figure 6: lines c and e are open, a, b, and d are closed) (Brasileiro et al., 2019).

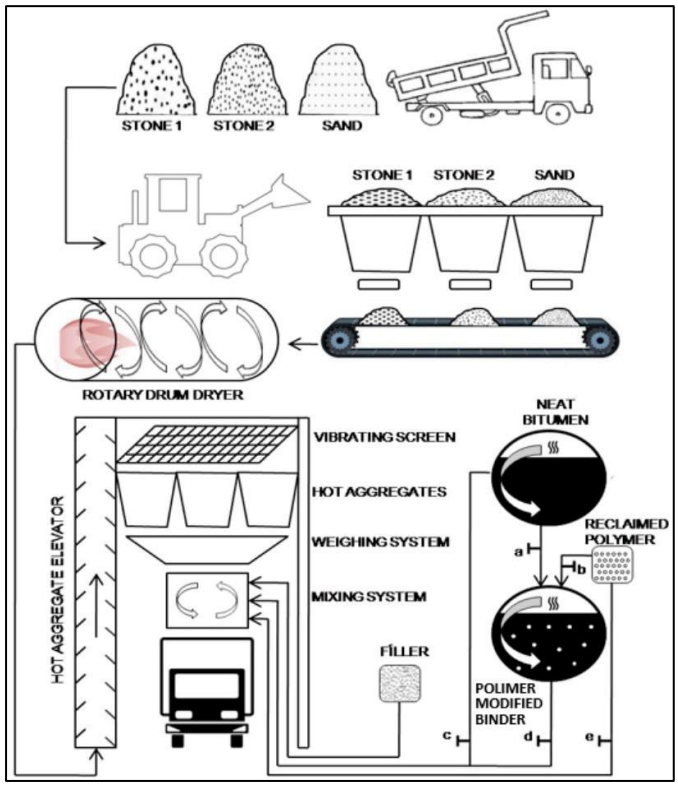

Figure 6. Organizational scheme of the plant-mixing procedure for HMA (Brasileiro et al., 2019)

D.1.5 HMA modification, polymers, and performance benefits

To improve the mechanical properties of HMA, many additives have been used to modify binders and HMA mixtures, such as hydrated lime (Aragao et al., 2008). Moreover, from a sustainability point of view, the addition of RAP is considered a standard procedure in modern asphalt mixes, usually sponsored by regulatory obligations for its use. In this context, virgin

polymers or those originating from waste plastics fall into the category of bitumen modifiers (Nizamuddin et al., 2020; World Bank et al., 2023).

The figures below illustrate the different types of modifications carried out on the binder in HMA mixtures, as well as the plastics generally used.

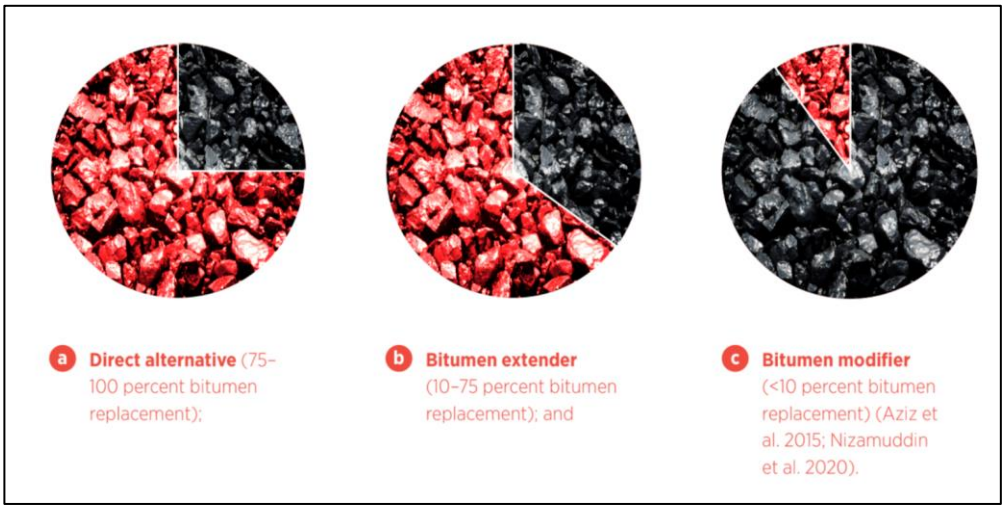

Figure 7. Bitumen replacement classification (World Bank et al., 2023)

	Average (%)	Range (%)	Median (%)
PP	13	0 to 50	5
Rubber	11	0 to 50	9
HDPE	7	0 to 20	6
LDPE	6	2 to 15	5
Polyethylene	6	0.2 to 25	5
PET	4	0 to 30	2
PS	3	0 to 6	3
Other	1	0 to 3	0.4

Figure 8. Percentage of bitumen substituted by plastic waste (World Bank et al., 2023)

The plastics shall pass quality criteria, and shall be sorted, cleaned, shredded and washed before introduction into HMA mixtures (World Bank et al., 2023). Furthermore, the smaller the dimensions of the plastics, the larger the surface area and binding between the bitumen and plastic is warranted (Gopinath et al., 2020). Regulation by Indian transportation authority advise that waste plastic shreds shall be 2 to 3 millimetres in dimension to ensure distribution and coating of the aggregates (Indian Roads Congress IRC:SP:98, 2013). Moreover, studies suggest that waste plastic shreds shall be introduced between 5 % to 10 % of the bitumen weight, where 8% is the advised optimal value (B. Mishra & M.K. Gupta, 2018; Indian Roads Congress IRC:SP:98, 2013; Vasudevan et al., 2012).

Bitumen modifiers include synthetic or recycled polymers having elastomeric, plastomeric, or reactive polymeric properties (Nizamuddin et al., 2020; World Bank et al., 2023). The choice of polymer is related to the desired enhancement of bitumen characteristics. The addition of reactive and plastomer polymers (EVA, EMA PIB, etc.) improves the resistance to deformation due to traffic loading and the stiffness. On the other hand, elastomers (SBS, SIS, SB, SBR, etc.) enhance the resistance to fatigue due to the improved elastic nature of bitumen (Nizamuddin

et al., 2020; World Bank et al., 2023). Plastomers may lead to the increased resistance of pavements to permanent deformation (rutting) at high temperatures and come at a low price and increase binder stiffness (Nizamuddin et al., 2020; World Bank et al., 2023). In a general scope, bitumen modifiers augment the performance of roadways regarding rutting resistance, durability, viscoelasticity and softening point (Aziz et al., 2015; Nizamuddin et al., 2020; Vasudevan et al., 2012). At extreme temperatures polymers decrease the thermal sensitivity of bitumen, improving resistance to fatigue cracking in low temperatures and rutting in high temperatures (Aziz et al., 2015; Nizamuddin et al., 2020). Additionally, the use of plastic waste to modify bitumen has also shown improvements for the Marshall characteristics (Shaikh et al., 2017). Congruently, the presence of waste plastics from 5 % to 12% of binder weight in bituminous pavements has shown improved resistance to water-induced damage (Sasidharan et al., 2019; World Bank et al., 2023) and a slight increase in air voids in HMA (Aziz et al., 2015; World Bank et al., 2023) and an elongation of the road service life (Sojobi et al., 2016).

D.1.6 Sustainability, LCA, & CEA

The recycling of waste plastics and their utilization in road pavement construction plays a key role in rendering this sector further sustainable and energy-efficient, as studies have reported that one tonne of waste plastic was necessary for every 1 kilometre of pavement built, which is associated with a reduction of 3 tonnes per kilometre of carbon dioxide emissions compared to typical construction methods (Vasudevan et al., 2012). Beyond the recycling of inorganic waste plastics, a decrease of bitumen utilisation in HMA is also achieved by the introduction of waste plastics as reported by various studies (Behl et al., 2012; Sasidharan et al., 2019; Vasudevan et al., 2012).

Moreover, the life cycle analysis (LCA) of waste plastic roads indicates reduction in their environmental impact compared to traditional roads, similarly considering greenhouse emissions (Lastra-González et al., 2022; World Bank et al., 2023).

So far, thorough cost-effectiveness (CEA) analyses are lacking for plastic-roads (World Bank et al., 2023), however, the field of plastic-roads proposes a promising circular economy for the industry. Nonetheless, a recent study carried out by the world bank concludes that plastic-roads are indeed cost-effective, by analysing data for the last 20 years (World Bank et al., 2023).

D.1.7 Alternative innovation

An innovative alternative to HMA which incorporates waste plastics, is the warm mix asphalt (Almeida et al., 2021). Warm mix asphalt is produced at lower temperatures, namely at 100 °C, achieved by means of three modifications: chemical additives, organic additives and foaming processes (Almeida et al., 2021). The reduced mixing temperature cuts energy consumption throughout the production and compaction process, possibly reducing 70 % of carbon dioxide emissions with respect to normal HMA (Almeida et al., 2021; Wu et al., 2021).

D.1.8 Hazards and drawbacks

The recyclability of plastic-roads is yet to be thoroughly assessed, as few scientific studies have provided input about its usability (Willis et al., 2020), especially due to the unavailability of RAP from plastic roads (P-RAP) with service life beyond 15 years (Lu et al., 2023). If P-RAP is deemed unfit for reuse, it would be a problematic end-of-life aspect of this modern pavement material (Lu et al., 2023).

Furthermore, the environmental impact of plastic-roads should be further evaluated, as it is yet unknown whether micro-plastics are generated during their service life (World Bank et al., 2023). The emission of micro-plastics may occur due to wearing and mechanical surface abrasion by travelling vehicle tires, expelling micro- and nano-plastics (Evangeliou et al., 2020; Leads & Weinstein, 2019; Sommer et al., 2018). Tire wear particles, brake wear particles, and road sources (such as plastics in modified asphalts or road marking paints) are three sorts of vehicle road traffic emissions (Evangeliou et al., 2020). The world bank defines micro-plastics as pieces less than 5 millimetres in dimension, dispersed in the environment because of plastic pollution (World Bank et al., 2023). Statistically, Brahney et. al 2021 have reported that about 84 percent of micro-plastic emissions to the atmosphere in the western U.S. are released from roads and vehicle brakes (Brahney et al., 2021).

During production, transport, and compaction temperature, both plastic and bitumen components of the modified HMA intermix at high temperatures, and the plastics may absorb some light components of Bitumen (Fonseca et al., 2022) which may render both components undistinguishable for environmental tracing.

Another ecological hazard related to plastic-roads is the leaching of toxic inorganic substances of plastic origin to the environment during road service life as well as during the production phase (Sasidharan et al., 2019). Moreover, hazardous chlorine-based fumes which may be freed during road paving remain a chemical hazard due to plastic presence (A. Chakraborty & S. Mehta, 2017). Nonetheless, levels of such fumes remain negligible without marked harmful effects, as studies have shown (A. Chakraborty & S. Mehta, 2017; Greg White, 2019).

Furthermore, contaminants and additives present in waste plastics are heterogeneous in nature and not standardized in recycling classes (Rochman et al., 2019). Added usually for colour and elasticity, these additives do not achieve strong bonds with the plastic polymers, and consequently can leach into the road environment of plastic-roads (Li et al., 2016; Wright & Kelly, 2017) .

D.1.9 Mechanical behaviour - Fatigue, stiffness, and water susceptibility

Numerous indicators of mixture performance may highlight the role of waste plastics in HMA, such as rutting resistance, stiffness modulus, fatigue performance, Indirect tensile strength, and water sensitivity. Among various parameters, this study will focus on the fatigue resistance, stiffness, and water susceptibility of modified HMA samples.

Several studies imply that recycled waste plastics lead to the improved rutting resistance due to the stiffness increase of the mixtures (Willis et al., 2020). This increase in stiffness however may have negative impact on fatigue and cracking resistance. This should be further

investigated by laboratory fatigue studies on long-term aged mixtures to simulate pavement fatigue conditions (Willis et al., 2020).

When the pavement support (base, subbase, or subgrade) becomes insufficient to transmit the applied loading, fatigue cracking starts to propagate (Aragao et al., 2008). This may occur due to inadequate drainage, stripping, excessive loading beyond design expectation, or scarce compaction and quality of construction (Aragao et al., 2008). Wearing courses being thin in dimension, experience fatigue cracking from the bottom of the asphalt layer and move towards the surface due to tensile loading (Brown et al., 2001). On the contrary, in thick pavements the cracks propagate from the surface of the asphalt towards the bottom of the layer (Brown et al., 2001). If cracking is allowed to develop, the risk of damage of the pavement increases due to vehicle dynamic loading and water infiltration (see Figure 10).

The fatigue testing analysis may be carried out in two modes (see Figure 9): stress-controlled or strain-controlled conditions (Huang, 2004). In the first, the cyclic force is maintained constant, and the strain is let to develop in the sample. In the strain-controlled mode, the strain is fixed, and the stresses decline gradually with cyclic strain. Generally, strain-controlled tests represent the material behaviour of the thin layers accurately under cyclic load, to allow a rigorous evaluation of its fatigue conduct. Studies advise that stress-controlled fatigue loading represents the behaviour of thick asphalt layers (Ghuzlan & Carpenter, 2000). Experimentally, it is observed that strain-controlled tests lead to higher number of cycles to failure than the stress-controlled tests (Ghuzlan & Carpenter, 2000).

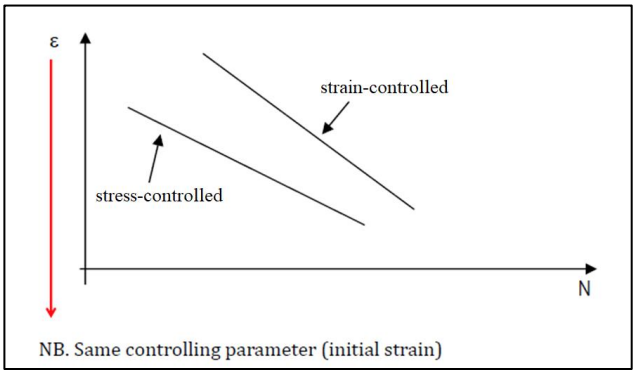

Figure 9. Fatigue lines for two failure modes: stress- and strain-controlled testing

The failure life of samples under fatigue can be assessed by means of the dissipated energy between consecutive loading cycles or the cumulative dissipated energy until failure (Ghuzlan & Carpenter, 2000). Failure eventually occurs when micro-cracks propagate to form visible macro-cracks leading to the splitting of the tested sample (Ghuzlan & Carpenter, 2000). The traditional fatigue method defines failure as the number of cycles at which the stiffness modulus is reduced by 50 % of its initial value (Orešković et al., 2019; Van Dijk & Visser, 1977). Usually the initial value of the modulus at the 100^{th} cycle is taken, however, this approach may be challenging, as defining the initial value of the modulus may be influenced by non-linearity (Di Benedetto et al., 2011; Orešković et al., 2019). In this study, the fatigue life is estimated using the energy ratio approach, where it is the number of loading cycles corresponding to the maximum energy ratio (see Figure 11). At this maximum, macro-cracks are assumed to propagate. Additionally, this research will consider the fracture cycle (specimen breaking) as additional criteria to assess the fatigue life of the mixture specimens.

Figure 10. Fatigue damaged pavement (Aragao et al., 2008)

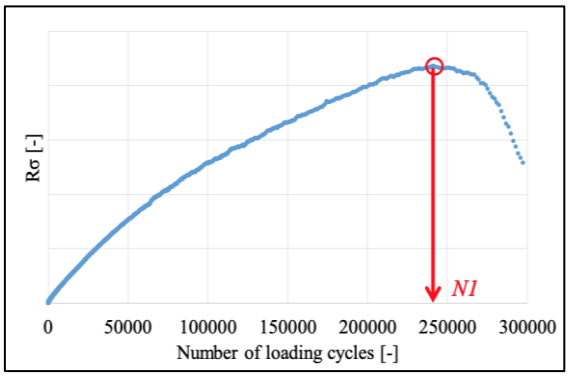

Figure 11. Fatigue life according to the Energy Ratio approach (Orešković et al., 2019)

It has been shown that the initial strain (ε_0) applied to the sample influences the number of cycles reached at failure (N_f). Commonly the initial strain or stress are plotted in a bi-logarithmic plane vs the number of cycles reached to failure, to obtain a so-called fatigue line as shown in figure 12. Exploiting the fatigue line, the critical strain equivalent to 10^6 load cycles (ε6) can be estimated, which serves as a performance indicator of the mixture. A higher (ε6) value signifies a better resistance to fatigue. The fatigue tests available are various in methodology and depend on the sample geometry and available testing equipment, such as four-point-bending test on prisms, indirect tensile cyclic loading (IT-CY) or continuous indirect tensile cyclic loading (CIT-CY) on cylinders. The frequency of the sample load application in fatigue test depends on the adopted test normative, however, a cyclic loading frequency of 10 Hz fairly represents a vehicle speed of circa 80 km/h (50 mph) (Aragao et al., 2008; Huang, 2004). Regularly, fatigue damage ensues at moderate service temperatures (Huang, 2004), and it may be representative to test samples for fatigue performance at 20 °C (Aragao et al., 2008). Further details about the CIT-CY testing method adopted in this research is available in Chapter P.

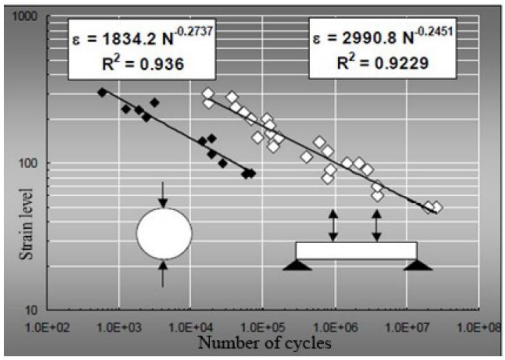

Figure 12. Fatigue lines in bi-logarithmic plane

During cyclic loading of fatigue samples, three phases depict the behaviour of the stiffness modulus as shown in Figure 13. In the first phase, the stiffness modulus rapidly decreases, then varies linearly for a long number of load cycles in the second phase (initiation mode). At the beginning of the second phase, micro-cracks begin to develop in the sample, further propagating until macro-cracks develop at the beginning of the third phase (propagation mode), when a rapid drop in the stiffness modulus is witnessed, until eventual physical failure occurs after a relatively minor number of load cycles.

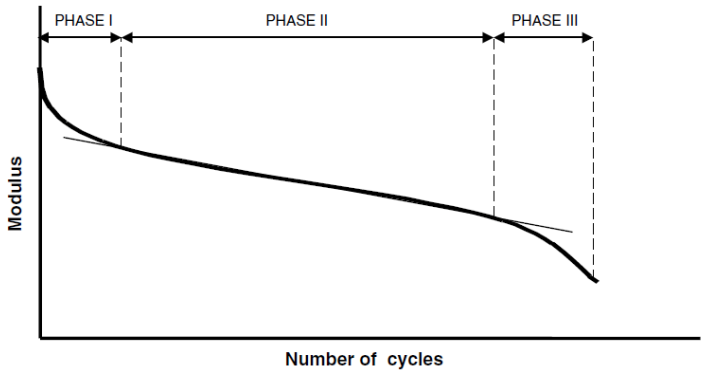

Figure 13. Stiffness modulus vs number of cycles during Fatigue test

The estimation of the stiffness modulus of waste plastic modified HMA samples undergoing fatigue tests is a preliminary tool to evaluate the impact of the modification on the fatigue performance (Eskandarsefat et al., 2022). Generally, the presence of waste plastic is associated with increased stiffness and thus a higher modulus. The stiffness modulus is utilized to estimate the initial strain for a given level of stress, where higher modulus would imply a lower initial strain and better fatigue performance (Eskandarsefat et al., 2022).

Using LDPE, studies report the IT-CY stiffness modulus increases for plastic-modified HMA, as well as better fatigue performance tested in stress-controlled conditions (Little D.N., 1992; Yin et al., 2020). Findings show that the LDPE introduction enhanced fatigue life of samples testing in stress-controlled mode, when fatigue tests are applied at relatively low strain classes (Little D.N., 1993; Yin et al., 2020).

Furthermore, waste-plastic modified HMA can be additionally evaluated by the ITSR, which indicates the degree of water susceptibility of the mixture. By comparing the ITS of dry- and wet-conditioned samples, the ITSR value is determined. Studies regarding LDPE & HDPE modified HMA mixtures indicate the increase of ITS values in dry conditions, however the same was not noticed in wet conditions, thus rendering moisture resistance unchanged by using waste plastics (Capitão et al., 2022). Further explanation of the ITS test methodology is presented in chapter O.

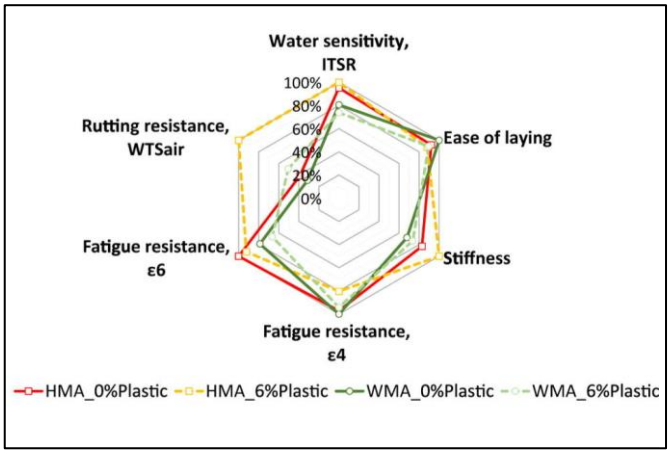

Figure 14. Relative performance of asphalt mixtures with and without plastics in hot-mix asphalt and warm-mix asphalt mixtures (Almeida et al., 2021)

Figure 14 represents several performance indicators for hot- & warm-mix (see D.1.7) asphalt modified with waste plastics. In practical terms, the challenge for today's constructer is optimizing the mixture composition to obtain satisfactory results for the expected service life conditions. This includes the understanding of the behaviour of waste plastics in the HMA mixtures on the volumetric, mechanical, environmental and safety performance level.

The following chapters exemplify the methodology followed to evaluate the mixtures in scrutiny.

E. LOCATION, MATERIAL, AND SAMPLING

The hot-mix asphalt mixtures under study originate from a plant-produced asphalt batch on real scale, which was paved on a local rural road SP220 section (ca. 500 m) between two roundabouts in Brandizzo (Piedmont), Italy (see Figure 15 & Figure 16). The HMA was collected from the construction site on 26/05/2023 during the paving operations in sampling bags (see Figure 17 to Figure 24) and transported to the materials laboratory of the department of environment, land, and infrastructure engineering (DIATI) of the Polytechnic of Turin. This road portion is expected to serve heavy-vehicle traffic due to the presence of several commercial warehouses in the vicinity as seen in Figure 16.

The modified HMA mixtures contain recycled polymers obtained from the processing of plastic waste originating from common household plastic waste collected from the metropolitan city of Turin (Italy). After primary plastic waste collection, sorting, differentiation, and recycling, the remaining heterogeneous plastic waste was shredded and added to the HMA mixtures in plant by means of the dry method (Refer to D.1.4.1). Finally, three HMA mixtures were paved as wearing course on three sub-segments of this road. The mixture differentiation is presented in Table 3:

Mixture ID	RAP content by mixture weight [%]	Plastic shred content by mixture weight [%]	Mechanical compaction temperature [˚C]
U24	24	**0**	160
U24PS0,5	24	**0,5**	160
U24PS1	24	**1,0**	160

Table 3. Composition of sampled wearing course HMA mixtures for laboratory investigation

U24 which contains no plastics (control mixture) was paved on one direction of travel, while the other two mixtures with plastic shreds were paved on the opposing travel direction, in two equal sub-segments.

On construction site, a total of 8 bags of ca. 25 kg each were sampled and collected for all the three mixtures. They were stored in a dry location in the laboratory, with stable climatic conditions. Consequently, the mixtures were heated in a furnace and the bags were divided into smaller quantities to facilitate individual sampling for laboratory testing, and to avoid additional furnace re-heating of the material which leads to further undesired ageing of the bituminous mixtures.

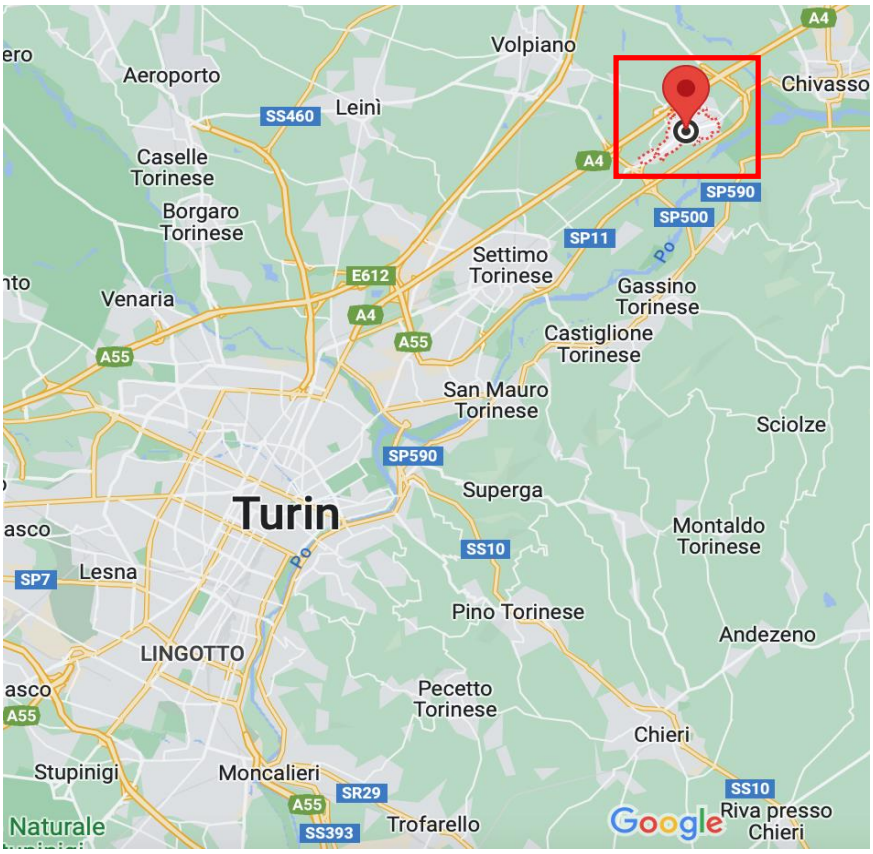

Figure 15. In red frame: the town of Brandizzo (Piedmont), Italy. [Source: Google Maps (2023) Torino]

Figure 16. Local rural road SP 220 segment in Brandizzo where the three HMA mixtures were paved.

[Source: Google Maps (2023) Brandizzo]

Figure 17. Asphalt paving works on SP220

Figure 18. Asphalt paving works on SP220

Figure 19. Asphalt paving works on SP220

Figure 20. Asphalt paving works on SP220

Figure 21. HMA batch for SP220

Figure 22. Temperature control of HMA batch

Figure 23. Loose HMA sampling for laboratory testing

Figure 24. Sampled HMA for testing

F. BINDER CONTENT BY IGNITION

The verification of the binder content of a bituminous mixture can be carried out by means of the ignition test described in BS EN 12697-39:2020. The binder content is an important volumetric characteristic which in turn influences the mechanical properties of the mixture.

The three mixtures underwent the ignition test to determine the binder content. Furthermore, by means of sieve analysis (refer to chapter G.), the ignition test permits to assess the granulometric distribution of the mixture aggregates skeleton which remains intact at the end of the test. The binder content and particle size distribution analysis allow to characterize the mixture as well as verify the producer adherence to the target mixture.

In Method B, the standard BS EN 12697-39:2020 envisages the use of a furnace and an external balance, as well as sample baskets and a catch pan to carry out the ignition test (see Figure 26).

The sample of the mixture is determined as a function of the nominal maximum aggregate size (NMAS) according to the following table provided by the norm:

Nominal maximum aggregate size mm	Mass of sample g	Maximum constant mass limit g
4	1 000 to 1 400	0,15
5,6 or 6,3 or 8 or 10	1 000 to 1 600	0,15
11,2 or 12,5 or 14 or 16	1 000 to 1 700	0,20
20 or 22,4	1 000 to 2 400	0,25
31,5	1 000 to 3 000	0,30
40 or 45	1 000 to 4 000	0,40

Table 4. Ignition test sampling mass as a function of NMAS as per BS EN 12697-39:2020

The mixtures in study being designated as wearing courses have NMAS less than or equal to 16 mm, thus the chosen sample mass was 1400 grams.

F.1 Procedure

1) The furnace was preheated to the test temperature (540 °C);
2) The sample (see Figure 25) was heated in an oven at 110 °C to dry it to a constant mass and allow workability;
3) The mass (W_t)of the empty and clean sample baskets and catch pan were measured by means of an external balance (see Figure 27);
4) The sample was homogeneously dispersed onto the two layers of the sample basket, and then weighed ($W_{t+m,\ BI}$) on the external balance;
5) The sample basket and catch pan were placed into the furnace until no mass loss was recorded;
6) The sample basket and catch pan were removed from the furnace, placed under a safety shield, and allowed to cool down to room temperature, and consequently their mass ($W_{t+m,\ AI}$) was recorded using the external balance;

F.2 Calculations

All masses shall be expressed in g to the nearest 0,1 g.

The total mass of bituminous mixture before the ignition $W_{S,W}$ is calculated as follows:

$$W_S = W_{t+s} - W_t$$

where

W_S *is the dried total mass of the bituminous mixture prior to ignition, in grams (g);*

W_{t+s} *is the total mass of bituminous mixture, sample basket(s) and catch pan prior to ignition, in grams (g);*

W_t *is the mass of the sample basket(s) and catch pan, in grams (g).*

The total mass of aggregate remaining after ignition W_a in grams is calculated as follows:

$$W_a = W_{t+a} - W_t$$

where

W_a *is the total mass of aggregate remaining after ignition, in grams (g);*

W_{t+a} *is the mass of bituminous mixture, sample basket(s) and catch pan after ignition, in grams (g);*

W_t *is the mass of the sample basket(s) and catch pan, in grams (g).*

The corrected binder content of the sample by mass of the bituminous mixture sample B, in percent, is calculated as follows:

$$B = \frac{(W_s - W_a)}{W_s} \times 100 - C_F$$

where

B *is the corrected binder content of the bituminous mixture sample, in percent (%);*

W_s *is the dried total mass of the bituminous mixture prior to ignition, in grams (g);*

W_a *is the total mass of aggregate remaining after ignition, in grams (g);*

CF *is the calibration value, in percent (%). (Overlooked in results)*

Figure 25. Loose HMA Sample

Figure 26. Ignition test furnace, baskets with catch pans, and carry shovel

Figure 27. Measurement of W_t using external balance

Figure 28. Sample spreading in basket before ignition

Figure 29. Sample basket after ignition test

F.3 Results

Ignition Test						
Mixture	U24		U24PS0,5		U24PS1	
Sample	1	2	1	2	1	2
Sample mass before ignition [g]	1406,4	1403,2	1399,2	1400,5	1404	1413,2
Sample mass after ignition [g]	1317,2	1313,8	1308,5	1308,8	1314,8	1322,5
$M_{bitumen+plastic}$ [g]	89,2	89,4	90,7	91,7	89,2	90,7
$M_{plastic}$ [g]	**0**	**0**	**7,0**	**7,0**	**14,0**	**14,1**
$M_{bitumen}$ [g]	**89,2**	**89,4**	**83,7**	**84,7**	**75,2**	**76,6**

Table 5. Ignition test results, masses of mixture components

Ignition Test							
Binder + Plastic content [%] by mixture weight				***Binder + plastic content [%] by aggregate weight***			
Sample	**U24**	**U24PS0,5**	**U24PS1**	Sample	**U24**	**U24PS0,5**	**U24PS1**
1	6,34	6,48	6,35	1	6,77	6,93	6,78
2	6,37	6,55	6,42	2	6,80	7,01	6,86
Mean	**6,36**	**6,51**	**6,39**	**Mean**	**6,79**	**6,97**	**6,82**
Std dev	0,020	0,040	0,040	Std dev	0,021	0,057	0,057

Table 6. Binder and plastic content results from Ignition tests. Binder includes virgin bitumen and bitumen from RAP

Ignition Test							
Binder Content [%] by mixture weight				***Binder Content [%] by aggregate weight***			
Sample	**U24**	**U24PS0,5**	**U24PS1**	Sample	**U24**	**U24PS0,5**	**U24PS1**
1	6,34	5,98	5,35	1	6,77	6,40	5,72
2	6,37	6,05	5,42	2	6,80	6,47	5,79
Mean	**6,36**	**6,02**	**5,39**	**Mean**	**6,79**	**6,44**	**5,76**
Std dev	0,020	0,040	0,040	Std dev	0,021	0,049	0,049

Table 7. Binder content results from Ignition tests. Binder includes virgin bitumen and bitumen from RAP

Further results from the ignition test are reported in Annex I for each individual mixture.

F.4 Remarks

In the mixtures in question, the binder content effectively includes virgin bitumen, and bitumen originating from RAP. The RAP binder content is not disclosed by the producer, and therefore its contribution to the total bitumen content cannot be verified. All the above constituents are not recoverable after the ignition test, including the plastic shreds. However, as noticed in sampling and compaction procedures, not all plastic shreds have a binding characteristic, as they do not melt as was visually evident at compaction temperature (refer to Chapter I.). It can be said that some un-melted plastic shreds may play a mediatory role as aggregates in behaviour.

As evident in the results, the mixtures have a relatively high binder content for a wearing HMA course for a rural road. As described in *Linee guida per la costruzione e manutenzione delle pavimentazioni stradali* (Consiglio Superiore dei Lavori Pubblici, 2022), a wearing course mixture of aggregates AC12 should contain 5 % to 6,5 % binder by weight of aggregates in the mixture. This range was not respected in the mixtures in study (see table 6). If plastic shred contribution is excluded from the binder phase content, it is apparent that the bitumen content in the mixtures decreases with increasing plastic shred content (see table 7).

Moreover, *Linee guida per la costruzione e manutenzione delle pavimentazioni stradali* (Consiglio Superiore dei Lavori Pubblici, 2022) requires at least 10% of RAP content by mixture weight for wearing courses. This is guaranteed as all three mixes contain 24% RAP.

Tabella 6.8

Tipologia	AC32	AC22	AC20	AC16	AC12	AC10	PA11	SMA11
Impiego	Base	Base	Binder[1]	Binder[2]	Usura[3]	Usura[4]	Usura	Usura
	Granulometria							
Setacci [mm]	Passante [%]							
63	100							
31,5	90-100	100						
22		90-100	100					
20	69-82	-	90-100	100				
16		55-85	-	90-100	100		100	100
12,5		-	-	-	90-100	100		-
11,2		-	-	-	-	-	90-100	90-100
10		-	56-68	73-80	-	90-100		-
8	45-56	35-60	-	-	70-90	70-90	20-40	50-65
6,3		-	-	-	-	-		-
5,6		-	-	-	-	-		35-45
4		25-50	37-48	45-56	40-55	40-55		-
2	21-31	20-35	23-33	28-38	25-38	25-38	15-25	20-30
0,5	10-17	6-21	11-17	14-22	14-20	14-20	8-16	-
0,25	6-12	4-16	6-12	7-14	10-15	10-15		-
0,063	4-7	4-8	4-7	4-8	6-10	6-10	5-8	8-12
Contenuto di legante [%] (riferito alla massa degli aggregati)								
	4,0-5,3	4,0-5,5	4,2-5,8	4,5-6,0	5,0-6,5	5,0-6,5	5,0-6,0	6,0-7,5

(1) per spessori compresi tra 6 e 12 cm
(2) per spessori compresi tra 4 e 6 cm
(3) per spessori uguali o superiori a 4 cm
(4) per spessori inferiori a 4 cm

Table 8. Sieve Passing requirements and percentage binder content (by aggregate weight) for wearing course and AC12 aggregates (Consiglio Superiore dei Lavori Pubblici, 2022)

G. DETERMINATION OF PARTICLE SIZE DISTRIBUTION – SIEVING METHOD

The verification of the particle size distribution of the HMA was carried out as per BS EN 933-1:2012, by means of washing and dry sieving. The particle size distribution is represented via the granulometric curve, which allows the description of the mixture aggregate skeleton.

G.1 Procedure

The test sample weight was determined based on the aggregate size as shown in table 9 below, as prescribed in BS EN 933-1:2012:

Aggregate size D (maximum) mm	mass of aggregates kg	volume of lightweight aggregates (litres)
90	80	-
32	10	2,1
16	2,6	1,7
8	0,6	0,8
≤ 4	0,2	0,3

Table 9. Minimum size of test portions as in BS EN 933-1:2012

The maximum aggregate size expected for a wearing course is 16 mm, and thus the test samples were 2,6 kg for each of the three mixtures.

The norm requires the heating of the test sample at 110 ± 5 °C to a constant mass prior to washing. However, the samples underwent the ignition test at 540 °C (see Figure 30) and were cooled right before performing the sieve analysis procedure. Therefore, the heating process is waived for the following procedure.

Washing

1) Measure the dry mass (M_1) of the sample obtained from the ignition test;
2) Place the aggregate material from the ignition test in a container above a 0,063 mm sieve (see Figure 31), ensuring that no fine particle (filler powder) is lost;
3) Fill with enough water to cover the test portion, and manually agitate and stir the mixture to allow the separation of the aggregates and suspension of the fines (see Figure 32 & Figure 33). Repeat three times;
4) Dry the retained residue on the 0,063 mm sieve in an oven at 110 ± 5 °C overnight to a constant mass (see Figure 34 & Figure 35). Record the mass (M_2) after oven drying and subsequent cooling.

Sieving

1) Measure and record the empty mass of each sieve of the column;
2) The dried sample shall be poured into the sieving column (see Figure 36 & Figure 37). It is composed of several connected sieve pans placed in decreasing order of sieve mesh size, from top to bottom;
3) After manually shaking the column for a few minutes, it is placed into a mechanical vibrator for about 15 minutes, to ensure complete sieving (Figure 38);
4) Remove each sieve pan and weigh it on an external balance, including the bottom pan.

G.2 Calculations

As expressed in BS EN 933-1:2012, the mass retained on every sieve is calculated as a percentage of the initial dry mass M_1. The cumulative passing percentage at each sieve down to 0,063 mm sieve is then calculated.

The percentage of fines passing the 0,063 mm sieve is calculated based on this relationship:

$$f = \frac{(M_1 - M_2) + P}{M_1} \times 100$$

where

M_1 is the dried mass of the sample in kg;
M_2 is the dried mass of the residue retained on the 0,063 mm sieve in kg;
P is the mass of the screened material remaining in the pan in kg;

If the sum of the masses retained on all sieves and P differ more than 1% from the mass M_2, the test shall be repeated.

Figure 30. Remaining aggregates after Ignition test

Figure 31. Aggregates and filler in washing sieve

Figure 32. Manual washing and stirring of the aggregates

Figure 33. Draining of aggregates after washing

Figure 34. Drying of washed aggregates in oven

Figure 35. Dried aggregates

Figure 36. Sieving column

Figure 37. Manual sieving of the washed & dry aggregates

Figure 38. Mechanical sieving of the aggregates using vibrator equipment

Figure 39. Retained aggregates on sieves after weighing

G.3 Results

For each mixture, one ignition test sample underwent the particle size distribution analysis, and consequently the following granulometric curves were obtained:

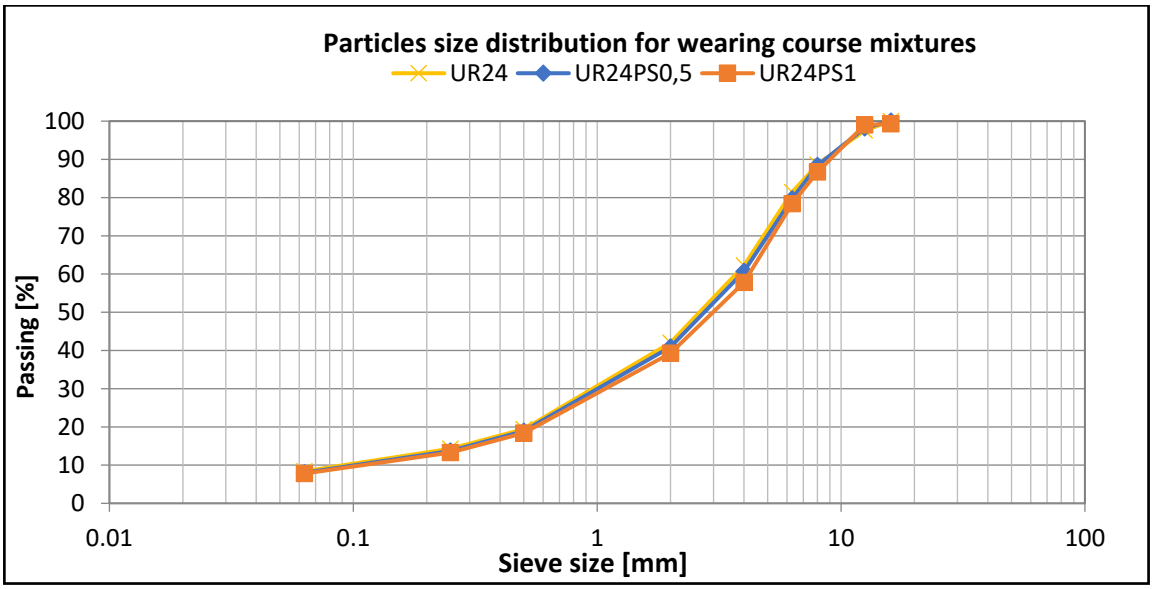

Figure 40. Particle size distribution for wearing course mixtures

G.1 Remarks

The particle size distribution curves show an identical aggregate composition for the three wearing course mixtures. From the curves, it is evident that the mixtures are composed of dense-graded aggregates, which contain a sufficient number of small-sized aggregates, which generally reduces the void content of the mixture.

As described in *Linee guida per la costruzione e manutenzione delle pavimentazioni stradali* (Consiglio Superiore dei Lavori Pubblici, 2022) and table 10 below, the mixtures belong to the category AC12 for wearing courses.

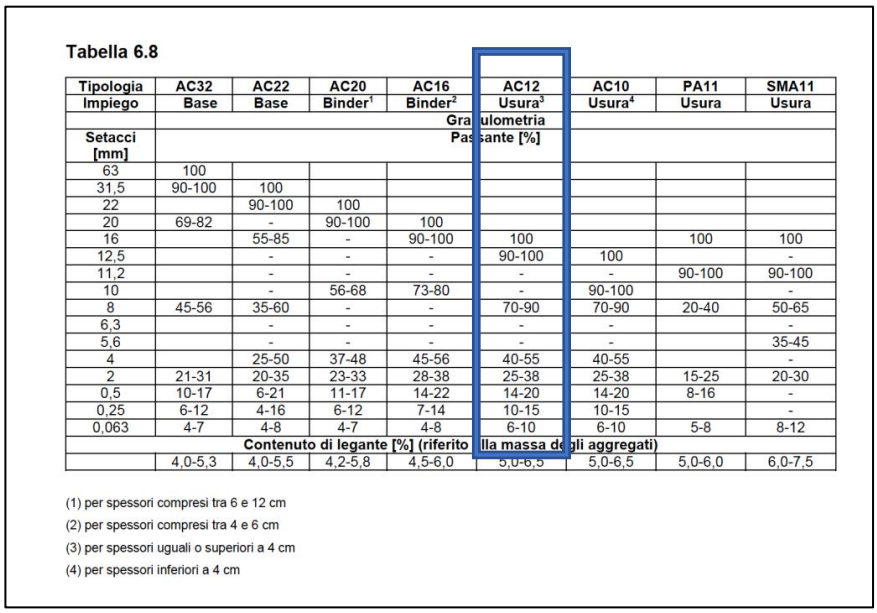

Tabella 6.8

Tipologia Impiego	AC32 Base	AC22 Base	AC20 Binder[1]	AC16 Binder[2]	AC12 Usura[3]	AC10 Usura[4]	PA11 Usura	SMA11 Usura
Setacci [mm]	Granulometria Passante [%]							
63	100							
31,5	90-100	100						
22		90-100	100					
20	69-82	-	90-100	100				
16		55-85	-	90-100	100		100	100
12,5		-	-	-	90-100	100		-
11,2		-	-	-	-	-	90-100	90-100
10		-	56-68	73-80	-	90-100		-
8	45-56	35-60	-	-	70-90	70-90	20-40	50-65
6,3		-	-	-	-	-		-
5,6		-	-	-	-	-		35-45
4		25-50	37-48	45-56	40-55	40-55		-
2	21-31	20-35	23-33	28-38	25-38	25-38	15-25	20-30
0,5	10-17	6-21	11-17	14-22	14-20	14-20	8-16	-
0,25	6-12	4-16	6-12	7-14	10-15	10-15		-
0,063	4-7	4-8	4-7	4-8	6-10	6-10	5-8	8-12
Contenuto di legante [%] (riferito alla massa degli aggregati)								
	4,0-5,3	4,0-5,5	4,2-5,8	4,5-6,0	5,0-6,5	5,0-6,5	5,0-6,0	6,0-7,5

(1) per spessori compresi tra 6 e 12 cm
(2) per spessori compresi tra 4 e 6 cm
(3) per spessori uguali o superiori a 4 cm
(4) per spessori inferiori a 4 cm

Table 10. Aggregate passing limits for sieve analysis, wearing course and AC12 aggregates (Consiglio Superiore dei Lavori Pubblici, 2022)

Further results from the sieve analysis tests are reported in Annex II for the individual mixtures.

H. THEORETICAL MAXIMUM DENSITY

The theoretical maximum density (TMD) of an asphalt mixture indicates the voidless mass of a mixture. In order to calculate the TMD, a volumetric procedure is carried out, as outlined by BS EN 12697-5:2018. The TMD represents a key indicator of a mixture, which is also required for the verification of the air void content of compacted asphalt specimens.

The mixture test samples shall be prepared as per BS EN 12697-28:2020. The sample is reheated in a suitable oven at a temperature not exceeding the appropriate value defined by the standard, until the sample is sufficiently workable to be mixed and divided. The material shall not be heated for more than 4 hours in the oven to minimize the loss of the volatile constituents of the binder as stated in BS EN 12697-28:2020.

H.1 Procedure

The following procedure was carried out on the loose bituminous mixtures under study to prepare a TMD sample which delivers two TMD values per test:

1) A loose sample shall be prepared to carry out this test, having a mass of at least 50 times the Nominal maximum aggregate size (NMAS in mm) of the mixture and not less than 250 g. In all three mixtures, NMAS was defined by means of the particle size distribution (sieve analysis) as in G.3;
2) The mixture shall be heated up to 110 ± 5 ˚C in an oven, in order to achieve material workability;
3) After cleaning a flat surface from any bituminous residue using a solvent, spread the heated material and manually loosen and disaggregate clumps and course aggregates from fine ones, to achieve sufficient separation (see Figure 41);
4) Allow the material to cool down for some minutes and repeat the disaggregation procedure once again to ensure adequate separation;
5) Create a pile of the mixture and quarter the material, to create 2 homogeneous halves as described by BS EN 12697-28:2020 (see Figure 42);
6) The volume (V_p) of the calibrated pycnometer including its cap is known. The mass (m_1) of the pycnometer and cap with the mixture shall be measured and recorded (see Figure 43);
7) Place the two mixture halves in two pycnometers, then measure and record the mass (m_2) of the pycnometers with the mixture including the cap;
8) Fill with de-aired distilled water, in order to carry out de-airing of the mixture by means of a mechanical vacuum system, as per the volumetric method (see Figure 44). The pycnometer shall be filled with de-aired distilled water until around 3 fingers above the mixture surface;
9) During the de-airing procedure, the pycnometers shall be shaken manually and regularly in order to facilitate de-airing;
10) Once the de-airing procedure is completed (after at least 30 minutes), dismantle the vacuum equipment and place the pycnometer cap. The pycnometer is filled with de-aired distilled water until the cap tip, and the mass (m_3) of the pycnometer, cap, mixture, and de-aired distilled water is measured and recorded again. The pycnometer exterior surface shall be dried before measurement;

11) Measure and record the temperature of the de-aired distilled water inside the pycnometer;
12) Discard the water and the mixture material.

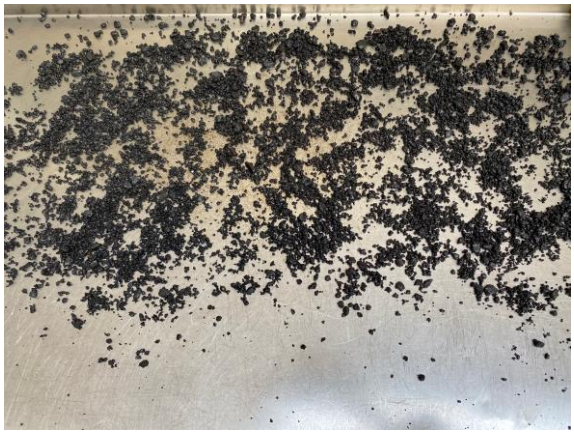

Figure 41. Material disaggregation and spreading

Figure 42. Material quartering

Figure 43. Measurement of m_1

Figure 44. Mixture de-airing using vacuum equipment

H.2 Calculations

All masses shall be expressed in g to the nearest 0,1 g. The volume of the pycnometer shall be expressed in m^3 to the nearest 0,5 x 10^6 m^3. All proportions shall be expressed in % to the nearest 0,1 %.

The density of water at the test temperature in megagram per cubic metre (Mg/m^3) to the nearest 0,0001 Mg/m^3 is calculated as follows:

$$\rho_w = 1{,}00025205 + (\frac{7{,}59 \times t - 5{,}32 \times t^2}{10^6})$$

where

ρ_w *is the density of water at test temperature, in megagram per cubic metre (Mg/m^3);*
t *is the temperature of the water in degrees Celsius (°C).*

The theoretical maximum density ρ_{mv} of the bituminous mixtures determined by the volumetric procedure is calculated as follows:

$$\rho_{mv} = \frac{(m_2 - m_1)}{10^6 \times V_p - \frac{(m_3 - m_2)}{\rho_w}}$$

where

ρ_{mv} *is the maximum density of the bituminous mixture, as determined by the volumetric procedure, in megagrams per cubic metre (Mg/m^3) to the nearest 0,001 Mg/m^3;*

m_1 *is the mass of the pycnometer plus head piece and spring, if any, in grams (g);*
m_2 *is the mass of the pycnometer plus head piece, spring and test sample, in grams (g);*
m_3 *is the mass of the pycnometer plus head piece, spring, test sample and water or solvent, in grams (g);*
V_p *is the volume of the pycnometer, when filled up to the reference mark, in cubic metres (m^3);*
ρ_w *is the density of the water or solvent at test temperature, in megagrams per cubic metre (Mg/m^3) to the nearest 0,0001 Mg/m^3.*

Result repeatability: $r = 2{,}77 \times \sigma_r = 0{,}011\ Mg/m^3\ (using\ water)$

H.3 Results

Theoretical Maximum Density (TMD) [Mg/m^3]			
Material sample	**U24**	**U24PS0,5**	**U24PS1**
1	2,527	2,541	2,523
2	2,538	2,534	2,524
Repeatability (using water)	0,011	0,007	0,001
3	2,542*	2,531	2,529
4	2,521*	2,540	2,530
Repeatability (using water)	0,021*	0,009	0,001
Mean	**2,533**	**2,537**	**2,526**

Table 11. the theoretical maximum density of the three mixtures under study

**Values rejected due to repeatability limit exceedance*

H.4 Remarks

The mixtures U24 and U24PS0,5 exhibit rather similar values of the TMD, while that of U24PS1 is slightly lower accompanied with the presence of a higher plastic shred content.

As seen in Table 11, one TMD test (in red) is rejected for U24 as it exceeds the repeatability limitation of 0,011 Mg/m^3. It was not comprised in the calculation of the mean.

The mixture U24PS1 containing 1% of plastic shreds was heated up to 130 ˚C instead of 110 ˚C to allow better workability, as the mixture tended to form clusters due to the high plastic content with the respect to the other mixtures. It was generally noticed that this mixture left higher binder residues on the working surface and working gloves.

Some plastic shreds were visible with the naked eye upon mixture disaggregation. Not all melt or become soluble, as some maintain their geometry. It can be assumed that some plastics play a minor role as aggregates in addition to becoming part of the binder.

I. PLASTIC SHREDS IN MIXTURE

I.1 Mixture plastic origin

The HMA for wearing course was produced in production plant and to scale, using the dry method to introduce the plastic shreds. Therefore, individual tests on the binder, plastics and aggregates cannot be carried out separately.

The urban and household waste plastic present in the mixtures is considered as modifier plastic, predominantly being LDPE in chemical composition. The introduced plastics originate from the residue of sorted plastics that remain from what is sold to manufacturers for reuse. Hence, what remains is a heterogeneous mix of plastic, that is in general consistent in its constitutive fractions, however with different performance and mechanical properties.

I.2 Mixture plastic laboratory inspection

The following procedure was carried out in order to obtain a sample of the plastics that were introduced into the mixture by the production plant:

1) In an oven, the loose HMA mixtures containing plastic shreds were heated up to compaction temperature (160 ± 5 ˚C).
2) Manually, the visible plastic shreds were selected and removed from the mixtures for visual inspection (see Figure 45 & Figure 46).
3) The selected plastic shreds were suspended in a petroleum based solvent for 30 minutes to remove the bitumen film coating from their surface (see Figure 47).
4) The shreds were cleaned with paper and washed with water, then laid and sorted according to shape, size, and type (see Figure 48 & Figure 49).

I.3 Observations

Based on visual inspection, it is established that the HMA mixtures contain a heterogeneous blend of recycled waste plastic shreds of different origins, geometry, density, chemistry, and polymeric composition. Their behaviour is not uniform since some were soft in texture, others deformed or melted, while some remained stiff and intact. It can be concluded that at compaction and production temperature not all the plastics melt, and not all partake in the binder component of the mixtures. This is due to the diverse melting points of the heterogeneous plastics in the mix. The presence of diverse plastics means that some will melt and coat aggregates, while other will remain intact and perform as aggregates, depending on their melting temperatures. The shreds are present in a range of dimensions up to 2 mm in thickness, and up to 1,5 cm in width as seen in Figure 48.

Figure 45. Heated HMA loose samples with random plastic shred pieces selected from the pans

Figure 46. Plastic shreds coated in Bitumen from the mixture

Figure 47. Plastic shreds soaked in petroleum based solvent to remove bitumen coat

Figure 48. Plastic shreds blend clean of Bitumen

Figure 49. Plastic shreds separated by type. Top left: intact hard plastics; Top right: melted and deformed soft plastics; Bottom: melted and deformed hard plastics

J. SPECIMEN PREPARATION BY GYRATORY COMPACTION

The norm BS EN 12697-31:2019 outlines the procedure of specimen preparation by means of a gyratory shear compactor for HMA mixtures. The geometric information derived from the compaction process allow the calculation of the SSD bulk density (refer to chapter K.) of the specimens produced, as well as their void content. This information in turn allows to determine the compaction curve (degree of compaction) and workability at a pre-defined target number of gyrations or target height, each corresponding to a target void content and its bulk density. Various mechanical tests implemented in this research have requirements among others related to void content, height, and diameter of the specimens with respective tolerances. Using the gyratory shear compactor, such specimens may be produced respecting the above-mentioned prerequisites.

The compaction of specimens requires a gyratory shear compactor, ovens, a mould and round metallic inserts (see Figure 52). As described in BS EN 12697-31:2019: the mould should maintain its temperature (with tolerances) throughout the test. The compaction is realised by two contemporary movements: a low static compression, and shearing action. The shearing action is achieved by the motion of the sample axis, which produces a conical surface of revolution having an apex O with an angle of 2ϕ at the apex (refer to Figure 50 & Figure 51). The ends of the test piece shall ideally remain perpendicular to the axis of the conical surface (as in BS EN 12697-31:2019). The gyratory shear compactor of the DIATI laboratory used for the specimen production has been calibrated for height measurements, and applies and maintains a compaction stress of 600 kPa. The norm BS EN 12697-31:2019 further defines the technical requirements of the gyratory shear compactor, as well as the moulds and round metallic inserts. The gyratory shear compactor simulates the kneading action of roller machines and it allows the assessment of the evolution of compaction as the acquisition software registers the variation of specimen height as a function of the number of gyration. During compaction, a rearrangement of the mixture aggregates happens, due to the combined action of normal and shear stresses caused by the rotation and angle of inclination. The angle is 1,25°, while the rate of rotation is 30 gyrations/minute. This combined action simulates the forces which are applied by rollers to the HMA pavement in road construction phases.

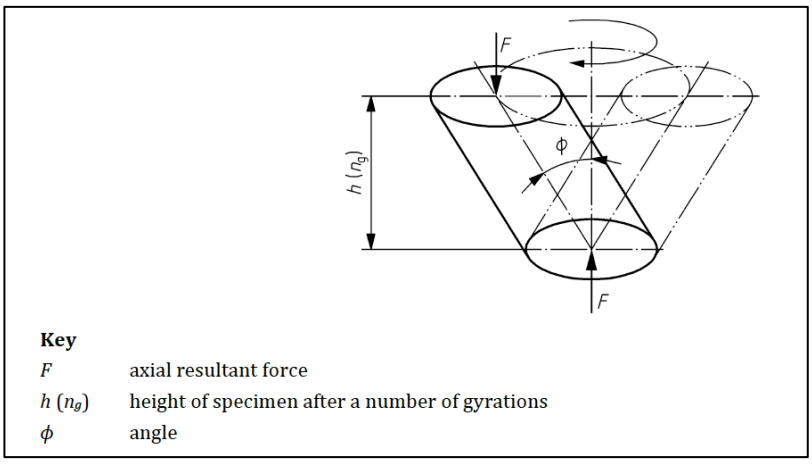

Figure 50. Test piece inclined motion diagram due to force eccentricity at one end, resulting in a tilting moment [BS EN 12697-31:2019]

For the mixtures in study, the compaction temperature selected is 160 ˚C, as the mixtures were paved on the road SP220 at this temperature. The aim is to replicate the compaction energy employed in the construction site at the same temperature, to obtain representative specimens. Furthermore, based on the results from trial compacted specimens at 200 gyrations, the final test specimens were produced to a pre-defined target number of gyrations N_{100} in order to employ the same compaction energy among all specimens of the mixtures. Furthermore, as explained in BS EN 12697-31:2019, the specimen diameter chosen was 100 mm, as the NMAS of the mixtures is less than 16 mm. The final height accepted for the compacted specimens is 60,0 ± 2 mm. The chosen diameter and height of the specimens is in accordance with all geometrical conditions of the various tests employed in this study.

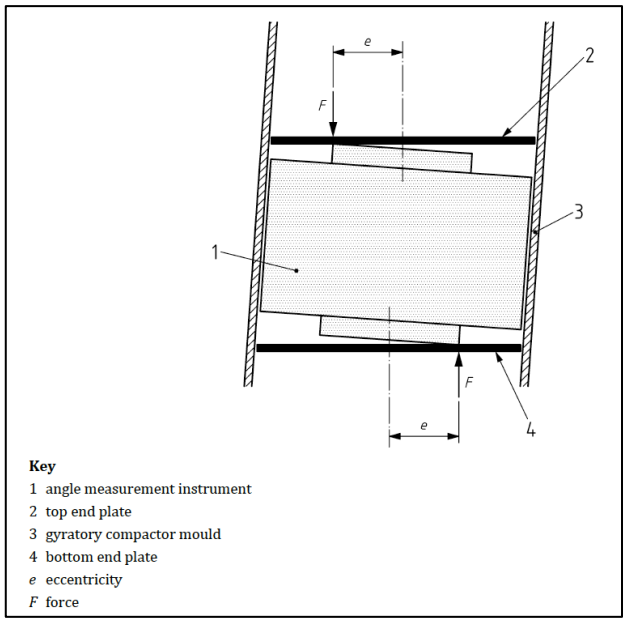

Figure 51. Tilting moments (top and bottom) induced by the angle measurement instrument [BS EN 12697-31:2019]

J.1 Procedure

The following represents the procedure followed to produce specimens by the gyratory shear compactor, as per BS EN 12697-31:2019:

1) Place the 100 mm moulds and inserts at compaction temperature (160 ± 2 ˚C) in an oven for at least 2 h (see Figure 53);
2) Bring the loose mixture sample to the compaction temperature. Avoid heating longer than necessary to evade added ageing of the mixture;
3) Upon reaching compaction temperature, place the mould and lower insert on the balance, and insert a filter paper. Tare the mass of the balance (see Figure 54);
4) Fill the mould with the calculated mass of the loose mixture inside the moulds by means of a funnel;
5) Place again the filled moulds in the oven and wait to reach compaction temperature once again;
6) Upon reaching the compaction temperature, remove the mould from the oven, and carry out a short and quick homogenisation of the mould content by means of a

metallic spatula. Avoid applying excessive force to avoid compaction of the loose mixture;

7) Insert a filter paper on the top of the loose mixture in the mould, followed by the top insert using a magnetic device;
8) Place the mould in the oven at compaction temperature again for at least 15 minutes to guarantee temperature uniformity;
9) Remove the mould from the oven and quickly transport the filled mould to the compactor and spray lubricant on the top insert and the base of the compactor chamber;
10) Insert the mould inside the compaction chamber, rotate until it interlocks and is set (see Figure 55 & Figure 56). First, check if the upper metal piston plate in the compaction chamber for 100 mm specimens is installed;
11) Start the compaction to the defined number of gyrations N_{100} and record the height of the specimen for every gyration by means of a digital software;
12) At the end of compaction, remove the mould from the compactor and extract the specimen from the mould by means of a hydraulic lift piston (see Figure 57);
13) Remove the top insert and the filter;
14) Manually flip the specimen by means of a wooden base plate and remove the bottom insert and filter (see Figure 58 & Figure 59);
15) Store the HMA specimen in a dry and cool place and allow to cool down to room temperature overnight.

After being allowed to cool down, the day following compaction the specimens underwent height measurement to be compared with the reported final height by the compactor machine at N_{100}, as well as to perform the SSD bulk density tests. After that, the specimens were placed in dry and level shelves to develop stiffness for 14 days.

J.2 Calculations

As stated in BS EN 12697-31:2019, the mixture sample mass to be inserted into the mould for compaction shall be estimated according to the following relationship:

$$M = 10^{-3} \times \pi \times \frac{D^2}{4} \times h_{min} \times \rho_{TMD}$$

where

M *the mass of a dry mixture to be introduced in the mould (g);*
D *is the internal diameter of the mould (mm);*
h_{min} *is the minimum height of compacted specimen, corresponding to zero % voids (mm);*
ρ_{TMD} *is the theoretical maximum density of the mixture; TMD (Mg/m^3).*

For a given type of gyratory compacter, h_{min} will be constant. The ratio of h_{min} to the internal diameter of the mould D shall be in the interval of 0,66 to 1,05.

Using the formula above and before producing compacted specimens for testing, trial specimens were created at N_{200} gyrations using a sample mass corresponding to 0% final voids in order to obtain a characteristic compaction curve representing the behaviour of each mixture (see results in Annex IV). From these trials, the projected air void content at N_{100}

gyrations was determined, as well as the correction factor. Both values are needed to calculate the mass of the loose sample to be introduced into the mould for a target void content at N_{100}, fixed height of 60 ± 2 mm and diameter of 100 mm. The following relationships were used to determine the mass introduced into the mould:

$$M_{mould} = (\rho_{SSD\,target\ voids} * V_x) * \frac{1}{cf}$$

$$\rho_{SSD\,target\ voids} = (1 - \frac{v_{target}}{100}) \times TMD$$

The analysis of the height data conveyed by the gyratory shear compactor interface was carried out using the following relationships to estimate the degree of compaction and void content of the specimens at every gyration:

V_x	Geometric volume of the specimen	$\pi*(D^2/4)*h(n_G)$
C_{ux}	% of compaction in which the wall effect due to imperfect sample-mould wall adherence is not considered	$100.(M_{effective}/V_x)/TMD$
C_x	% of compaction considering the wall effect	$(C_{ux}\cdot\rho_{SSD}\cdot V_{xfinal})/M_{effective}$
v_{real} (%)	Real % of voids in the sample	$100\text{-}C_x$
v_{geom} (%)	Theoretical geometric % of voids in the sample	$100\text{-}C_{ux}$
cf	Correction factor	C_x/C_{ux}

where

v_{target}	*the target air void content of the specimen (%);*
$\rho_{SSD\,target\ voids}$	*the theoretical bulk density of specimen at target air void content (Mg/m³);*
$M_{effective}$	*the mass of the specimen measured after compaction and cooling (g);*
D	*the internal diameter of the mould (mm);*
$h(n_G)$	*the specimen height achieved at the n^{th} gyration (mm);*
ρ_{SSD}	*the bulk density of the mixture (Mg/m³).*

To determine the compaction curve, the following relationship is presented:

$$C_x(n_G) = C_1 + k*\log(n_G)$$

The self-compaction (C_1) and workability (k) of the specimen mixtures can be obtained from compaction curve by means of trend-line function of the Compaction $C_x(n_G)$ in % vs. gyration number n_G [Log] curve. Where the self-compatibility is the y-intercept of the curve, while the workability is the compaction curve trendline gradient.

Figure 52. Specimen moulds with base and top inserts

Figure 53. Heating of Specimen moulds and inserts in the oven

Figure 54. Filling and weighing the moulds before compaction

Figure 55. Inserting the mould in the gyratory shear compactor chamber

Figure 56. Locking of the mould inside the gyratory shear compactor chamber

Figure 57. Compacted specimen extraction from the mould

Figure 58. Compacted sample cooling after extraction

Figure 59. Compacted sample (top view)

J.3 Results

Gyratory Shear Compactor Specimen Properties							
U24							
ID	N	d	Target H	Achieved H	M_{sample}	v_{real}	c_x
[-]	[girations]	[mm]	[mm]	[mm]	[g]	[%]	[%]
U24A	100	100	60 ± 2	60,1	1168,9	0,70	99,30
U24B				59,8	1168,8	0,75	99,25
U24C				59,4	1167,6	0,42	99,58
U24D				60,4	1167,5	1,14	98,86
U24E				59,6	1168,4	0,76	99,24
U24F				60,4	1170,0	0,91	99,09
U24G				61,2	1171,8	1,80	98,20
U24H				60,0	1170,5	0,90	99,10
U24I				59,9	1169,7	0,56	99,44
U24J				59,6	1166,0	0,88	99,12
U24K				60,3	1169,7	0,63	99,37
U24L				60,2	1172,1	0,51	99,49
U24M				59,9	1170,0	0,95	99,05
U24N				60,5	1171,5	0,84	99,16
U24O				60,4	1169,8	1,18	98,82
U24P				59,4	1169,1	0,42	99,58
U24Q				60,0	1169,6	0,23	99,77
U24R				60,4	1170,2	0,78	99,22
U24S				59,3	1167,2	0,37	99,63
U24Gbis*				60,4	1169,0	0,93	99,07
			Mean	**60,06**	**1169,37**	**0,78**	**99,22**
			Std. Dev.	0,47	1,55	0,35	0,35

Table 12. Compaction results for U24 Specimens
**replacement specimen for U24G which was impaired*

Gyratory Shear Compactor Specimen Properties							
U24PS0,5							
ID	**N**	**d**	**Target H**	**Achieved H**	**M_{sample}**	**v_{real}**	**c_x**
[-]	**[girations]**	**[mm]**	**[mm]**	**[mm]**	**[g]**	**[%]**	**[%]**
U24PS0,5A	100	100	60 ± 2	59,50	1140,80	2,42	97,58
U24PS0,5B				60,20	1140,10	3,43	96,57
U24PS0,5C				60,10	1143,50	3,22	96,78
U24PS0,5D				60,90	1144,20	3,68	96,32
U24PS0,5E				60,90	1142,90	4,43	95,57
U24PS0,5F				60,10	1142,40	3,71	96,29
U24PS0,5G				60,80	1142,70	4,20	95,80
U24PS0,5H				59,70	1142,30	2,98	97,02
U24PS0,5I				60,20	1141,80	3,02	96,98
U24PS0,5J				59,80	1140,00	3,04	96,96
U24PS0,5K				60,30	1142,50	3,14	96,86
U24PS0,5L				59,70	1143,50	2,80	97,20
U24PS0,5M				60,70	1142,10	3,75	96,25
U24PS0,5N				60,70	1142,30	3,75	96,25
U24PS0,5O				61,10	1141,50	4,40	95,60
U24PS0,5P				60,90	1142,60	4,28	95,72
U24PS0,5Q				60,20	1142,70	2,69	97,31
U24PS0,5R				59,90	1143,00	2,84	97,16
U24PS0,5S				60,40	1141,20	3,51	96,49
			Mean	**60,32**	**1142,22**	**3,44**	**96,56**
			Std. Dev.	0,48	1,11	0,64	0,60

Table 13. Compaction results for U24PS0,5 Specimens

Gyratory Shear Compactor Specimen Properties							
U24PS1							
ID	**N**	**d**	**Target H**	**Achieved H**	**M_{sample}**	**v_{real}**	**c_x**
[-]	**[girations]**	**[mm]**	**[mm]**	**[mm]**	**[g]**	**[%]**	**[%]**
U24PS1A	100	100	60 ± 2	60,0	1143,9	3,20	96,80
U24PS1B				60,4	1144,3	2,77	97,23
U24PS1C				60,0	1145,1	2,48	97,52
U24PS1D				60,6	1146,9	2,52	97,48
U24PS1E				60,4	1145,5	2,84	97,16
U24PS1F				59,6	1144,8	1,92	98,08
U24PS1G				59,7	1145,2	2,08	97,92
U24PS1H				60,6	1145,1	2,72	97,28
U24PS1I				60,5	1144,4	3,13	96,87
U24PS1J				60,4	1143,6	2,79	97,21
U24PS1K				59,7	1143,6	2,51	97,49
U24PS1L				59,8	1145,7	2,48	97,52
U24PS1M				60,8	1144,6	3,77	96,23
U24PS1N				60,3	1144,2	2,48	97,52
U24PS1O				59,6	1145,4	2,02	97,98
U24PS1P				60,8	1144,9	3,43	96,57
U24PS1Q				59,5	1144,6	2,14	97,86
U24PS1R				60,9	1145,3	3,91	96,09
U24PS1S				60,3	1146,3	2,63	97,37
U24PS1Bbis**				60,6	1145,7	3,39	96,61
			Mean	**60,23**	**1144,96**	**2,76**	**97,24**
			Std. Dev.	0,45	0,85	0,56	0,56

Table 14. Compaction results for U24PS1 Specimens

***replacement specimen for U24PS1B which was impaired*

Mixture	# of specimens	$H_{achieved}$ [mm]	M_{sample} [g]	TMD [Mg/m³]	SSD density [Mg/m³]	v_{real} [%]	C_x [%]	Workability [-]	Self-compaction [%]
Mean values									
Diameter = 100 mm; N_{100}; T = 160 ˚C									
U24	20	60,06	1169,37	2,533	**2,513**	**0,78**	99,22	**8,34**	**82,72**
U24PS0,5	19	60,32	1142,22	2,537	**2,449**	**3,44**	96,56	**7,95**	**80,79**
U24PS1	20	60,23	1144,96	2,526	**2,457**	**2,76**	97,24	**8,00**	**81,32**

Table 15. Specimen compaction and volumetric properties for all mixtures

Further results and figures of compaction curves of trial and definitive specimens are reported in Annex IV.

J.4 Remarks

All specimens were homogenized and compacted at the same temperature and to the same number of gyrations N_{100}, since the trial specimens showed a very low air void content with increasing gyration count. Compacting to the same final number of gyrations ensures the compaction energy is administered uniformly in all specimens. That being said, the air void content varied among the specimens of each mixture category as seen in the results above. Further details about air void content determinations are presented in K.3 for the SSD bulk density of compacted specimens.

It is evident from the compaction curves that three mixtures achieve relatively low air void contents, rendering them less porous and closed in nature. The mean air void content is maximum (3,44 %) in U24PS0,5 and lowest (0,78 %) in U24, while U24PS1 achieves an intermediate value (2,76 %). For similar binder content, it is apparent that the presence of plastic shreds increases the air voids in the mixture specimens; however, this relationship is not proportional. The low void content in U24 and U24PS1 represents a risk for what concerns dewatering, noise limitation, and thermal expansion at high temperatures. At low void contents, the mixture tends to be plastic and volatile in performance (*Asphalt Pavement Construction - Asphalt Institute*, 2022).

The compaction curves of the mixtures deliver similar results for the self-compaction, where the lowest value (80,79 %) is achieved by U24PS0,5, rendering it less prone to segregation. Furthermore, U24PS0,5 achieves the lowest workability value (7,95), which requires more energy for its compaction compared to the other mixtures.

Plastics were occasionally visible on the surface of some compacted specimens, however, in intact form.

K. BULK DENSITY OF GYRATORY COMPACTED SPECIMENS

The norm BS EN 12697-6:2020 describes the methodology to calculate the bulk density of compacted gyratory cylindrical HMA samples. The norm defines the bulk density as 'the mass per unit volume, including air voids of a specimen at known test temperature'. From the bulk density, the air void content in the sample can be computed, based on the TMD which was determined prior to compaction. The bulk density is a vital parameter to evaluate the compaction degree and the performance of asphalt mixes by means of the air void content, especially for what concerns their relationship with mechanical properties.

In this study, the bulk density was calculated by employing the SSD method, as defined by BS EN 12697-6:2020. The SSD method implies that the surface of the compacted sample is dry, while the inner voids are completely occupied with water. The bulk density is computed from the mass of the specimen and its volume, which is obtained from its mass in air and its mass in water.

K.1 Procedure

The following represents the procedure to perform the SSD bulk density test, as per BS EN 12697-6:2020:

All SSD bulk density tests were carried out one day post specimen compaction, at room temperature.

1) Measure the dry mass (m_1) of the compacted samples using a balance (see Figure 60);
2) Place the specimen in the water bath, for about 40 minutes (see Figure 61);
3) Every 10 minutes, shake the specimen manually while submerged in water, to facilitate the expulsion of air from the inner voids;
4) Measure the mass of the saturated specimen immersed in water, by means of a balance in the water bath (see Figure 62);
5) Remove the specimen from the water bath, and dry its surface using a moist cloth (See Figure 63);
6) Measure the mass of the SSD specimen (m_3) immediately using a balance;
7) Measure the temperature of the water bath and record it.

K.2 Calculations

As stated in BS EN 12697-6:2020, the density of water at test temperature is calculated as follows:

$$\rho_w = 1{,}00025205 + \left(\frac{7{,}59 \times t - 5{,}32 \times t^2}{10^6}\right)$$

where

t *the temperature of water (˚C);*

ρ_w *the density of the water at test temperature in Mg/m³.*

As stated in BS EN 12697-6:2020, the bulk density (SSD) of the cylindrical sample is calculated as follows:

$$\rho_{bssd} = \frac{m_1}{m_3 - m_2} \times \rho_w$$

where

ρ_{bssd} *the bulk density (SSD) (Mg/m³);*

m_1 *the mass of the dry specimen (g);*

m_2 *the mass of the specimen in water (g);*

m_3 *the mass of the saturated surface-dried specimen (g);*

ρ_w *the density of the water at test temperature in Mg/m³.*

The bulk density shall be expressed to the nearest 0,001 Mg/m³.
All masses shall be determined in gram to the nearest 0,1 g.

From the bulk density calculated, the real and geometric air void contents can be determined based on the specimen height achieved at the end of the specimen compaction at N_{100}. These calculations are further clarified in J.3.

Figure 60. Measurement of the dry mass (m_1) of the compacted sample

Figure 61. Compacted samples in water bath

Figure 62. Measurement of the water saturated mass (m_2) of the compacted sample

Figure 63. Drying of the water saturated sample using a moist cloth for the SSD mass (m_3) measurement

K.3 Results

Specimen	M_1 [g]	M_2 [g]	M_3 [g]	T_{water} [°C]	ρ_w [Mg/m³]	ρ_{bssd} [Mg/m³]	ρ_{tmd} [Mg/m³]	v_{real} at N_{100} [%]	v_{geom} at N_{100} [%]
U24A	1168,9	706,1	1169,6	24,6	0,9972	**2,515**	2,533	**0,70**	2,22
U24B	1168,8	706,2	1169,9	24,6	0,9972	**2,514**	2,533	**0,75**	1,74
U24C	1167,6	706,4	1168,1	24,6	0,9972	**2,522**	2,533	**0,42**	1,18
U24D	1167,5	703,2	1168,2	24,6	0,9972	**2,504**	2,533	**1,14**	2,82
U24E	1168,4	705,3	1168,9	24,6	0,9972	**2,513**	2,533	**0,76**	1,44
U24F	1170,0	705,8	1170,7	24,6	0,9972	**2,510**	2,533	**0,91**	2,62
U24G	1171,8	703,8	1173,8	23,4	0,9975	**2,487**	2,533	**1,80**	3,74
U24H	1170,5	706,4	1171,6	23,4	0,9975	**2,510**	2,533	**0,90**	1,93
U24I	1169,7	707,3	1170,6	23,4	0,9975	**2,518**	2,533	**0,56**	1,83
U24J	1166,0	702,9	1166,2	23,8	0,9974	**2,510**	2,533	**0,88**	1,65
U24K	1169,7	706,6	1170,2	23,8	0,9974	**2,517**	2,533	**0,63**	2,48
U24L	1172,1	709,7	1173,8	22,8	0,9977	**2,520**	2,533	**0,51**	2,12
U24M	1170,0	705,7	1171,0	22,8	0,9977	**2,509**	2,533	**0,95**	1,80
U24N	1171,5	707,5	1172,9	22,8	0,9977	**2,511**	2,533	**0,84**	2,65
U24O	1169,8	704,5	1170,8	22,8	0,9977	**2,503**	2,533	**1,18**	2,63
U24P	1169,1	707,1	1169,6	22,8	0,9977	**2,522**	2,533	**0,42**	1,05
U24Q	1169,6	708,6	1170,4	22,8	0,9977	**2,527**	2,533	**0,23**	2,00
U24R	1170,2	706,9	1171,7	20,7	0,9981	**2,513**	2,533	**0,78**	2,60
U24S	1167,2	706,2	1167,7	22,6	0,9977	**2,523**	2,533	**0,37**	1,05
U24Gbis	1169,0	704,7	1169,8	20,2	0,9982	**2,509**	2,533	**0,93**	2,70
					Mean	**2,513**	2,533	**0,78**	2,11
					Stand. Dev.	**0,009**	0,000	**0,35**	0,68

Table 16. Bulk density test results and air void content for U24 gyratory compacted specimens

Specimen	M_1 [g]	M_2 [g]	M_3 [g]	T_{water} [°C]	ρ_w [Mg/m³]	ρ_{bssd} [Mg/m³]	ρ_{tmd} [Mg/m³]	v_{real} at N_{100} [%]	v_{geom} at N_{100} [%]
U24PS0,5A	1140,8	684,5	1144,2	24,0	0,9974	**2,475**	2,537	**2,42**	3,76
U24PS0,5B	1140,1	679,7	1143,9	24,0	0,9974	**2,450**	2,537	**3,43**	4,94
U24PS0,5C	1143,5	683,6	1148,2	24,0	0,9974	**2,455**	2,537	**3,22**	4,49
U24PS0,5D	1144,2	682,6	1149,7	24,0	0,9974	**2,443**	2,537	**3,68**	5,69
U24PS0,5E	1142,9	679,4	1149,6	24,0	0,9974	**2,424**	2,537	**4,43**	5,80
U24PS0,5F	1142,4	680,8	1147,3	24,0	0,9974	**2,442**	2,537	**3,71**	4,59
U24PS0,5G	1142,7	678,8	1147,9	23,4	0,9975	**2,430**	2,537	**4,20**	5,66
U24PS0,5H	1142,3	682,6	1145,6	23,4	0,9975	**2,461**	2,537	**2,98**	3,95
U24PS0,5I	1141,8	682,9	1145,9	23,4	0,9975	**2,460**	2,537	**3,02**	4,79
U24PS0,5J	1140,0	681,4	1143,7	24,0	0,9974	**2,459**	2,537	**3,04**	4,31
U24PS0,5K	1142,5	681,1	1144,9	24,0	0,9974	**2,457**	2,537	**3,14**	4,89
U24PS0,5L	1143,5	681,9	1144,6	22,8	0,9977	**2,466**	2,537	**2,80**	3,85
U24PS0,5M	1142,1	680,6	1147,3	22,8	0,9977	**2,441**	2,537	**3,75**	5,55
U24PS0,5N	1142,3	679,7	1146,5	22,8	0,9977	**2,441**	2,537	**3,75**	5,54
U24PS0,5O	1141,5	677,7	1147,3	22,8	0,9977	**2,425**	2,537	**4,40**	6,22
U24PS0,5P	1142,6	677,4	1147,1	20,7	0,9981	**2,428**	2,537	**4,28**	5,82
U24PS0,5Q	1142,7	683,2	1145,3	20,7	0,9981	**2,468**	2,537	**2,69**	4,72
U24PS0,5R	1143,0	683,4	1146,3	20,7	0,9981	**2,465**	2,537	**2,84**	4,22
U24PS0,5S	1141,2	679,2	1144,4	22,6	0,9977	**2,448**	2,537	**3,51**	5,16
					Mean	**2,449**	2,537	**3,44**	4,95
					Stand. Dev.	**0,0153**	0,000	**0,60**	0,74

Table 17. Bulk density test results and air void content for U24PS0,5 gyratory compacted specimens

Specimen	M_1 [g]	M_2 [g]	M_3 [g]	T_{water} [°C]	ρ_w [Mg/m³]	ρ_{bssd} [Mg/m³]	ρ_{tmd} [Mg/m³]	v_{real} at N_{100} [%]	v_{geom} at N_{100} [%]
U24PS1A	1143,9	681,6	1148,1	24,0	0,9974	**2,446**	2,526	**3,20**	3,92
U24PS1B	1144,3	683,3	1147,9	24,0	0,9974	**2,457**	2,526	**2,77**	4,52
U24PS1C	1145,1	684,5	1148,1	23,5	0,9975	**2,464**	2,526	**2,48**	3,82
U24PS1D	1146,9	685,4	1149,9	23,5	0,9975	**2,463**	2,526	**2,52**	4,62
U24PS1E	1145,5	683,7	1149,2	23,5	0,9975	**2,455**	2,526	**2,84**	4,42
U24PS1F	1144,8	686,0	1146,8	23,7	0,9974	**2,478**	2,526	**1,92**	3,20
U24PS1G	1145,2	685,9	1147,7	22,9	0,9976	**2,474**	2,526	**2,08**	3,33
U24PS1H	1145,1	683,1	1147,9	22,9	0,9976	**2,458**	2,526	**2,72**	4,77
U24PS1I	1144,4	680,7	1147,2	22,9	0,9976	**2,447**	2,526	**3,13**	4,67
U24PS1J	1143,6	681,9	1146,3	24,0	0,9974	**2,456**	2,526	**2,79**	4,58
U24PS1K	1143,6	682,8	1145,9	24,0	0,9974	**2,463**	2,526	**2,51**	3,46
U24PS1L	1145,7	683,6	1147,5	22,8	0,9977	**2,464**	2,526	**2,48**	3,45
U24PS1M	1144,6	678,1	1147,8	22,8	0,9977	**2,431**	2,526	**3,77**	5,13
U24PS1N	1144,2	682,5	1145,8	22,8	0,9977	**2,464**	2,526	**2,48**	4,37
U24PS1O	1145,4	687,0	1148,6	22,8	0,9977	**2,476**	2,526	**2,02**	3,18
U24PS1P	1144,9	680,2	1148,6	20,7	0,9981	**2,440**	2,526	**3,43**	5,10
U24PS1Q	1144,6	684,9	1147,0	20,7	0,9981	**2,472**	2,526	**2,14**	3,05
U24PS1R	1145,3	678,3	1149,0	22,5	0,9977	**2,428**	2,526	**3,91**	5,22
U24PS1S	1146,3	684,1	1149,0	22,5	0,9977	**2,460**	2,526	**2,63**	4,20
U24PS1Bbis	1145,7	681,0	1149,3	22,5	0,9977	**2,441**	2,526	**3,39**	4,72
					Mean	**2,457**	2,526	**2,76**	4,19
					Stand. Dev.	**0,014**	0,000	**0,56**	0,71

Table 18. Bulk density test results and air void content for U24PS1 gyratory compacted specimens

Further results of SSD bulk density tests, air void content, and compaction are reported in Annex IV.

K.4 Remarks

All specimens were homogenized and compacted at the same temperature and to the same number of gyrations N100. Nevertheless, the air void content varied among the specimens of each mixture category as seen in the results above.

The results show that the air void content is highest for the mixture U24PS0,5, where the mean is about 3,44 %, while that of U24PS1 is around 2,76%, and that for U24 0,78%. These results evidently place only U24PS0,5 within the CSLP requirements for a wearing course for a local road (Consiglio Superiore dei Lavori Pubblici, 2022). This in turn would represent difficulties regarding the hydraulic draining capacity of the wearing course, which may thus result in hazardous traffic conditions. Furthermore, low voids also are generally correlated with higher traffic noise levels.

As described in *Linee guida per la costruzione e manutenzione delle pavimentazioni stradali* (Consiglio Superiore dei Lavori Pubblici, 2022), a wearing course mixture of aggregates AC12 must contain void contents from 3 % to 6 %. However, apart from U24PS0,5, the material mixes are very dense, as these limits could not be respected at N_{100}. This is further confirmed by the high degrees of compaction achieved by the specimens (see Annex IV). This was apparent from the trial gyratory compaction samples at N_{200}, which showed extremely low void content for all mixtures (see Annex IV). Therefore, the decision to compact specimens at N_{100} was taken to avoid further low void contents. The low void content can be traced back to the fact that the mixtures contain a high binder content, as well as fine aggregates (dense-graded particle size distribution).

Moreover, the mixtures show significant standard deviations for specimen air void content at the same compaction energy employed at N_{100}.

Nel caso di conglomerati bituminosi di tipo chiuso (AC), a meno di specifiche esigenze progettuali supportate da opportuni studi di carattere sperimentale, la miscela di progetto deve rispettare le specifiche tecniche indicate nella Tabella 6.10.

Tabella 6.10.

Parametro	Normativa di riferimento	Unità di misura	Valori richiesti		
V_m a 10 rotazioni	UNI EN 12697-8	%	11-15		
V_m a 100 rotazioni	UNI EN 12697-8	%	3-6		
V_m a 180 rotazioni	UNI EN 12697-8	%	≥ 2		
			Base	Binder	Usura
Resistenza a trazione indiretta a 25°C a 100 rotazioni (*ITS*)	UNI EN 12697-23	N/mm²	0,95-1,65[a] 1,10 -1,75[b]	0,85-1,55[a] 0,95-1,65[b]	0,75-1,45[a] 0,85-1,55[b]
Coefficiente di trazione indiretta a 25°C a 100 rotazioni (*CTI*) c	-	-	≥ 70[a] ≥ 80[b]	≥ 0,70[a] ≥ 0,80[b]	≥ 65[a] ≥ 75[b]
Sensibilità all'acqua (*ITSR*)	UNI EN 12697-12	%	≥ 80[a] ≥ 90[b]	≥ 80[a] ≥ 90[b]	≥ 80[a] ≥ 90[b]

(a) Conglomerati prodotti con bitume normale

(b) Conglomerati prodotti con bitume modificato o polimeri di addizione

Table 19. Performance requirements for wearing course and AC12 aggregates (Consiglio Superiore dei Lavori Pubblici, 2022)

L. SHORT- & LONG-TERM AGEING

L.1 Short-term Ageing

The loose mixtures underwent short term-ageing conditions upon heating at various temperatures (from 110 to 160 ˚C) in ovens in order to achieve workability and requirements for purposes such as material batch divisions as well as gyratory compaction specimen preparation, as denoted in each respective standard. Additionally, the natural short-term ageing due to the production, transportation, and oxidation with the progress of time is ordinary. Based on all the previous, it can be assumed that the mixtures endured short-term ageing uniformly.

L.2 Long-term Ageing

Following the methodology described in AASHTO R 30-02 (2015), the long-term ageing of specimens was carried out as per the following steps:

1) Upon gyratory compaction, the specimens were left to cool down overnight.
2) One day following compaction, the specimens were placed in a conditioning oven at 85 ± 3 ˚C for 120 ± 0,5 hours (see Figure 64).
3) At the end of the conditioning period, the oven was turned off and the specimens were allowed to reach room temperature with the oven doors open overnight.

Note: specimen bulk density test was carried out prior to the long-term ageing procedure. Moreover, the dimensions (height and diameter) of the specimens were recorded before and after the long-term ageing procedure, to highlight any possible volumetric expansion behaviour (refer to chapter M.).

Figure 64. Long-term Ageing of specimens in conditioning oven

M. COMPACTED SPECIMEN BEHAVIOUR

After the realization of gyratory compacted specimens, measurements of the cylinder height and diameter was carried out. The height was recorded at four equidistant points using a calliper, as well as two diameters (see Figure 65 and Figure 66).

The increase in dimension is reported with respect to the final dimension registered by the gyratory compactor at the target gyration (N_{100}).

Material	Mean height increase		Mean diameter increase	
	H = 60 ± 2 mm		D = 100 ± 3 mm	
	[mm]	[%]	[mm]	[%]
U24	0,18	0,30	0,15	0,15
U24 LTA	0,20	0,33	0,24	0,24
U24PS0,5	0,34	0,57	0,19	0,19
U24PS0,5 LTA	0,40	0,66	0,26	0,26
U24PS1	0,42	0,70	0,22	0,22
U24PS1 LTA	0,51	0,85	0,40	0,40

Table 20. compacted specimen height and diameter increase, LTA (long-term aged)

Further data and graphs are reported in Annex V for each individual mixture.

M.1 Remarks

Based on the above, it is evident that the compacted specimens display varying increases in height and diameter after compaction. Clearly, this dimensional growth propagates both with increasing plastic content and long-term ageing. The plastic shreds appear to exhibit spring-like behaviour, by gaining and storing energy (compaction or thermal) which is in turn discharged afterwards, causing lateral and medial expansion in the specimens.

Figure 65. Specimen height and diameter measurement points

Figure 66. Specimen height and diameter measurement with a calliper

N. STIFFNESS MODULUS (ITSM – IT-CY TEST)

The stiffness modulus is an important indicator of the mechanical properties of cylindrical compacted HMA samples. It allows the estimation of the material capacity to resist mechanical tensile loading as well as its behaviour during service life conditions, at various temperatures and loading frequencies. From such data, master curves can be constructed to characterise the material properties.

In this study the stiffness modulus was calculated for all tested samples at various temperatures, in order to better understand the behaviour of the mixtures, as well as its correlation to the air void content in both short- & long-term aged samples. The determination of the stiffness modulus followed the standard BS EN 12697-26:2018. The UTM-30 machine was used to carry out the indirect tensile test to cylindrical specimens IT-CY (BS EN 12697-26:2018 - Annex C) test for stiffness modulus determination for compacted samples.

N.1 Procedure

Generally, a load amplitude shall be applied without causing damage to the tested specimens (usually below 50 micro-strains no damage occurs). For the determination, specimens shall be conditioned for at least for 4 hours in a climatic chamber at the desired test temperature. Prior to the test, the samples should be stored at room temperature on a flat surface, and then tested at the age of 14 to 42 days since their production. The stiffness modulus shall be determined from the average of the results of at least 4 specimens. The specimen dimensions depend on the NMAS value of the mixture tested as shown in Table 21 below. For the mixtures in study, specimens of 100 ± 3 mm in diameter and 60 ± 2 mm in height were tested.

Maximum grain size mm	**Specimen diameter** mm	**Specimen height** mm
≤ 16	100 ± 3 150 ± 3	40 to 60 ± 2
> 16 to < 32	150 ± 3	60 ± 2
≥ 32	150 ± 3	90 ± 2

Table 21. Specimen dimension as per BS EN 12697-26:2018 – Annex C

The testing equipment shall include a steel loading frame, and a load actuator capable of applying a vertical repeated load pulse with rest period. The loading should be haversine in waveform as shown in Figure 67. The loading time from the begin of the test until the peak shall be between 50 and 125 ms ± 5 mm.

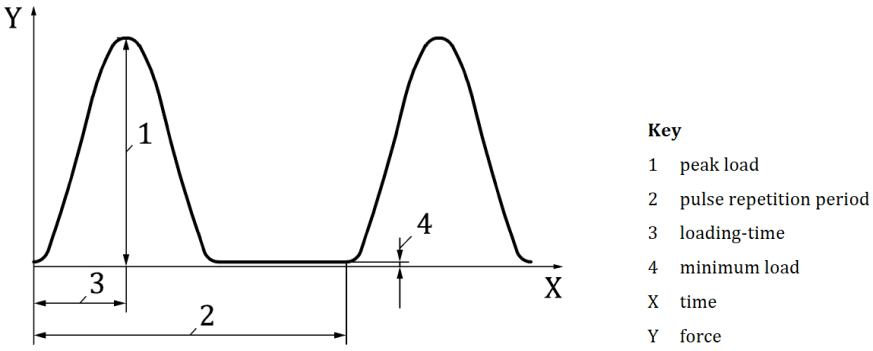

Figure 67. Pulse loading function characteristics as per BS EN 12697-26:2018 – Annex C

The value of the peak load shall be controlled to reach a target peak transient horizontal deformation of 5 µm of the specimen diameter, for a reference temperature of 10 °C. For other testing temperatures, the following table can be consulted.

Temperature °C	**Recommended maximum horizontal deformation** µm
−5	2,5
10	5,0
15	6,5
20	7,5
25	9,0

Table 22. Recommended maximum horizontal deformation for 100 mm diameter samples as per BS EN 12697-26:2018 – Annex C

The deformation shall be measurement by monitoring the transient horizontal diametric deformation of the specimen. This can be achieved by means of linear variable differential transformers (LVDTs) mounted on both sides of the rigid frame. The LVDT shall be fastened symmetrically but not overly tight, by using a special screwdriver to apply a constant torque of 25 cNm.

A minimum of 10 conditioning pulses shall be administered to the specimen, to allow the machine to regulate the loading required to achieve the target deformation and time. After conditioning, 5 load pulses are applied and the modulus calculated as the average of the 5 pulses. The specimen shall then be rotated by (90 ± 10) ° around its horizontal axis, and the test carried out again. The mean value of this test shall be within + 10% and -20% of the average calculated for the first test. If this is valid, the mean of both tests will be calculated as the stiffness modulus of the tested specimen. Otherwise the test results are rejected.

N.2 Calculations

As stated in BS EN 12697-26:2018, the following relationship is used to calculate the stiffness modulus:

$$E = \frac{F \cdot (\nu + 0{,}27)}{(z.h)}$$

where

z *the amplitude of the resilient horizontal deformation obtained during the loading cycle (mm);*

h *average thickness of the specimen (mm);*

ν *Poisson's ratio, if unknown it can be assumed 0,35 for all test temperatures;*

E *stiffness modulus (kN/mm²);*

F *applied load from the actuator (kN).*

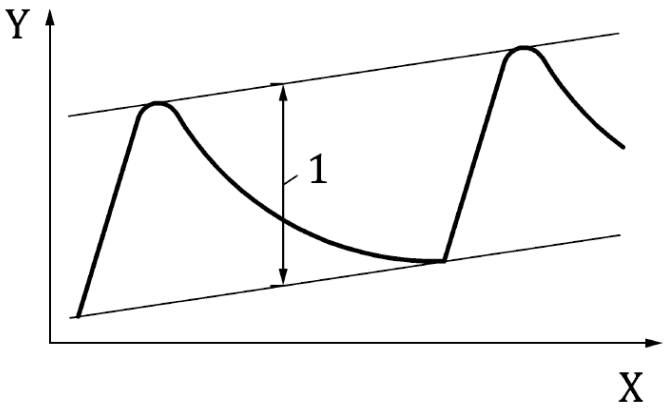

Key

X	time
Y	deformation
1	resilient deformation, z

Figure 68. The resilient deformation z, calculated from the pulse load, as per BS EN 12697-26:2018 – Annex C

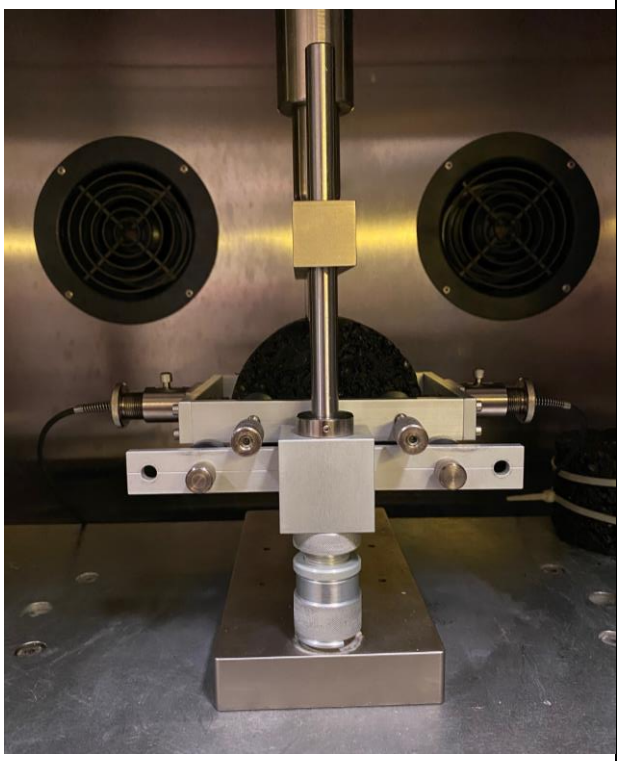

Figure 69. LVDTs, steel load-frame, and sample in testing chamber of UTM-30

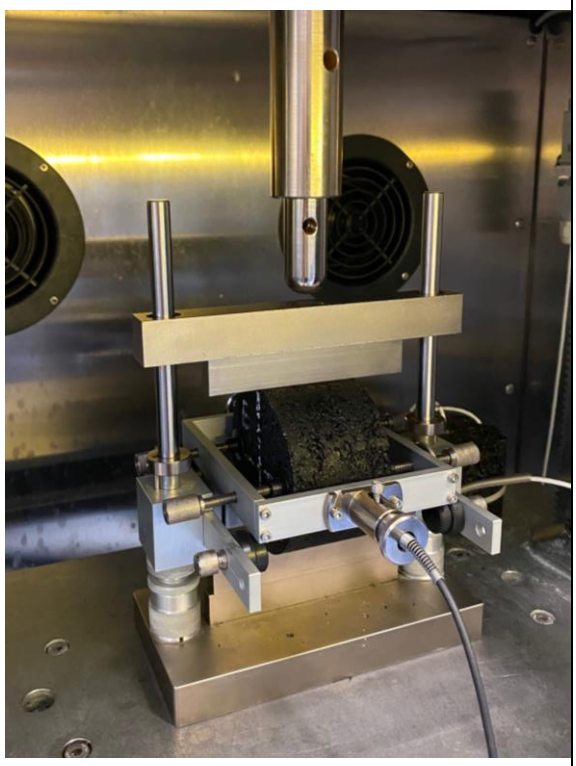

Figure 70. Loading configuration for IT-CY stiffness modulus test

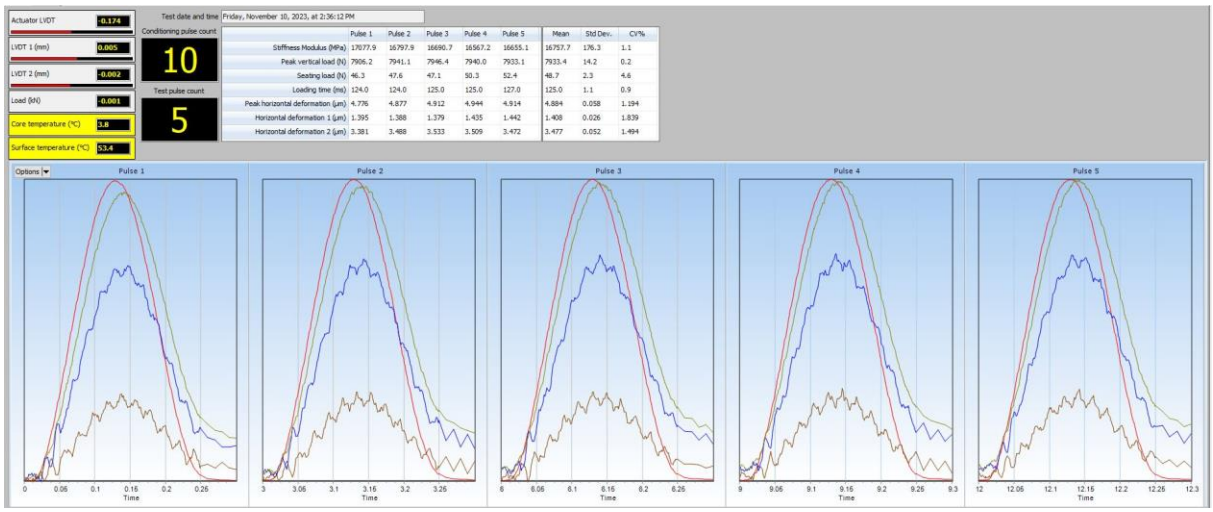

Figure 71. Sample results for the 5 load pulses and deformations produced by the testing software during ITSM IT-CY test

N.3 Results

Test Parameters	
Waveshape	Haversine
Loading time (ms)	125
Loading pulse width (ms)	250
Rest period (ms)	2750
Pulse repetition period (ms)	3000
Number of conditioning pulses	10
Target temperature (°C)	10, 20, 25, 30
Contact load (N)	50
Estimated Poisson's ratio	0,35
Target horizontal micro-strain	Variable
Target horizontal deformation (µm)	5, 7, 9, 10

Table 23. Input parameters for IT-CY test software for stiffness modulus

ITSM IT-CY **d = 100 mm**	**Stiffness Modulus test parameters**			
	Test Temperature [℃]			
	10	**20**	**25**	**30**
Target Horiz. Def. [µm]	5	7	9	10

Table 24. Target horizontal deformation used for software input for IT-CY stiffness modulus test for various temperatures, for 100 mm cylindrical specimens

ITSM IT-CY	**Mean Stiffness Modulus [Mpa] Test Temperature [℃]**				**Mean v_{real}**
Mixture	**10**	**20**	**25**	**30**	**[%]**
U24 STA	16111	7643	5233	3181	0,76
U24 LTA	17282	8947	NA	3833	0,83
U24PS0,5 STA	16169	7962	6216	3679	3,42
U24PS0,5 LTA	17594	9406	NA	4518	3,48
U24PS1 STA	15614	7283	5337	3009	2,80
U24PS1 LTA	16758	8630	NA	3963	2,67

Table 25. Mean stiffness modulus for all tested mixture specimens at various temperatures, and air void contents

Further individual results with standard deviation of tests, and graphs of stiffness modulus vs air void content are reported in Annex VI.

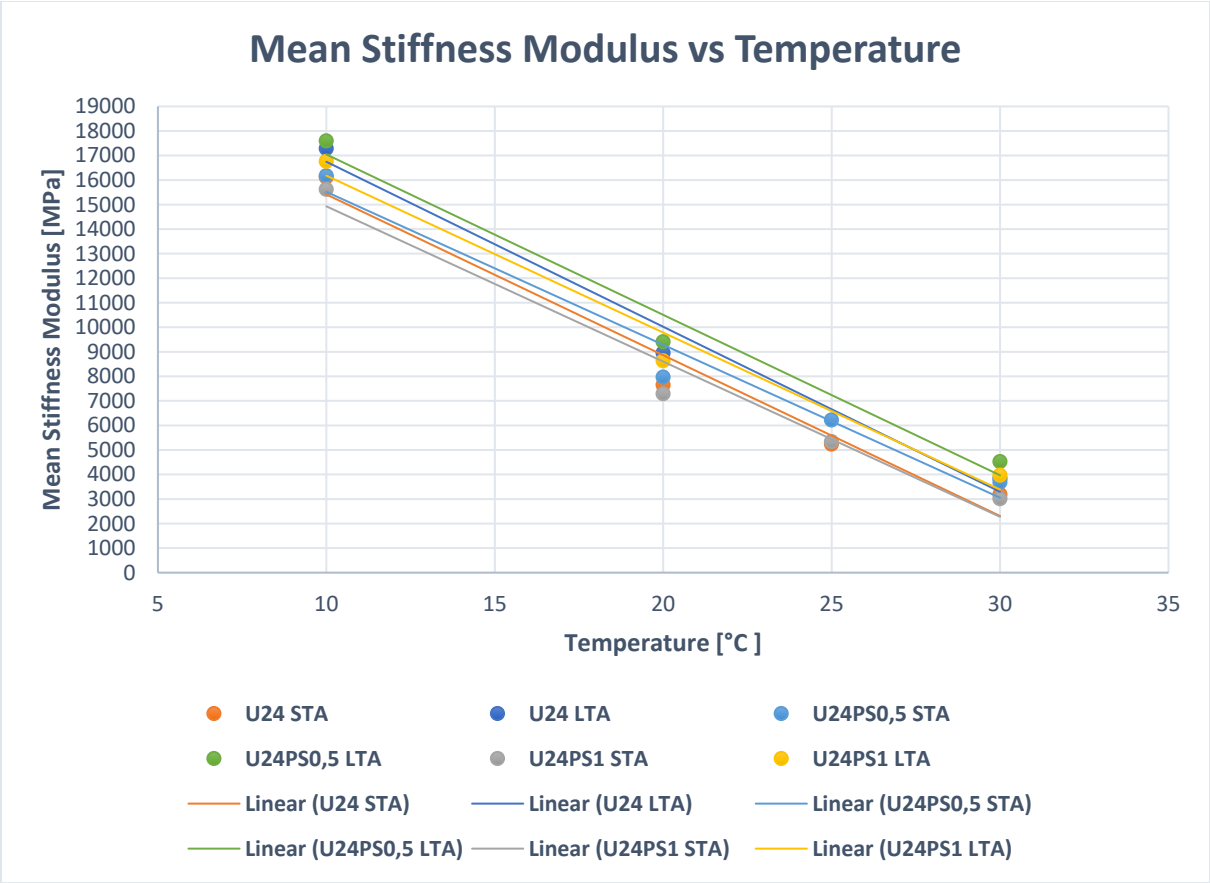

Figure 72. Test results: Mean stiffness modulus [MPa] vs Temperature [°C]

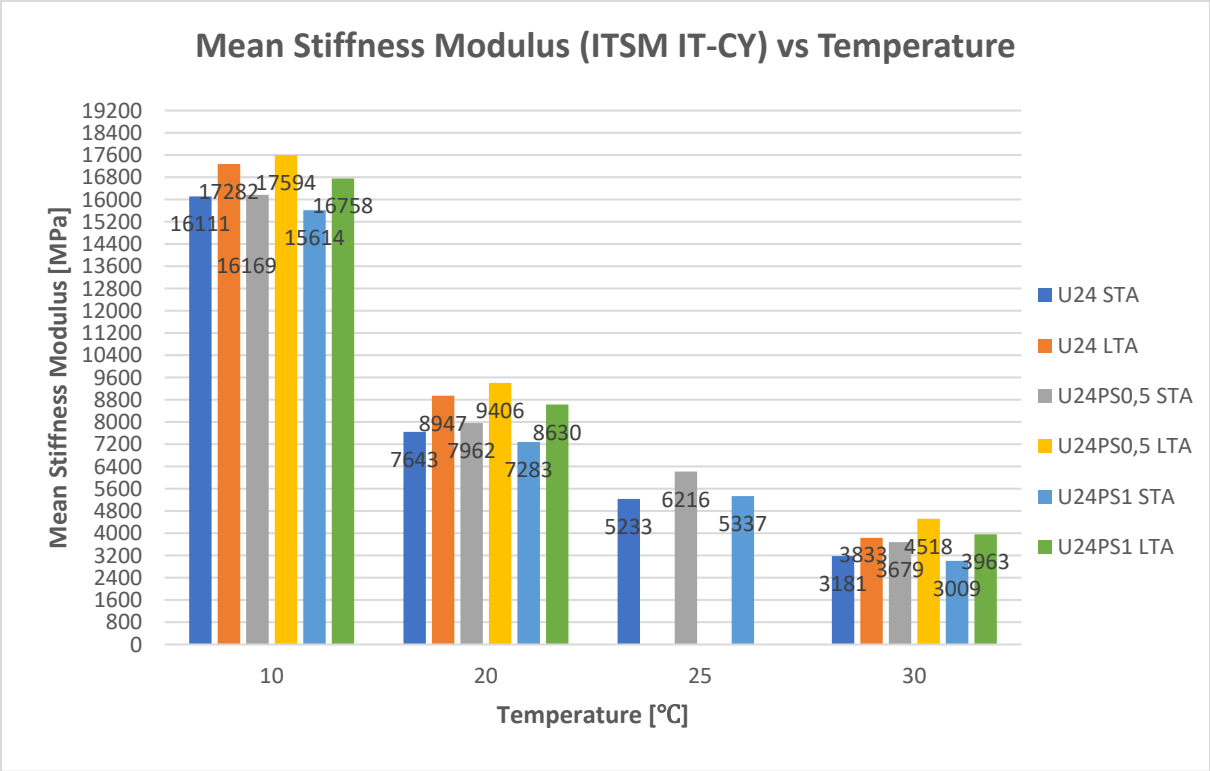

Figure 73. Test results: Mean Stiffness modulus [MPa] vs Temperature [°C]

N.4 Remarks

It is evident that the stiffness modulus for the samples proportionally decreases with increasing testing temperature as shown in Figure 72.

Even with largely increasing air void content in the mixtures with plastic shreds, the stiffness modulus value achieved by U24 is maintained for all temperatures in the mixtures with plastics. This shows the stiffening effect provided by plastic presence in the modified asphalt, which compensates the negative effects on stiffness by the increasing air void content. Thus, it can be said that the presence of plastic shreds provides improvements to the mixture stiffness performance.

The increase of the stiffness modulus in long-term aged specimens with respect to short-term aged ones, confirms that ageing of the mixtures causes stiffening. This is witnessed in the three mixtures, irrespective of the plastic shred content.

O. INDIRECT TENSILE STRENGTH

The norm BS EN 12697-23:2017 defines the Indirect tensile strength test as follows: “the indirect tensile strength test measures the maximum tensile stress calculated from the peak load applied to a cylindrical specimen loaded diametrically until break at specified test conditions. The test requires a compression testing machine, Marshall-type confirming to EN 12697-34, or similar apparatus, having a recommended minimum capacity of 28 kN and capable of applying loads to test specimens at a constant rate of deformation of (50 ± 2) mm/min after a transitory period less than 20% of the loading time. The rate of deformation shall be maintained”.

The norm requires at least three samples to conduct the test. For cylindrical specimens of 100 ± 3 mm nominal diameter, NMAS should not surpass 22 mm. The specimens shall have an age between 48 hours and 42 days from the time of their preparation. The samples shall be conditioned in a water bath or thermostatically controlled air chamber. They shall be conditioned for 4 hours at the test temperature (in this study at 25 ± 2 ˚C) in a climatic chamber. The temperature at which the test is conducted impacts the ITS value.

O.1 Procedure

The following represents the procedure to perform the ITS test, using the universal testing machine (UTM-30):

8) The specimen shall be placed below the testing piston in the apparatus (See Figure 74), at room temperature (15 to 25 ˚C);
9) The testing head and the loading strip should be aligned in order to guarantee diametrical loading;
10) The test shall be started by loading the specimen compressively and continuously at a constant deformation speed of 50 ± 2 mm/min after a transitory period less than 20% of the loading time;
11) The peak load reached shall be recorded, and the loading shall continue until the failure (break) of the specimen. The type of failure should be recorded (see Figure 75);
12) The ITS shall be Calculated in kPa.

In the case of wet ITS tests, the specimens were conditioned in a water bath inside a thermostatically controlled climatic chamber at 25 ± 2 ˚C for 7 days (refer to Figure 83), 14 days after compaction. This alternative conditioning methodology substitutes the one outlined in BS EN 12697-12:2018 and AASHTO T 283, due to absence of the necessary equipment.

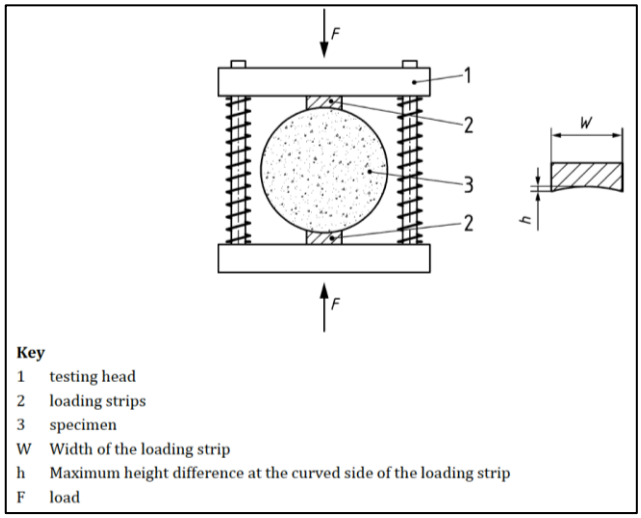

Figure 74. Loading configuration & apparatus for ITS test [EN 12697-23:2017 (E)]

The failure modes are described in BS EN 12697-23:2017 (E) and Figure 75 as follows:

a) Clear tensile break: the specimen is clearly broken along a diametrical line, except perhaps for small triangular sections close to the loading strips;
b) Deformation: specimens without a clearly visible tensile break line;
c) Combination: specimens with a limited tensile break line and larger deformed areas close to the loading strips.

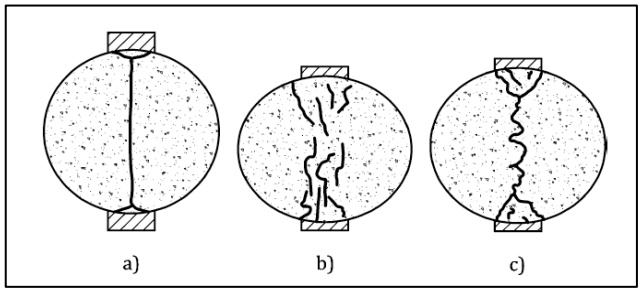

Figure 75. Types of Failure modes of cylindrical specimens under ITS testing [EN 12697-23:2017 (E)]

O.2 Calculations

As stated in BS EN 12697-23:2017 (E), the ITS is calculated as follows:

$$ITS = \frac{2P}{\pi\, D\, H} \times 1000$$

The average of three tests shall be computed.

where

ITS *is the indirect tensile strength in kPa;*
P *is the peak Load in N;*
D *is the diameter of the specimen in mm;*
H *is the height of the specimen in mm.*

The values are accepted if the difference in the ITS of the single test specimens is less than 17% of the average.

The water sensitivity is determined by the ratio of the ITS in wet conditions to the dry conditions, as described by method A in chapter 5 of BS EN 12697-12:2018. The indirect tensile strength ratio (ITSR) is calculated as follows:

$$ITSR = 100 \times \frac{ITS_w}{ITS_d}$$

where

ITSR *is the indirect tensile strength ratio in (%);*

ITS_w *is the average indirect tensile strength of the wet samples in (kPa);*

ITS_d *is the average indirect tensile strength of the dry samples in (kPa).*

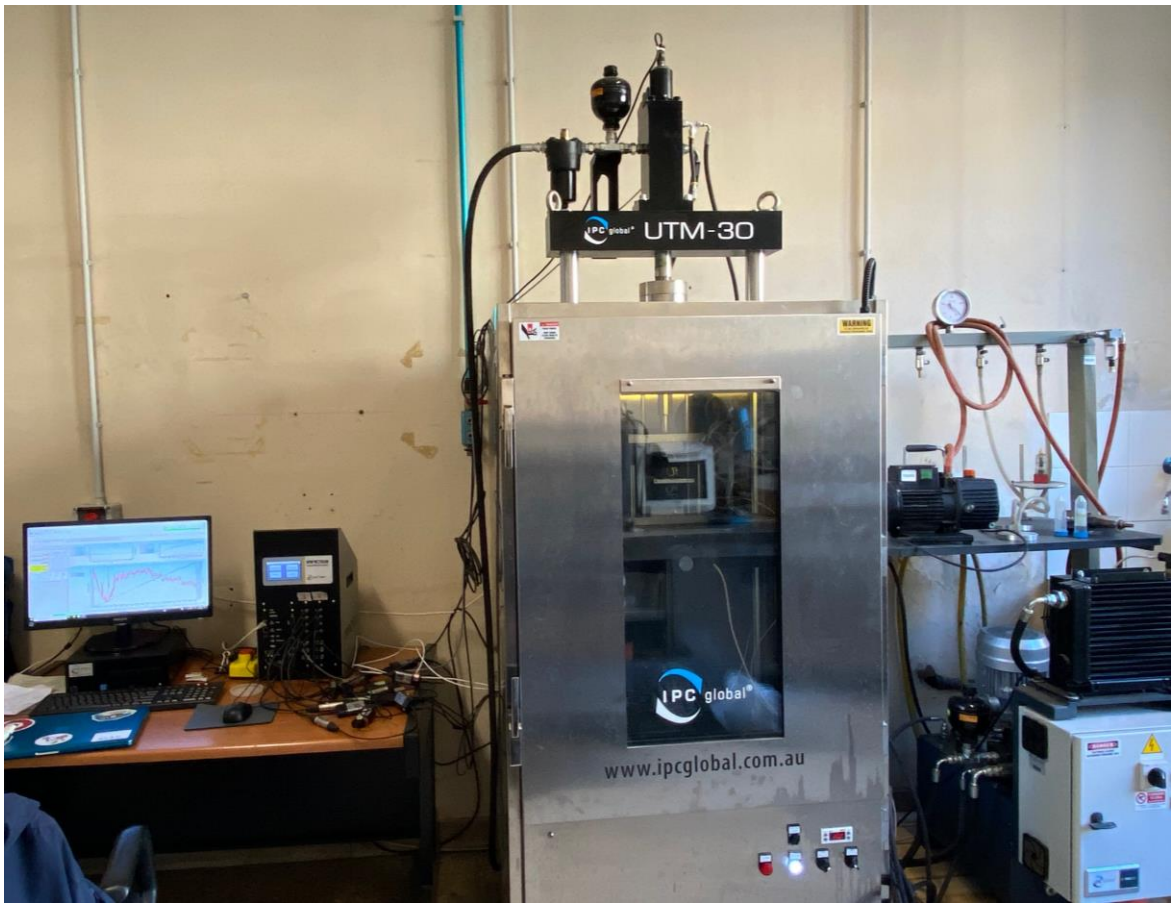

Figure 76. UTM-30 climate controlled testing chamber used for ITS tests, ITSM & CIT-CY tests (see chapter N. & Chapter P.)

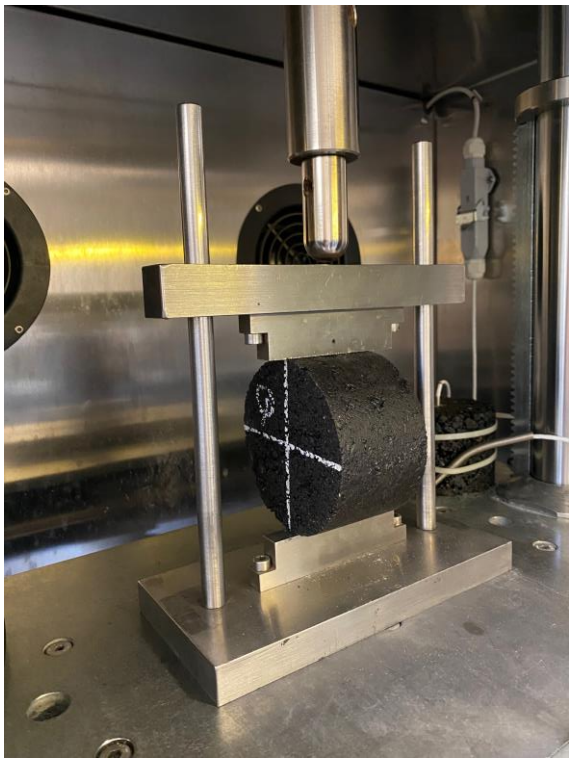

Figure 77. Specimen loading configuration in UTM-30

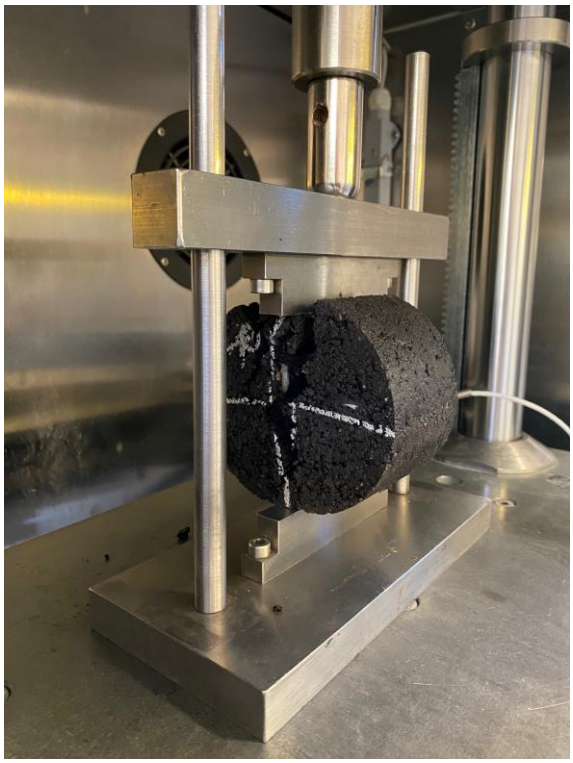

Figure 78. Failure of ITS Test specimen

Figure 79. Failed ITS test Specimen. It is evident that the failure line is symmetrical and runs diametrically

Figure 80. The failure mode represents a limited tensile break line and larger deformed areas close to the loading strips

Figure 81. ITS (dry) failure interface of specimen U24I

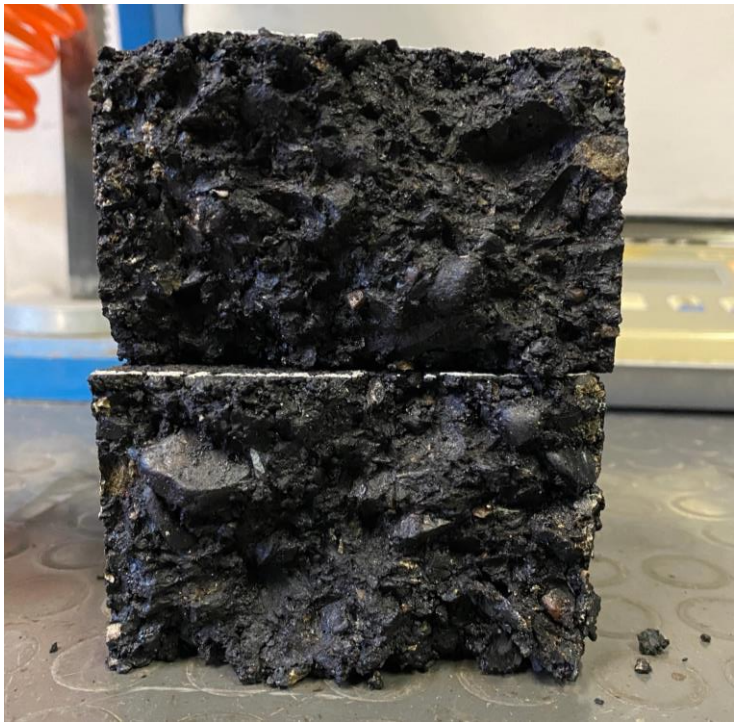

Figure 82. ITS (wet) failure interface of specimen U24PS0,5R

Figure 83. Conditioning of specimens in water at 25 degrees Celsius in a thermostatically controlled climatic chamber for ITS wet tests

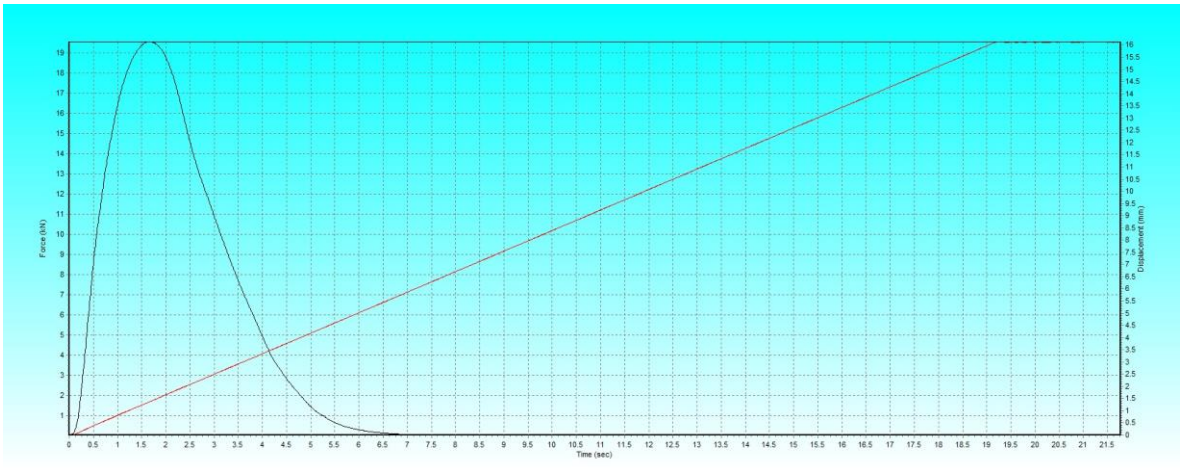

Figure 84. Exemplary results of the loading & displacement vs time diagram produced in UTS-30 software interface

O.3 Results

The ITS test was carried out at 25 ± 2 ˚C, for specimens produced by the gyratory shear compactor, having an equal age of at least 14 days. Additionally, prior to sample conditioning and performing the ITS tests, the Indirect tensile stiffness modulus (refer to chapter N.) at testing temperature was determined for the sake of having a better understanding of the mechanical properties of the samples. After the breaking of samples, the ITS ratio for wet and dry results was calculated to assess the water sensitivity of the mixture samples.

The results were obtained from 3 dry and 3 wet batch specimens for each of the three mixtures. The samples were compacted from the same lot and on the same day to ensure conformity. The samples chosen per batch displayed similar volumetric properties (air voids, bulk density, and height).

	Void Content	Stiffness Modulus - Dry	ITS Dry	Stiffness Modulus - Wet	ITS Wet	ITSR
			mean values for tested samples			
	[%]	[MPa]	[MPa]	[MPa]	[MPa]	[%]
U24	0,57	4983	**2,022**	5484	**2,155**	**106,6**
U24PS0,5	3,21	6056	**2,001**	6377	**2,127**	**106,3**
U24PS1	2,69	5478	**1,839**	5195	**2,060**	**112,0**

Table 26. Results summary of ITS wet and dry tests for the three mixtures

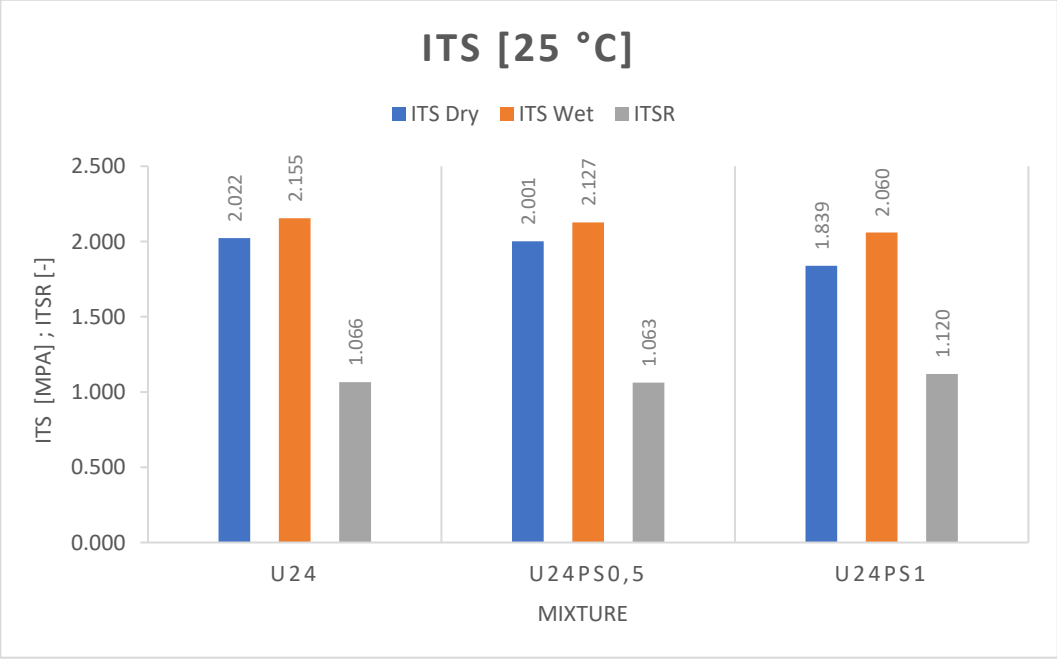

Figure 85. ITS wet and dry test results and ITSR for the three mixtures

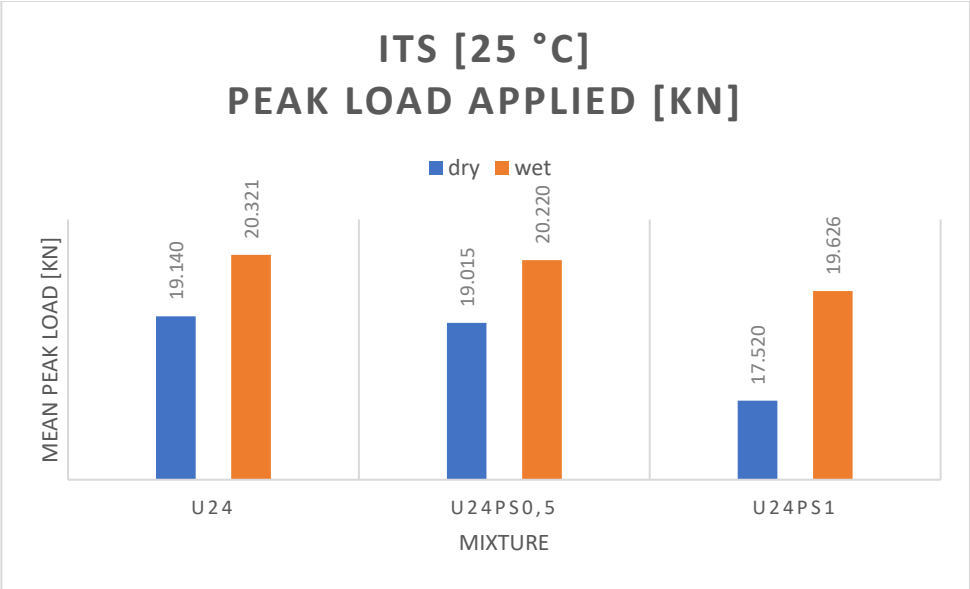

Figure 86. ITS wet and dry test results of the peak load for the three mixtures

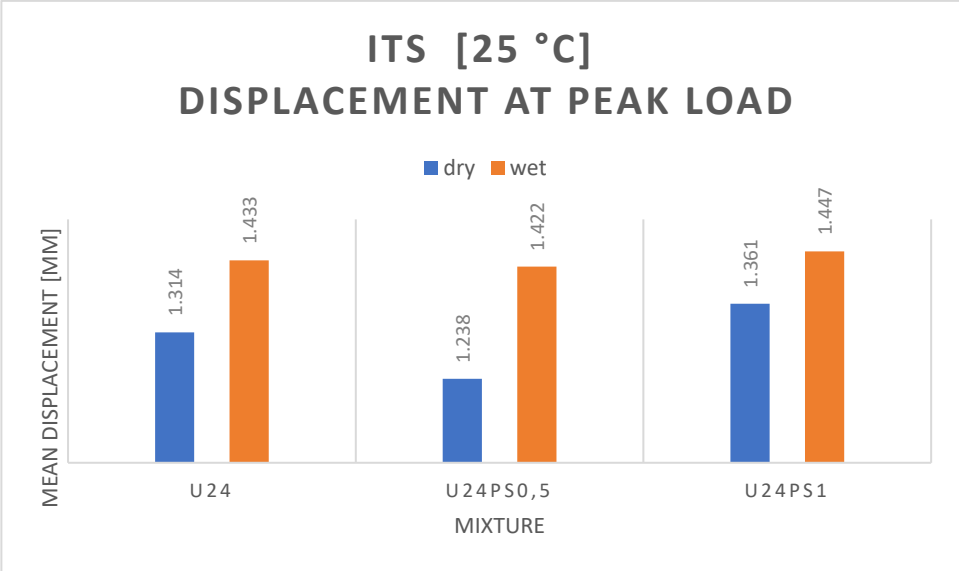

Figure 87. ITS wet and dry test results of the displacement at the peak load for the three mixtures

Further results and graphs of ITS tests are reported in Annex VII.

O.4 Remarks

The results indicate no effect of water on the mixtures, where the ITSR value varies for individual specimens from 100% to 112%. Therefore, it can be concluded that the material is resistant to water wearing effects. All three mixtures have relatively low air void content, thus permitting less infiltration of water. Across the three mixtures, the increase of air void content is associated with the decrease of the ITS value for dry and wet samples, however in a non-linear manner. Having higher void content and ITSM, the mixture containing 0,5% plastic shreds displays a higher dry and wet ITS value than those of 1% plastics, however less than those with no plastics. Moreover, by visual inspection of the broken dry and wet samples across the three mixtures, the failure surface does not demonstrate substantial bitumen film stripping, nor broken aggregates, as all were mostly intact (see Figure 81 and Figure 82). Generally, the break lines were diametrical and symmetric (see Figure 80), revealing a clear tensile break failure mode (mode a).

As specified in Table 27 below from *Linee guida per la costruzione e manutenzione delle pavimentazioni stradali* (Consiglio Superiore dei Lavori Pubblici, 2022), the ITS results obtained surpass the upper limits of the requirements for modified binders. Whereas the ITSR value is above the minimum threshold.

Nel caso di conglomerati bituminosi di tipo chiuso (AC), a meno di specifiche esigenze progettuali supportate da opportuni studi di carattere sperimentale, la miscela di progetto deve rispettare le specifiche tecniche indicate nella Tabella 6.10.

Tabella 6.10.

Parametro	Normativa di riferimento	Unità di misura	Valori richiesti		
V_m a 10 rotazioni	UNI EN 12697-8	%	11-15		
V_m a 100 rotazioni	UNI EN 12697-8	%	3-6		
V_m a 180 rotazioni	UNI EN 12697-8	%	≥ 2		
			Base	Binder	Usura
Resistenza a trazione indiretta a 25°C a 100 rotazioni (*ITS*)	UNI EN 12697-23	N/mm²	0,95-1,65[a] 1,10 -1,75[b]	0,85-1,55[a] 0,95-1,65[b]	0,75-1,45[a] 0,85-1,55[b]
Coefficiente di trazione indiretta a 25°C a 100 rotazioni (*CTI*) c	-	-	≥ 70[a] ≥ 80[b]	≥ 0,70[a] ≥ 0,80[b]	≥ 65[a] ≥ 75[b]
Sensibilità all'acqua (*ITSR*)	UNI EN 12697-12	%	≥ 80[a] ≥ 90[b]	≥ 80[a] ≥ 90[b]	≥ 80[a] ≥ 90[b]

(a) Conglomerati prodotti con bitume normale

(b) Conglomerati prodotti con bitume modificato o polimeri di addizione

Table 27. Performance requirements for wearing course and AC12 aggregates (Consiglio Superiore dei Lavori Pubblici, 2022)

P. CIT-CY FATIGUE PERFORMANCE TEST

The fatigue performance of HMA mixtures is an important structural indicator to their resistance to cracking, especially during the long-term road service life. Fatigue is defined by BS EN 12697-24:2018 as 'the reduction of strength of a material under repeated loading when compared to the strength under a single load'. This is relevant to understand the effects of plastic shreds in the studied mixtures in this study. The test will be carried on STA & LTA specimens aged between 14 and 42 days since their production, at a conditioning and test temperature of 20 °C.

The cyclic indirect tensile test on cylindrical shaped specimens (CIT-CY) was carried out as per the standard BS EN 12697-24:2018 – Annex F. The specimens are subjected to cyclic compressive load (sinusoidal) in the vertical plane, without rest periods. A resulting uniform tensile stress develops orthogonally along the direction of loading, causing the cylinder to fail by central splitting along the diameter. Generally, several failure criterions exist to evaluate the fatigue life of tested specimen, and results achieved are different depending on the chosen criteria. Usually the number of load cycles corresponding to when the initial complex stiffness modulus (typically after 100 load cycles) decreases by half its initial value is considered as the conventional failure criterion. In this study, the energy ratio criteria based on the dissipated energy concept was applied. Additionally, the fatigue life was assessed also at the cycles of specimen breaking, as a further comparison with the energy ratio criteria. The fatigue line can generally be assessed and plotted in a bi-logarithmic plane using the following relationship between the horizontal strain amplitude (ε_t) and number of cycles to fracture life (N_f): $\varepsilon_t = a \cdot N_f^b$, where a & b are mixture-specific parameters obtained.

The CIT-CY test using the UTM-30 machine is only executable in stress-controlled mode, which regulates the selected applied force and monitors the resulting deformation in the specimen. This method evaluates the performance of the mixture under cyclic indirect tensile load. The response of the bituminous mixtures will be of interest to understand the benefits or drawbacks brought about by the plastic shreds added in comparison to the normal HMA control mixture.

The frequency of the load application adopted in CIT-CY tests is 10 Hz, which simulate a vehicle speed of circa 80 km/h (50 mph) (Aragao et al., 2008; Huang, 2004). Regularly, fatigue damage ensues at moderate service temperatures (Huang, 2004), and therefore, it would be representative to test samples for fatigue performance at 20 °C (Aragao et al., 2008).

P.1 Procedure

For each loading conditions (stress amplitude, temperature, frequency), at least 3 specimens shall be tested, excluding an additional specimen used to estimate the loading parameters. In this study, a trial specimen was used to understand the material response and adjust the three applied stress amplitude levels for fatigue testing (see Table 31 for stress levels). The test envisages an application of a lower load level of 0,035 MPa. The test was conducted at loading of 10 Hz and 20 °C for specimens conditioned for at least 4 hours, and of 100 mm diameter and 60 mm height (see Table 28). In this study, only 2 repetitions were carried out for every stress level. The stress levels chosen guaranteed that the initial horizontal strain amplitudes ($\boldsymbol{\varepsilon_{a0}}$) in the specimen centre were all within the range of 25 µm/m to 100 µm/m. The fatigue life of the tested specimens must be between 10^3 and 10^6 load cycles. The loading stress levels chosen allowed to obtain failure in three ranges: [1000 to 10.000],

[10.000 to 100.000], and [100.000 to 1.000.000] loading cycles. This allowed a better representation of the fatigue line based on results that are well-distanced in loading level and number of failure cycles.

Prior to testing, specimens were stored on a flat surface for at least 14 days after compaction, at room temperature (around 20 °C), and allowed to develop stiffness (influenced by the storage time).

Table F.1 — Specimen dimensions

Maximum grain size mm	**Specimen diameter** Ω mm	**Specimen height** h mm
≤ 16	100 ± 3	40 ± 2
> 16 to < 32	150 ± 3	60 ± 2
≥ 32	150 ± 3	90 ± 2

Table 28. Specimen dimensions as a function of NMAS as per BS EN 12697-24:2018

P.2 Calculations

As stated in BS EN 12697-24:2018, the CIT-CY fatigue test calculations are as follows:

The vertical force applied is a controlled harmonic sinusoidal loading without any rest periods, according to the following formula:

$$F_t = F_m + F_a sin(2 \cdot \pi \cdot f \cdot t)$$

$$F_m = F_l + F_a$$

where

F_m *medium vertical force (kN);*
F_l *the lower vertical force (kN) of 35 kPa;*
F_a *vertical force amplitude force (kN);*
f *load frequency (Hz);*
t *test time (s).*

The parameters F_m, F_a, and F_l are determined by regression analysis (curve fitting) regarding the measured force values during the recorded interval.

The vertical load results in a horizontal stress, of a maximum value in the centre of the specimen as expressed in the following equation:

$$\sigma_a = \frac{2 \cdot F_a}{\pi \cdot h \cdot \Omega}$$

where

σ_a *amplitude of the horizontal tensile stress in the middle of the specimen (MPa)*
F_a *vertical amplitude force (kN);*
h *average specimen thickness (mm);*
Ω *specimen diameter (mm).*

The horizontal deformation parameters u_m, u_a, and u_d are obtained by regression analysis (curve fitting) of the following formula:

$$u(t) = u_m + u_a \cdot sin(2 \cdot \pi \cdot f \cdot t + \varphi) + u_d \cdot t$$

where

u_m *mean horizontal displacement (mm);*
u_a *horizontal displacement amplitude (mm);*
u_d *horizontal displacement rate (represents viscoplastic deflections) (mm/s);*
f *load frequency (Hz);*
t *test time (s);*
φ phase angle between vertical force and horizontal displacement function (degrees).

From the above, the maximum stress amplitude and lower stress level at the specimen centre can be calculated. The maximum initial tensile strain amplitude and the strain difference can be calculated by the following equations:

$$\varepsilon_a = (\frac{2 \cdot u_a}{\Omega}) \cdot \left[\frac{1 + 3\nu}{4 + \pi \cdot \nu - \pi}\right] \cdot 10^6$$

and

$$\Delta\varepsilon = 2 \cdot \varepsilon_a$$

where

ε_a *maximum horizontal strain amplitude in the middle of the specimen (mm/m)*
u_a *horizontal displacement amplitude (mm);*
ν *Poisson ratio = 0,35 (-);*
Ω *specimen diameter (mm);*
$\Delta\varepsilon$ *maximum strain difference in the middle of the specimen (mm/m).*

The specimen stiffness modulus at intervals can be determined as follows:

$$S_{mix,n} = \frac{\sigma_a}{\varepsilon_a} \cdot (1 + 3\nu) \cdot 10^6$$

where

n *load cycle number representing the recorded interval (-);*

$S_{mix,n}$ *stiffness modulus for load interval n (MPa);*

ε_a *maximum horizontal strain amplitude in the middle of the specimen (mm/m);*

ν *Poisson ratio = 0,35 (-);*

σ_a *amplitude of the horizontal tensile stress in the middle of the specimen (MPa).*

The energy ratio recorded at intervals is calculated as follows:

$$ER(n) = n \cdot S_{mix,n}$$

where

$ER(n)$ *energy ratio for load interval represented by load cycle number n (-).*

The fracture life is determined according to the energy dissipation method: the fracture life is calculated from the relationship between the load cycle number and energy ratio. The fracture life is at the maximum energy ratio, as shown in Figure 88.

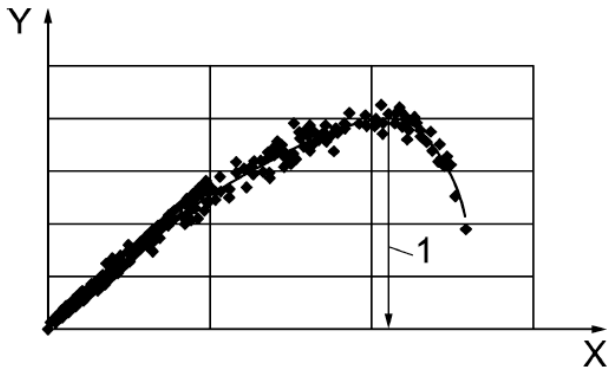

Key

Y energy ratio

X number of load cycles

1 fracture life

Figure 88. Energy ratio vs cycle number, maximum is the fracture life, BS EN 12697-24:2018

The fatigue line can be determined from the CIT-CY test results for the specimens using the least-square regression relationship which fits data of the logarithm of the tensile strain difference as an independent variable and the data of the logarithm of the fracture life as a dependent variable as shown below:

$$\lg(N_{f,w}) = \lg(k_\varepsilon) + n_\varepsilon \cdot \lg(\Delta\varepsilon)$$

$$N_{f,w} = k_\varepsilon \cdot (\frac{1}{\Delta\varepsilon})^{n_\varepsilon}$$

where

$N_{f,w}$ number of load cycles until fracture life according to the energy ratio criterion (-);

$\Delta\varepsilon$ *maximum strain difference in the middle of the specimen (mm/m);*

k_ε material constants of the fatigue function (-);

n_ε material constants of the fatigue function (-).

Figure 89. Climatic chamber for specimen conditioning

Figure 90. Steel apparatus to glue metal strips for LVDT clamping during tests

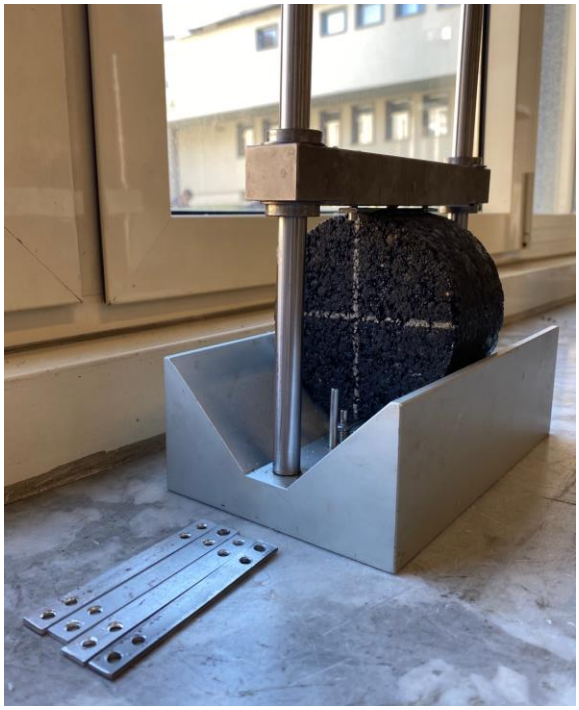

Figure 91. Metal strip gluing for LVDTs

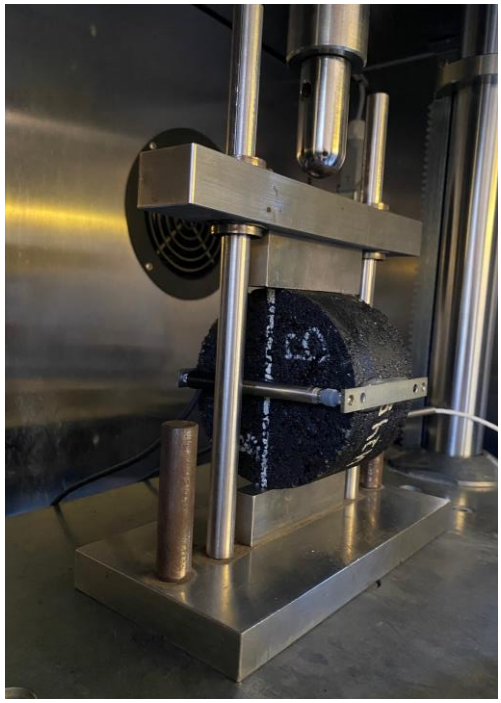

Figure 92. CIT-CY steel loading frame, LVDTs, and force actuator in UTM-30

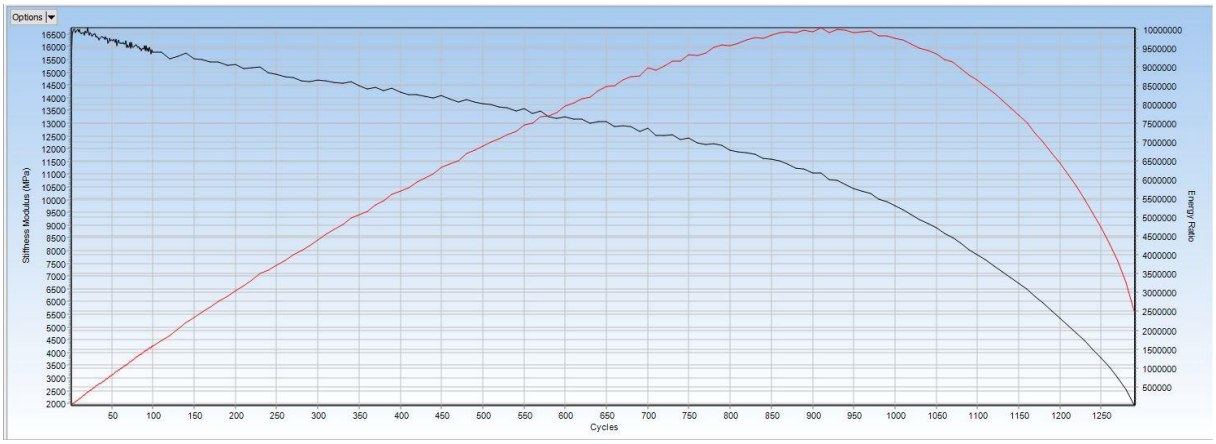

Figure 93. Trial sample fatigue curve produced by the testing software: stiffness modulus [MPa] and energy ratio [-] vs load cycle number [-]. Failure in the range of [1000 to 2000] cycles.

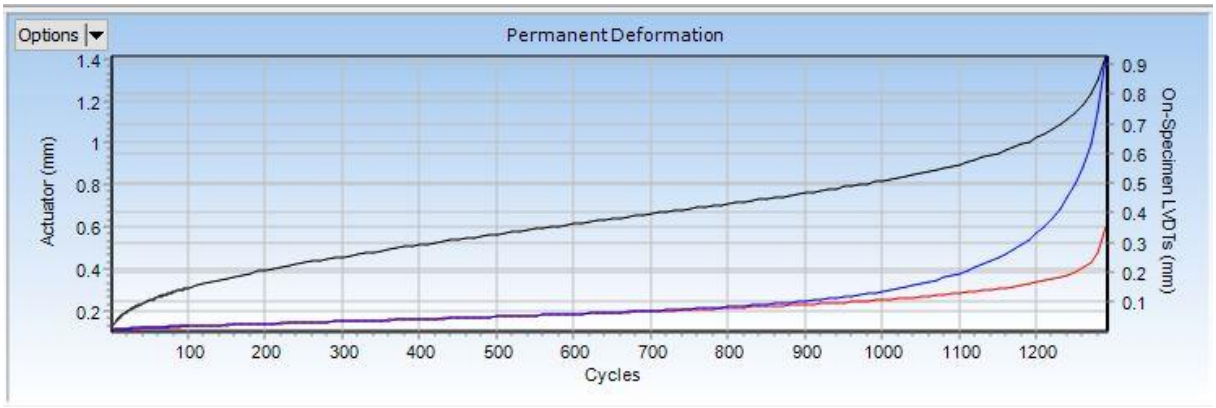

Figure 94. Trial sample fatigue curve for tested mixtures produced by the testing software: LVDT deformation amplitudes [µm/m] vs load cycle number [-]. Failure in the range of [1000 to 2000] cycles.

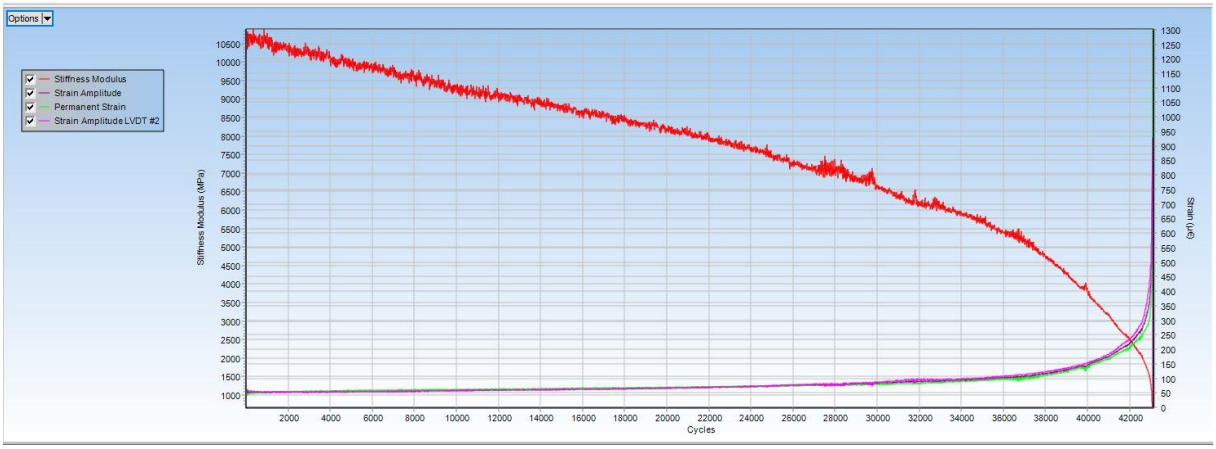

Figure 95. Specimen fatigue curve for tested mixtures produced by the testing software: stiffness modulus [MPa] and LVDT deformation amplitudes [µm/m] vs load cycle number [-]. Failure in the range of [42000 to 44000] cycles.

Figure 96. Broken CIT-CY fatigue specimens

Figure 97. Broken CIT-CY fatigue specimens. Clear symmetrical splitting line along the centreline

Figure 98. Broken CIT-CY fatigue specimens. No plastics visible along the splitting line, nor broken aggregates

Figure 99. Broken CIT-CY fatigue specimen batch for this study

P.3 Results

The following test results are presented:

- A graphical and mathematical representation of the fatigue line as well as the regression parameters k_ε and n_ε;
- The strain amplitude **ε**6 (μm/m) corresponding to a fatigue life of 10^6 cycles for the energy ratio failure criteria, as well as the sample break cycle criteria;
- The correlation coefficient, R^2;
- The number of load cycles $N_{f,w}(10\ \mu\mathrm{m/m})$ and $N_{f,w}(100\ \mu\mathrm{m/m})$ for strain differences $10\ \mu\mathrm{m/m}$ and $100\ \mu\mathrm{m/m}$.

Mixture	ε6 (μm/m)	CIT-CY Fatigue Equation	R^2 (-)	a	b	Avg. void cont. (%)	k_e	n_e	Avg. Stiffness Mod. [Mpa]
***Energy Ratio failure criteria**; Test temperature at 20 °C ± 0,5; Loading frequency 10 Hz; Specimen conditioning for 12 Hours; 60 ± 2 mm height & 100 mm diameter; Wearing Course*									
U24	26,7	$y = 540{,}467x^{-0{,}218}$	0,978	540,467	-0,218	0,73	3,527E+12	4,591	7643
U24 LTA	26,3	$y = 537{,}492x^{-0{,}218}$	0,975	537,492	-0,218	0,83	3,160E+12	4,578	8947
U24PS0,5	25,3	$y = 547{,}698x^{-0{,}223}$	0,976	547,698	-0,223	3,60	2,003E+12	4,492	7962
U24PS0,5 LTA	26,4	$y = 378{,}282x^{-0{,}193}$	0,984	378,282	-0,193	3,48	2,408E+13	5,191	9407
U24PS1	21,6	$y = 688{,}349x^{-0{,}251}$	0,992	688,349	-0,251	2,89	2,120E+11	3,991	7179
U24PS1 LTA	24,6	$y = 552{,}693x^{-0{,}225}$	0,998	552,69	-0,225	2,67	1,519E+12	4,442	8775

*Table 29. Specimen fatigue line functions, **ε**6 (μm/m), correlation coefficient, regression parameters and material properties – Energy ratio failure criteria*

Mixture	ε6 (μm/m)	CIT-CY Fatigue Equation	R^2 (-)	a	b	Avg. void cont. (%)	k_e	n_e	Avg. Stiffness Mod. [Mpa]
***Sample break failure criteria;** Test temperature at 20 °C ± 0,5; Loading frequency 10 Hz; Specimen conditioning for 12 Hours; 60 ± 2 mm height & 100 mm diameter; Wearing Course*									
U24	28,0	$y = 603{,}128x^{-0{,}222}$	0,981	603,138	-0,222	0,73	3,345E+12	4,505	7643
U24 LTA	26,9	$y = 614{,}253x^{-0{,}226}$	0,983	614,253	-0,226	0,83	2,177E+12	4,425	8947
U24PS0,5	26,9	$y = 596{,}280x^{-0{,}224}$	0,976	596,280	-0,224	3,60	2,457E+12	4,464	7962
U24PS0,5 LTA	28,1	$y = 422{,}200x^{-0{,}196}$	0,984	422,200	-0,196	3,48	2,486E+13	5,102	9407
U24PS1	23,2	$y = 741{,}990x^{-0{,}251}$	0,994	741,99	-0,251	2,89	2,728E+11	3,984	7179
U24PS1 LTA	26,6	$y = 572{,}001x^{-0{,}222}$	0,998	572,001	-0,222	2,67	2,635E+12	4,505	8775

*Table 30. Specimen fatigue line functions, **ε**6 (μm/m), correlation coefficient, regression parameters and material properties – Sample break failure criteria*

The following results use the Energy ratio failure criteria only. Further results for the sample breaking cycles criteria were also assessed for comparative purposes. They are presented in Annex VIII.

Fatigue CIT-CY	Mean stress level [kPa] applied to specimens		
	1	2	3
STA	175	270	440
LTA	215	300	475

Table 31. Applied stress levels for CIT-CY specimens

Fatigue CIT-CY	Stress level [kPa] applied to specimens (2 repetitions per level)			
	1	2	3	Trial level
U24	175	270	440	350
Mean εa_0 (µm/m)	32,6	50,8	89,8	68,4
Mean N_f	475075	35500	4815	13010
U24 LTA	215	300	475	
Mean εa_0 (µm/m)	40,7	55,6	99,2	/
Mean N_f	133070	33980	2335	/

Fatigue CIT-CY	Stress level [kPa] applied to specimens (2 repetitions per level)			
	1	2	3	Trial level
U24PS0,5	175	270	440	430
Mean εa_0 (µm/m)	38,6	53,1	87,9	84,8
Mean N_f	131610	44285	3900	3660
U24PS0,5 LTA	215	300	475	
Mean εa_0 (µm/m)	36,15	55,0	81,7	/
Mean N_f	185470	25260	2720	/

Fatigue CIT-CY	Stress level [kPa] applied to specimens (2 repetitions per level)			
	1	2	3	Trial level
U24PS1	175	270	440	440
Mean εa_0 (µm/m)	31,8	52,6	92,35	105,7*
Mean N_f	224585	26055	3330	2140
U24PS1 LTA	215	300	475	
Mean εa_0 (µm/m)	39,7	60,4	87,8	/
Mean N_f	120290	18840	3565	/

Table 32. Mean initial strain amplitude and failure cycles at the tested stress levels for the specimens of the three mixtures using the energy ratio criteria

**Value in red exceeds the initial strain limits, and was not included in the result analysis*

	ε6 (µm/m)		
Mixture	**Energy Ratio**	**Sample Break**	*Variation [%]*
U24	26,7	28,0	4,9
U24 LTA	26,3	26,9	2,3
U24PS0,5	25,3	26,9	6,3
U24PS0,5 LTA	26,4	28,1	6,4
U24PS1	21,6	23,2	7,4
U24PS1 LTA	24,6	26,6	8,1

*Table 33. The strain amplitude **ε**6 (µm/m) corresponding to a fatigue life of 10^6 cycles applying both failure criteria: energy ratio and sample break for failure cycles number*

	$N_{f,w}$ (ε)			
	ε = 5 µm/m (Δε = 10 µm/m)		**ε = 50 µm/m (Δε = 100 µm/m)**	
Mixture/Failure criteria	Energy ratio	Sample break	Energy ratio	Sample break
U24	2,18E+09	2,38E+09	55903	74367
U24 LTA	1,99E+09	1,76E+09	52699	66108
U24PS0,5	1,45E+09	1,86E+09	46764	63932
U24PS0,5 LTA	5,67E+09	6,75E+09	36501	53369
U24PS1	3,44E+08	4,48E+08	35136	46456
U24PS1 LTA	1,19E+09	1,87E+09	43125	58572

Table 34. The number of load cycles $N_{f,w}(10\ \mu m/m)$ and $N_{f,w}(100\ \mu m/m)$ for strain differences $10\ \mu m/m$ and $100\ \mu m/m$ applying both failure criteria: energy ratio and sample break for failure cycles number.

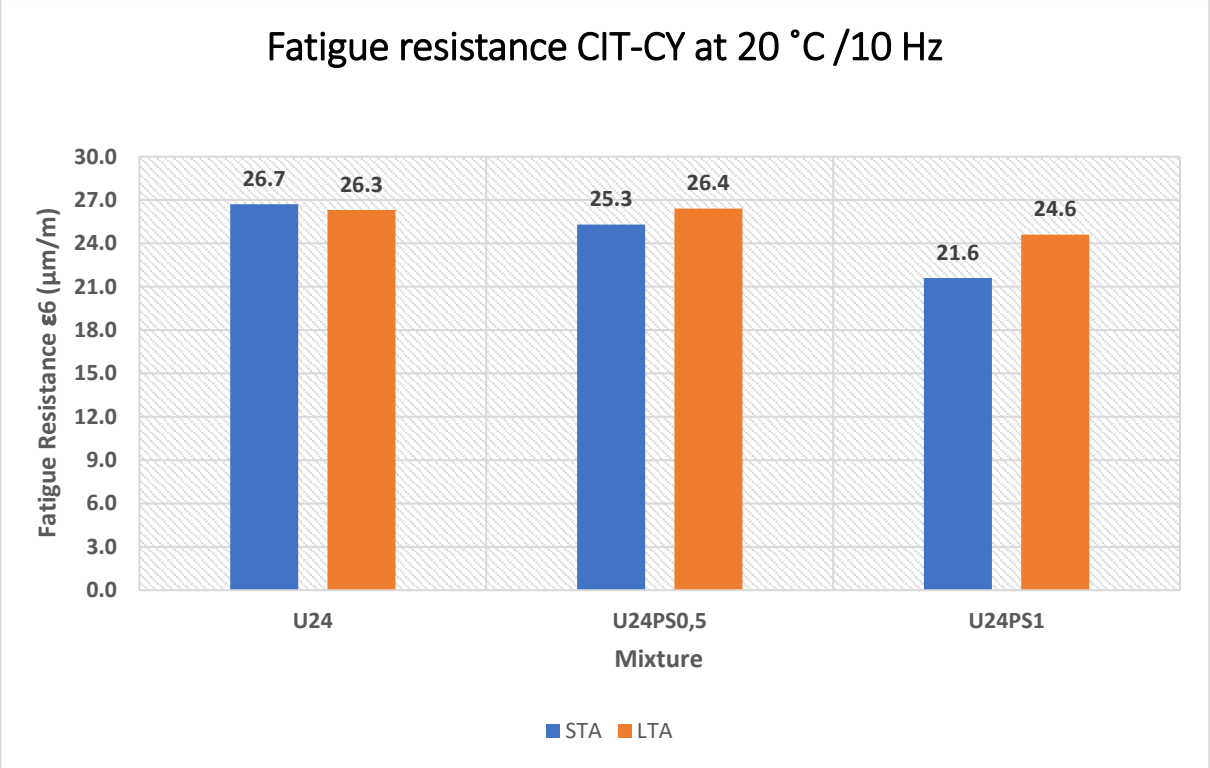

Figure 100. Fatigue resistance results: strain amplitude ε6 (µm/m) for the three mixtures using energy ratio failure criteria

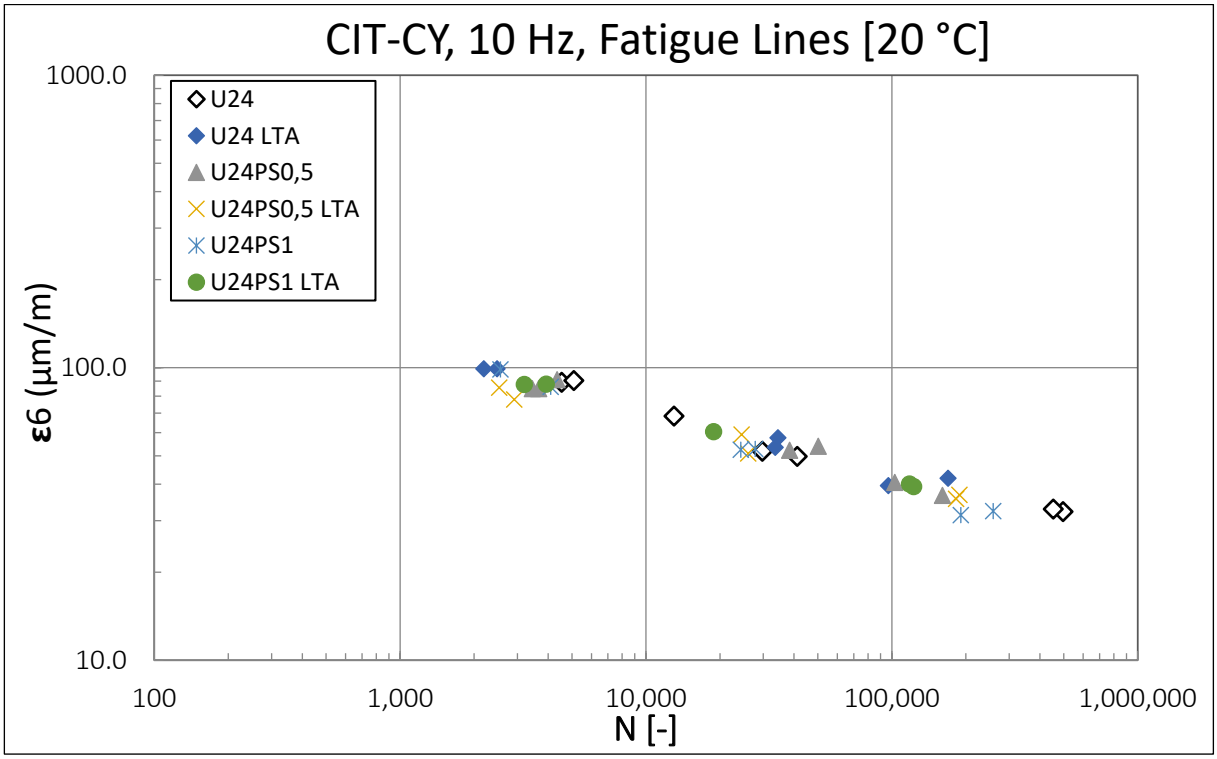

Figure 101. Fatigue lines: strain amplitude ε6 (µm/m) vs load cycles at failure using energy ratio failure criteria

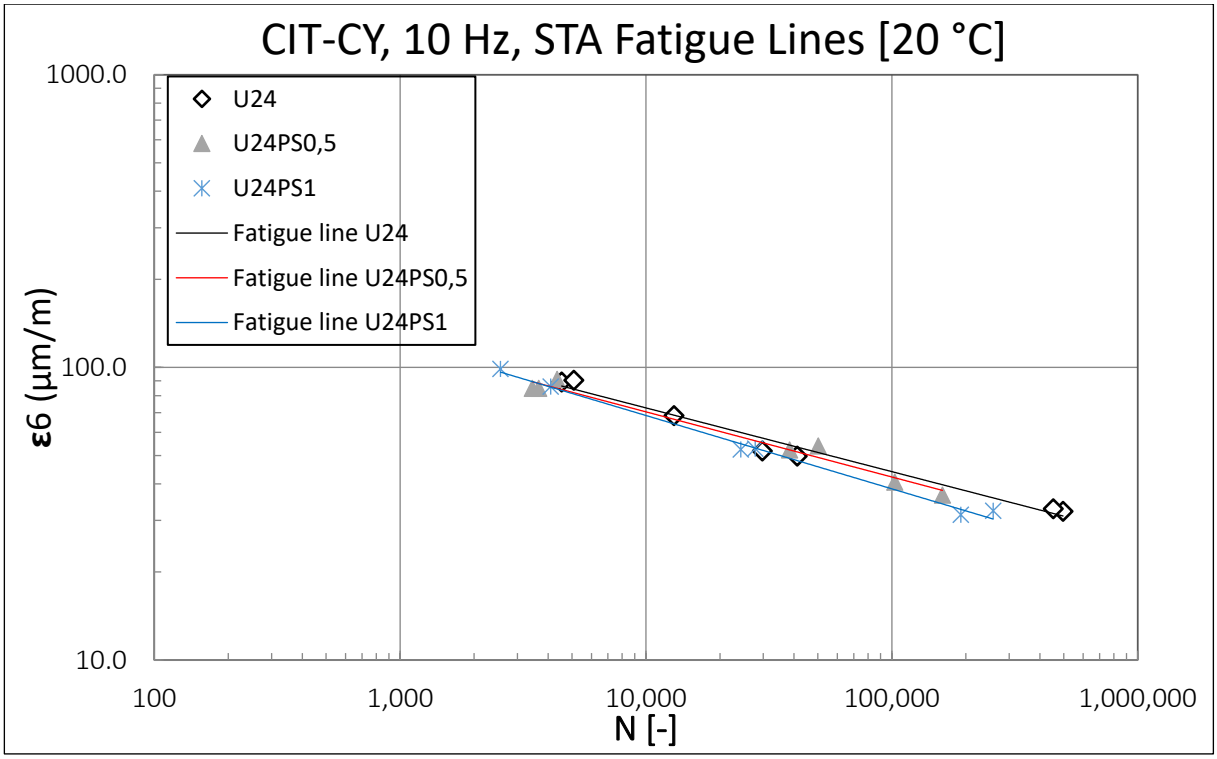

Figure 102. Fatigue lines: strain amplitude ε6 (µm/m) vs load cycles at failure for the STA specimens using energy ratio failure criteria

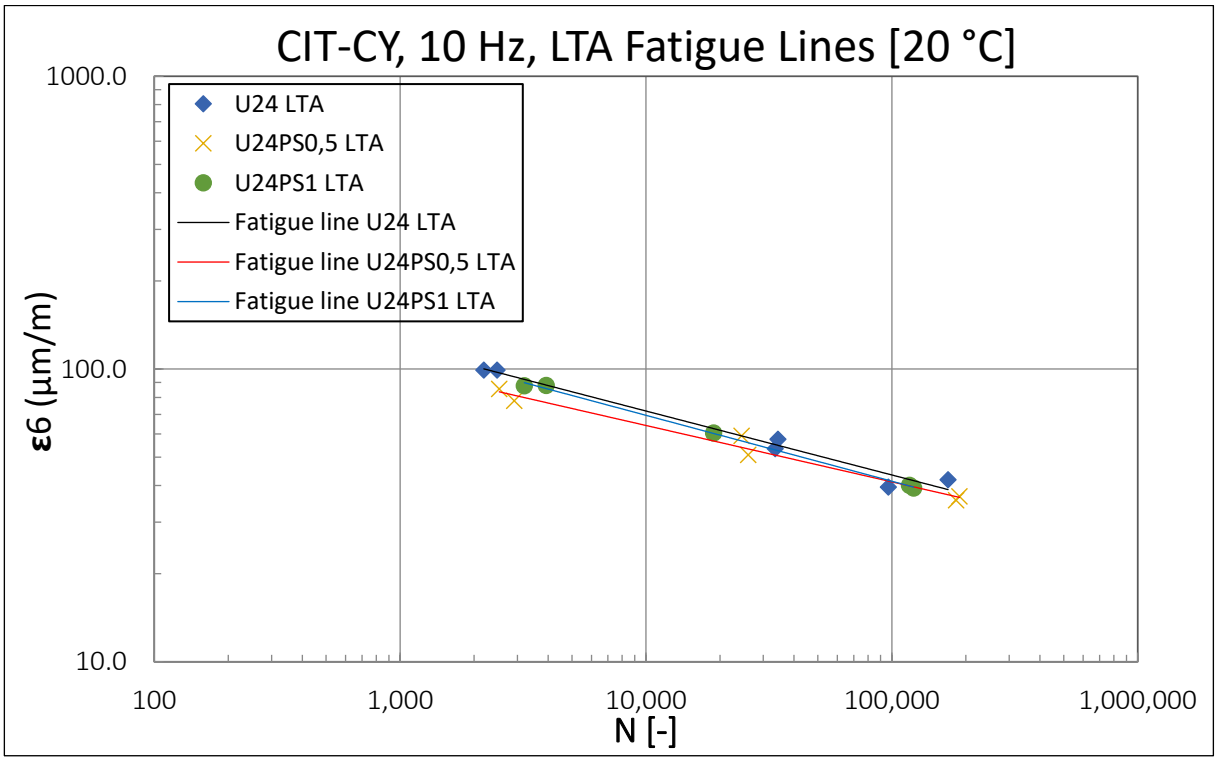

Figure 103. Fatigue lines: strain amplitude ε6 (µm/m) vs load cycles at failure for the LTA specimens using energy ratio failure criteria

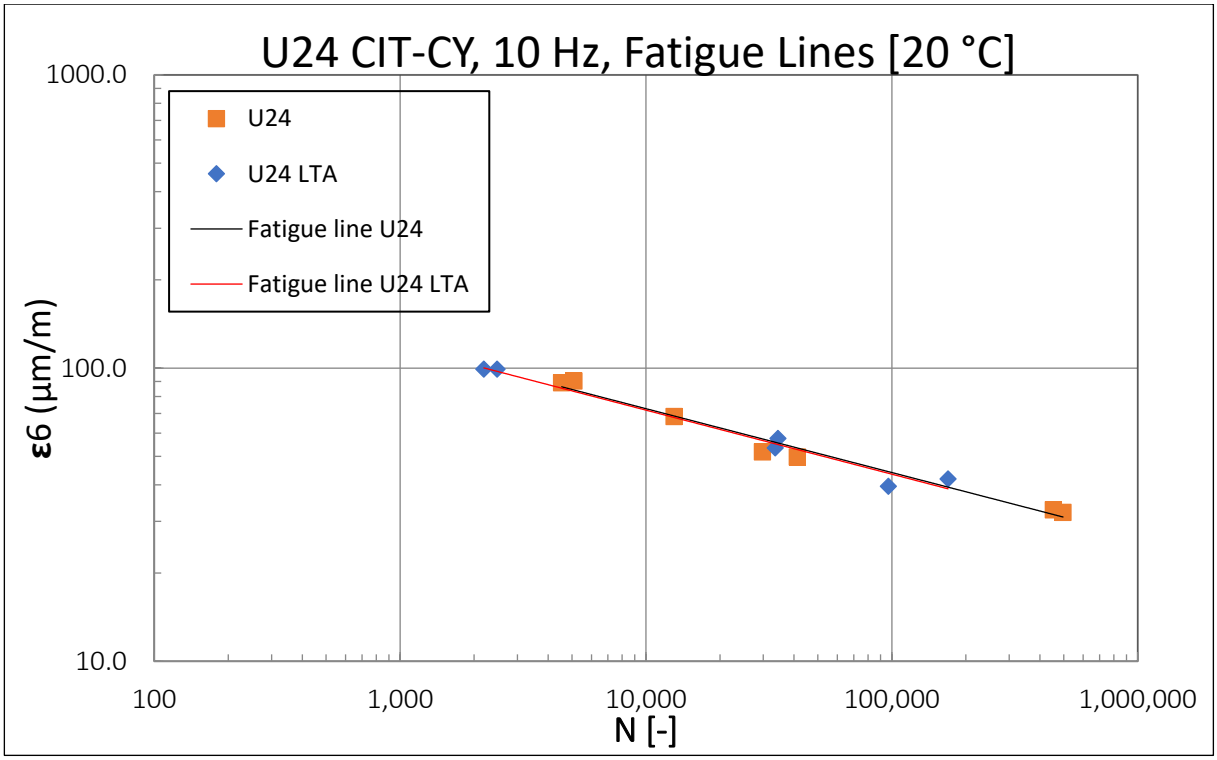

Figure 104. Fatigue lines: strain amplitude ε6 (µm/m) vs load cycles at failure for U24 specimens using energy ratio failure criteria

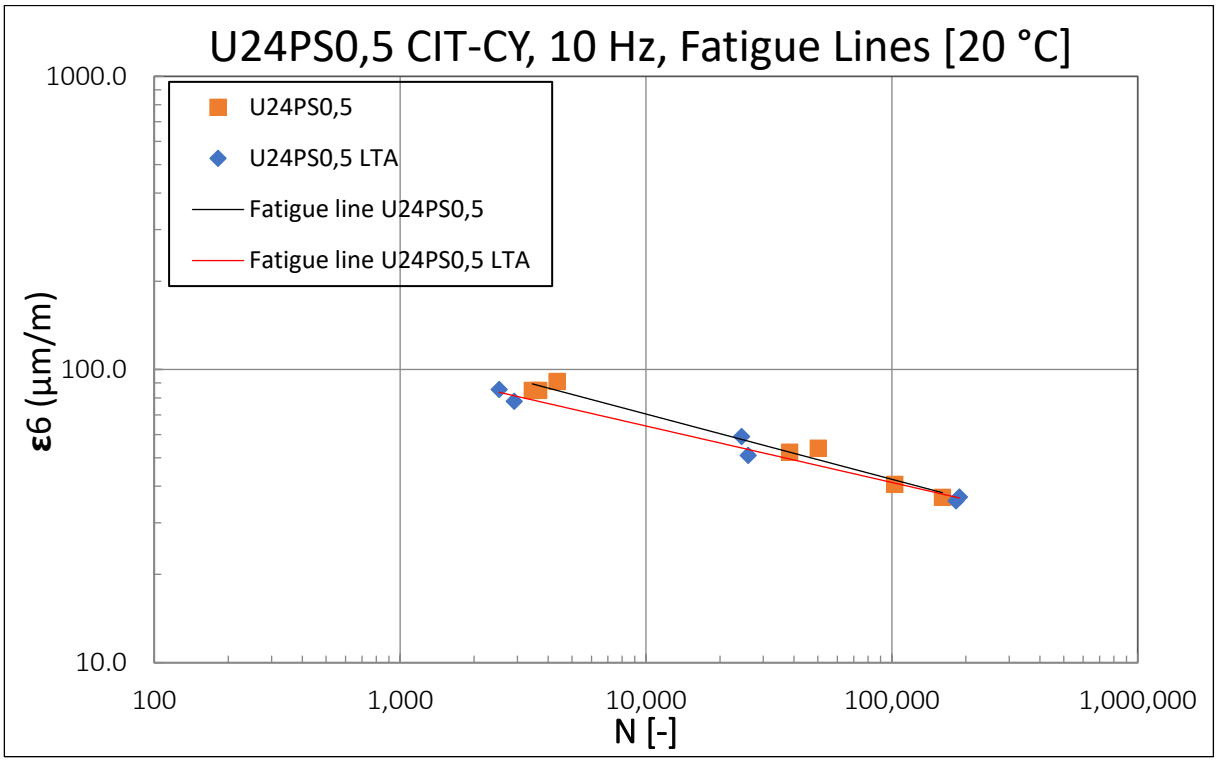

Figure 105. Fatigue lines: strain amplitude ε6 (µm/m) vs load cycles at failure for U24PS0,5 specimens using energy ratio failure criteria

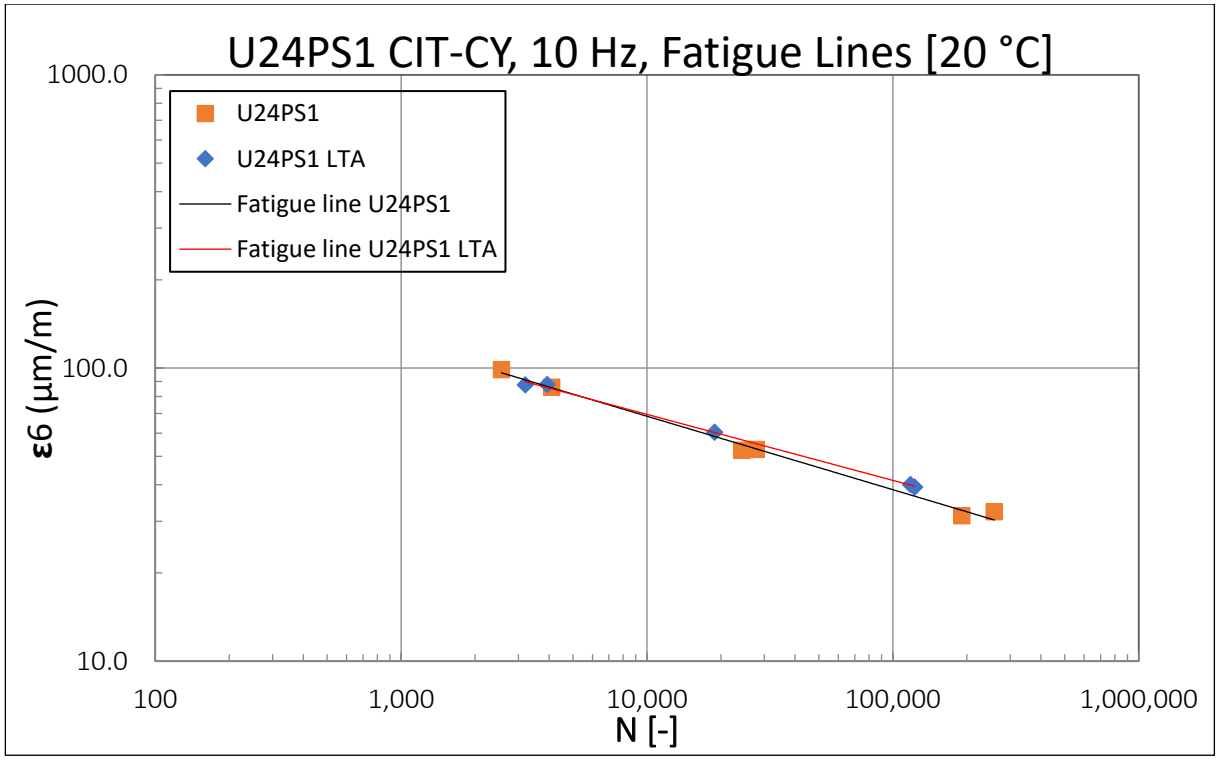

Figure 106. Fatigue lines: strain amplitude ε6 (µm/m) vs load cycles at failure for U24PS1 specimens using energy ratio failure criteria

Further detailed results and tables of CIT-CY tests, sample energy ratio, stiffness modulus, horizontal deformation curves, and curves of failure by sample break criteria are reported in Annex VIII.

P.4 Remarks

The fatigue curves show regular behaviour, except for some specimens that showed temporary oscillation of the stiffness modulus only at low stress level (level 1). The oscillations persisted no longer than a few 100 cycles and did not impact the general trend of the fatigue curves. The oscillation was by average about $\pm$ 500 MPa from the mean value of the stiffness modulus recorded. The oscillations are attributed to the high loading frequency of this test method, and the low vertical stress applied to the specimens at level 1.

Plastics were not visible at the fracture line of broken specimens, and aggregates were not fractured in most specimens.

The initial stiffness modulus (after 100 load cycles) in CIT-CY fatigue tests is always higher by a relatively constant quantity (an average of + 25 %) with respect to the stiffness modulus measured in ITSM tests. This is drawn back to the difference in the loading nature, imposed load amplitude & frequency, and the horizontal strain amplitude constraints between both tests.

Further detailed analysis of the CIT-CY results is presented in chapter R.

Q. RESULT SUMMARIES

Results comparison (*variations refer to the control mixture U24)*				*Limits CSLP AC12 Usura*
HMA Wearing course mixture (RAP content 24%)	**U24**	**U24PS0,5**	**U24PS1**	
Recycled plastic shred content by mixture weight [%]	0	0,5	1	
Mean Binder (incl. plastics) content [%] by mixture weight	6,36	6,51	6,39	
Variation [%]	*0,00*	*2,36*	*0,47*	
Mean Binder (incl. plastics) content [%] by aggregate weight	6,79	6,97	6,82	5,0 - 6,5
Variation [%]	*0,00*	*2,65*	*0,44*	
Mean TMD [Mg/m^3]	2,533	2,537	2,526	
Variation [%]	*0,00*	*0,16*	*-0,26*	
Number of gyratory compacted specimens at N_{100}				
Total STA	19	19	19	
STA followed by LTA	6	6	6	
Mean Specimen Bulk Density [Mg/m^3]	2,513	2,449	2,457	
Standard deviation	0,009	0,0153	0,014	
Variation [%]	*0,00*	*-2,55*	*-2,23*	
Mean Air voids [%] at N_{100}	0,78	3,44	2,76	3,0 - 6,0
Standard deviation	0,35	0,60	0,56	
Variation [%]	*0,00*	*341,03*	*253,85*	
Mean Height increase [mm] *				
STA, 60 ± 2 mm	0,00	0,16	0,24	
Standard deviation		0,14	0,20	
LTA, 60 ± 2 mm	0,00	0,20	0,31	
Standard deviation		0,16	0,13	
Mean Stiffness Modulus ITSM IT-CY [Mpa]				
STA, 10 ˚C	16111	16169	15614	
Standard deviation	1314	815	973	
Variation [%]	*0,00*	*0,36*	*-3,08*	
LTA, 10 ˚C	17282	17594	16758	
Standard deviation	829	1359	1261	
Variation [%]	*0,00*	*1,81*	*-3,03*	
STA, 20 ˚C	7643	7962	7283	
Standard deviation	199	368	538	
Variation [%]	*0,00*	*4,17*	*-4,71*	
LTA, 20 ˚C	8947	9406	8630	
Standard deviation	705	208	610	
Variation [%]	*0,00*	*5,13*	*-3,54*	
STA, 25 ˚C	5233	6216	5377	
Standard deviation	833	495	440	
Variation [%]	*0,00*	*18,78*	*2,75*	
STA, 30 ˚C	3181	3679	3009	
Standard deviation	146	160	240	
Variation [%]	*0,00*	*15,66*	*-5,41*	
LTA, 30 ˚C	3833	4518	3963	
Standard deviation	308	410	236	
Variation [%]	*0,00*	*17,87*	*3,39*	

Results comparison (*variations refer to the control mixture U24)*				*Limits CSLP*
HMA Wearing course mixture (RAP content 24%)	**U24**	**U24PS0,5**	**U24PS1**	*AC12 Usura*
Mean ITS_{dry} [MPa], 25 ˚C, 3 specimens STA	2,02	2,00	1,84	0,85 - 1,55
Standard deviation	0,245	0,073	0,071	
Variation [%]	*0,00*	*-1,03*	*-9,06*	
Mean ITS_{wet} [MPa], 25 ˚C, 3 specimens STA	2,15	2,13	2,06	
Standard deviation	0,063	0,103	0,112	
Variation [%]	*0,00*	*-1,30*	*-4,42*	
Mean ITSR [%], 25 ˚C	106,6	106,3	112,0	≥ 90
Variation [%]	*0,00*	*-0,28*	*5,11*	
Fatigue Line CIT-CY - Energy Ratio criteria: ε6 (µm/m)				
7 specimens STA, 20 ˚C, 10 Hz	26,7	25,3	21,6	
Variation [%]	*0,00*	*-5,24*	*-19,10*	
R^2 (-)	0,978	0,976	0,992	
Variation [%]	*0,00*	*-0,20*	*1,43*	
6 specimens LTA, 20 ˚C, 10 Hz	26,3	26,4	24,6	
Variation [%]	*0,00*	*0,38*	*-6,46*	
R^2 (-)	0,975	0,984	0,998	
Variation [%]	*0,00*	*0,92*	*2,36*	
Fatigue Line CIT-CY - Sample Break criteria: ε6 (µm/m)				
7 specimens STA, 20 ˚C, 10 Hz	28,0	26,9	23,2	
Variation [%]	*0,00*	*-3,93*	*-17,14*	
R^2 (-)	0,981	0,976	0,994	
Variation [%]	*0,00*	*-0,51*	*1,33*	
6 specimens LTA, 20 ˚C, 10 Hz	26,9	28,1	26,6	
Variation [%]	*0,00*	*4,46*	*-1,12*	
R^2 (-)	0,983	0,984	0,998	
Variation [%]	*0,00*	*0,10*	*1,53*	

Table 35. Result summaries of the experimental campaign

** The mean height increase is assumed to be associated to the expansive behaviour of plastics in the compacted samples. The mean height increase with respect to the achieved sample compaction height noticed for U24 (control mixture without plastics) may be related to machine calibration error. Therefore, the mean height increase of this mixture was deducted from the height increase of plastic shred mixtures to exclude machinery calibration error, if any.*

R. CONCLUSIONS AND RECOMMENDATIONS

R.1 Conclusions

From three plant-produced wearing course HMA mixtures with varying plastic shred content (0%, 0,5%, 1% by mixture weight) and 24% RAP, laboratory tests were employed. Volumetric and granulometric assessment was carried out on loose samples, as well as performance tests on compacted specimens by means of gyratory shear compaction at N_{100}, achieving various air void contents and followed by long-term ageing and conditioning.

For each mixture, 19 specimens were produced and underwent testing for the IT-CY stiffness modulus at 4 temperatures, ITS dry & wet, and CIT-CY fatigue tests. From the produced specimens, 6 specimens for each mixture underwent long-term ageing exclusively for CIT-CY testing. All tests were carried out between 14 and 42 days from the date of compaction or the end of oven long-term ageing (where applicable). The following conclusions have been reached from the experimental findings:

- The maximum air void content is achieved in U24PS0,5, U24PS1, and U24 in decreasing order. It can be concluded that the presence of plastic shreds is associated with an increase in the air void content, however, shows not a directly proportional affiliation between plastic dosage and air void propagation.

- Results confirm that presence of plastic shreds has no significant impact on total binder content (1,5 % increase on average), and on the TMD achieved. An insignificant decrease (about 2,4 % on average) in specimen bulk density is noticed. It is also associated with a non-proportional increase of mixture air void. This is confirmed by other literature outcomes (Aziz et al., 2015).

- The geometric expansion of specimen in height is directly correlated with the increase of plastic shred content in the mixture. This effect is further amplified in LTA specimens. The expansion of diameter further iterates this, however insignificantly.

- For each mixture, three specimens have been tested for ITS in dry and wet conditions, at 25 °C at constant deformation rate of 50 mm/minute. The results show no adverse impact of plastic shreds on the water susceptibility of the mixtures (ITS differences are all less than 10 %). The ITSR of mixture specimens is uniform and uninfluenced, as confirmed by other studies (Sasidharan et al., 2019; Capitão et al., 2022).

- The results show that the stiffness modulus of mixture specimens decreases with increasing temperature. This is coherent with other various research findings.

- The stiffness modulus of LTA specimens is consistently higher than that of STA for all mixtures, confirming the findings that ageing of HMA mixtures has stiffening effects. This outcome is witnessed in the three mixtures, irrespective of the plastic shred content. The maximum

stiffness modulus was recorded for U24PS0,5 at all temperatures and in STA and LTA conditions.

- Even with largely increasing air void content in the mixtures with plastic shreds, they maintain the value of stiffness modulus recorded for U24 at all temperatures. This shows the stiffening effect provided by plastic presence in the modified asphalt, which compensates here the undesirable effects of the increasing air void content on stiffness. Thus, it can be said that the presence of plastic shreds provides improvements to the mixture stiffness modulus performance.

- At least two specimens have been tested for CIT-CY fatigue at three strain levels, at 10 °C and 10 Hz loading frequency, in controlled-stress mode. The fatigue failure criteria adopted in this study is the Energy ratio (ER) as well as the sample Breaking criteria. Fatigue lines were fitted and presented by a power function. The regression coefficients of the fatigue lines were presented, and by comparing the strain (**ε**6) and the goodness of fitting (R^2) results, the fatigue performance of the mixtures was evaluated for a fatigue life of 10^6 loading cycles.

- The value of R^2 for all CIT-CY fatigue tests is sufficiently satisfactory and similar in value (above 0,97). The goodness of the fatigue lines is not affected by the mixture type nor mixture ageing. Only one outlier was recorded in all fatigue lines of the specimens, namely one U24 specimen at level 1 stress. This outlier had no substantial difference in stiffness and void content with respect to its batch, and its outlying behaviour can be traced to local imperfections.

- From 21 short-term aged specimens, and using both failure criteria, CIT-CY tests show negligible sensitivity to the increasing plastic shred content in mixtures. On the other hand, from 18 long-term aged specimens, CIT-CY fatigue tests show no impact by plastic presence with respect to the control mixture.

- The findings show that the introduction of plastic shreds slightly reduces the fatigue life of the STA samples containing 1% plastic shreds exclusively, as the critical strain (**ε**6) decreases with both failure criteria (-17,14 % for ER; -19,10% for sample breaking; % with respect to the control mixture).

- The critical strain (**ε**6) value is otherwise unchanged in all STA & LTA samples, even with increasing air void content in the samples with waste plastic shreds. This is a positive influence brought about by the plastic presence, in maintaining stiffness of the mixtures even with significantly growing air voids. This behaviour was similarly confirmed by stiffness modulus test results.

- Long-term ageing shows no detrimental impact on the fatigue life of the mixtures, as changes in the value of critical strain (**ε**6) are insignificant. The fatigue resistance of the mixtures does not decline in the long-term service life.

- For all mixtures, noteworthy variance in the number of cycles to failure is observed at lower strain levels only.

- Based on the above findings, the presence of plastic shreds may aid the modified mixture to intercept and deflect initial micro-cracks in the binder of asphalt pavements, since higher air voids did not decrease the fatigue life of the plastic modified mixtures.

- It must be highlighted that the three mixtures contain strongly varying air void content, which can mistakenly obscure the positive effect of plastic presence when comparing the fatigue life in both ageing conditions.

- Based on the above findings for the three mixtures in study, it can be said that U24PS0,5 may encompass the optimal compromise between increased air void & plastic shred content with respect to stiffness modulus, ITSR, and fatigue resistance for both ageing conditions.

R.2 Recommended future studies

- It recommended to compare specimens with similar air void content for all three mixtures, to eliminate the effect of void variation on stiffness and fatigue performance analysis.
- The findings of this study can be extended by further fatigue performance tests at lower temperatures, to highlight the behaviour of the mixtures under the combination of fatigue and thermal cracking.
- To better understand the effects of plastics in HMA wearing courses, it may be beneficial to carry out fatigue tests in controlled-strain conditions, as wearing courses are thin and behave in controlled-strain mode. In controlled-strain conditions the fatigue life of specimens is expected to be longer.
- Other fatigue testing methods (such as 4-point-bending & IT-CY) must be further investigated to illustrate the fatigue behaviour of the mixtures in a wider scope.
- The paved road section of SP220 with the HMA mixtures under study shall be monitored during regular intervals to assess the mechanical and structural properties of the pavement. Cored asphalt samples can be used to carry laboratory assessment of the integrity of the road during its service life.
- The results of this study may be used to compare the long-term ageing of the paved mixtures after 10 years' service life with the laboratory induced long-term ageing.
- Emission monitoring could be beneficial to understand the potential release of pollutants and hazardous toxins originating from plastics due to wearing and abrasion of HMA mixtures, as well as leaching phenomena monitoring.
- Monitoring of the hydraulic draining aptitude of the pavement is recommended due to low air void content in the mixtures, particularly in U24.
- Monitoring of traffic noise pollution levels is recommended due to the low air void content in the mixtures, particularly in U24.

BIBLIOGRAPHY

A. Chakraborty, & S. Mehta. (2017). Utilization & Minimization of Waste Plastic in Construction of Pavement: A Review. *International Journal of Engineering Technology Science and Research*, *4*(8).

Almeida, A., Capitão, S., Estanqueiro, C., & Picado-Santosc, L. (2021). Possibility of incorporating waste plastic film flakes into warm-mix asphalt as a bitumen extender. *Construction and Building Materials*, *291*, 123384. https://doi.org/10.1016/J.CONBUILDMAT.2021.123384

Aragao, F. T., Kim, Y.-R., & Lee, J. (2008). Research on Fatigue of Asphalt Mixtures and Pavements in Nebraska. *Nebraska Department of Transportation Research Reports*. https://digitalcommons.unl.edu/ndor/41

Asphalt Pavement Construction - Asphalt Institute. (2022). https://www.asphaltinstitute.org/engineering/frequently-asked-questions/asphalt-pavement-construction/#

Aziz, M. M. A., Rahman, M. T., Hainin, M. R., & Bakar, W. A. W. A. (2015). An overview on alternative binders for flexible pavement. *Construction and Building Materials*, *84*, 315–319. https://doi.org/10.1016/J.CONBUILDMAT.2015.03.068

B. Mishra, & M.K. Gupta. (2018). Use of plastic waste in bituminous mixes by wet and dry methods. *Proceedings of the Institution of Civil Engineers - Municipal Engineer*, *1*(11).

Behl, A., Jain, P., & Sharma, G. (2012). Study on waste polyvinyl chloride modified bitumen for paving applications. *ARRB Conference, 25th, 2012, Perth, …*, *1965*.

Brahney, J., Mahowald, N., Prank, M., Cornwell, G., Klimont, Z., Matsui, H., & Prather, K. A. (2021). Constraining the atmospheric limb of the plastic cycle. *Proceedings of the National Academy of Sciences of the United States of America*, *118*(16), e2020719118. https://doi.org/10.1073/PNAS.2020719118/SUPPL_FILE/PNAS.2020719118.SAPP.PDF

Brasileiro, L., Moreno-Navarro, F., Tauste-Martínez, R., Matos, J., & Rubio-Gámez, M. del C. (2019). Reclaimed polymers as asphalt binder modifiers for more sustainable roads: A review. *Sustainability (Switzerland)*, *11*(3). https://doi.org/10.3390/su11030646

Brown, E. R., Kandhal, P. S., & Zhang, J. (2001). Performance testing for hot mix asphalt.

Capitão, S., Almeida, A., & Picado-Santos, L. (2022). Volumetric properties, workability, and mechanical performance of waste plastic-modified asphalt mixtures. *Plastic Waste for Sustainable Asphalt Roads*, 117–144. https://doi.org/10.1016/B978-0-323-85789-5.00007-1

Consiglio Superiore dei Lavori Pubblici. (2022). *Linee guida per la costruzione e manutenzione delle pavimentazioni stradali*.

Di Benedetto, H., Nguyen, Q. T., & Sauzéat, C. (2011). Nonlinearity, heating, fatigue and thixotropy during cyclic loading of asphalt mixtures. *Road Materials and Pavement Design*, *12*(1), 129–158. https://doi.org/10.1080/14680629.2011.9690356

Eskandarsefat, S., Meroni, F., Sangiorgi, C., & Tataranni, P. (2022). Fatigue resistance of waste plastic-modified asphalt. *Plastic Waste for Sustainable Asphalt Roads*, 145–162. https://doi.org/10.1016/B978-0-323-85789-5.00008-3

Evangeliou, N., Grythe, H., Klimont, Z., Heyes, C., Eckhardt, S., Lopez-Aparicio, S., & Stohl, A. (2020). Atmospheric transport is a major pathway of microplastics to remote regions. *Nature Communications 2020 11:1*, *11*(1), 1–11. https://doi.org/10.1038/s41467-020-17201-9

Fonseca, M., Capitão, S., Almeida, A., & Picado-santos, L. (2022). Influence of Plastic Waste on the Workability and Mechanical Behaviour of Asphalt Concrete. *Applied Sciences (Switzerland)*, *12*(4). https://doi.org/10.3390/app12042146

Ghuzlan, K. A., & Carpenter, S. H. (2000). Energy-Derived, Damage-Based Failure Criterion for Fatigue Testing. *Https://Doi.Org/10.3141/1723-18*, *1723*, 141–149. https://doi.org/10.3141/1723-18

Gopinath, K. P., Nagarajan, V. M., Krishnan, A., & Malolan, R. (2020). A critical review on the influence of energy, environmental and economic factors on various processes used to handle and recycle plastic wastes: Development of a comprehensive index. *Journal of Cleaner Production*, *274*, 123031. https://doi.org/10.1016/J.JCLEPRO.2020.123031

Greg White. (2019). Evaluating recycled waste plastic modification and extension of bituminous binder for asphalt. *Eighteenth Annual International Conference on Pavement Engineering, Asphalt Technology and Infrastructure. Liverpool, England, United Kingdom, 27-28 February*. https://www.researchgate.net/publication/331465864_EVALUATING_RECYCLED_WASTE_PLASTIC_MODIFICATION_AND_EXTENSION_OF_BITUMINOUS_BINDER_FOR_ASPHALT

Huang, Y. Hsien. (2004). Pavement Analysis and Design. *Pearson Prentice Hall Upper Saddle River, NJ*, *2*, 401–409.

Indian Roads Congress IRC:SP:98. (2013). Guidelines for the use of Waste Plastic in Hot Bituminous Mixes (dry process) in Wearing Courses. *Indian Roads Congress*, *July*.

Kaza, S., Yao, L. C., Bhada-Tata, P., & Van Woerden, F. (2018). What a Waste 2.0: A Global Snapshot of Solid Waste Management to 2050. *What a Waste 2.0: A Global Snapshot of Solid Waste Management to 2050*. https://doi.org/10.1596/978-1-4648-1329-0

Lastra-González, P., Lizasoain-Arteaga, E., Castro-Fresno, D., & Flintsch, G. (2022). Analysis of replacing virgin bitumen by plastic waste in asphalt concrete mixtures. *International Journal of Pavement Engineering*, *23*(8), 2621–2630. https://doi.org/10.1080/10298436.2020.1866760

Leads, R. R., & Weinstein, J. E. (2019). Occurrence of tire wear particles and other microplastics within the tributaries of the Charleston Harbor Estuary, South Carolina, USA. *Marine Pollution Bulletin*, *145*, 569–582. https://doi.org/10.1016/J.MARPOLBUL.2019.06.061

Li, H. X., Getzinger, G. J., Ferguson, P. L., Orihuela, B., Zhu, M., & Rittschof, D. (2016). Effects of Toxic Leachate from Commercial Plastics on Larval Survival and Settlement of the Barnacle Amphibalanus amphitrite. *Environmental Science and Technology*, *50*(2), 924–931. https://doi.org/10.1021/ACS.EST.5B02781/SUPPL_FILE/ES5B02781_SI_001.PDF

Little D.N. (1992). Analysis of the Influence of Low Density Polyethylene Modification (Novophalt) of Asphalt Concrete on Mixture Shear Strength and Creep Deformation Potential. *American Society for Testing and Materials*, *1992*(1108). https://catalog.libraries.psu.edu/catalog/27993698

Little D.N. (1993). Enhancement of asphalt concrete mixtures to meet structural requirements through the addition of recycled polyethylene. In *Use of Waste Materials in Hot-Mix Asphalt, ASTM, STP 1193, Philadelphia, 210–230.*

Lu, D. X., Enfrin, M., Boom, Y. J., & Giustozzi, F. (2023). Future recyclability of hot mix asphalt containing recycled plastics. *Construction and Building Materials*, *368*. https://doi.org/10.1016/j.conbuildmat.2023.130396

Nizamuddin, S., Jamal, M., Gravina, R., & Giustozzi, F. (2020). Recycled plastic as bitumen modifier: The role of recycled linear low-density polyethylene in the modification of physical, chemical and rheological properties of bitumen. *Journal of Cleaner Production*, *266*. https://doi.org/10.1016/j.jclepro.2020.121988

Orešković, M., Trifunović, S., Mladenović, G., & Bohuš. (2019). Fatigue resistance of a grid-reinforced asphalt concrete using four-point bending beam test. *Bituminous Mixtures and Pavements VII-Proceedings of the 7th International Conference on Bituminous Mixtures and Pavements, ICONFBMP 2019*, 589–594. https://doi.org/10.1201/9781351063265-79/FATIGUE-RESISTANCE-GRID-REINFORCED-ASPHALT-CONCRETE-USING-FOUR-POINT-BENDING-BEAM-TEST-ORE

Rahman, M. T., Mohajerani, A., & Giustozzi, F. (2020). Recycling of waste materials for asphalt concrete and bitumen: A review. *Materials*, *13*(7). https://doi.org/10.3390/ma13071495

Rochman, C. M., Brookson, C., Bikker, J., Djuric, N., Earn, A., Bucci, K., Athey, S., Huntington, A., McIlwraith, H., Munno, K., Frond, H. De, Kolomijeca, A., Erdle, L., Grbic, J., Bayoumi, M., Borrelle, S. B., Wu, T., Santoro, S., Werbowski, L. M., … Hung, C. (2019). Rethinking microplastics as a diverse contaminant suite. *Environmental Toxicology and Chemistry*, *38*(4), 703–711. https://doi.org/10.1002/ETC.4371

Sasidharan, M., Eskandari Torbaghan, M., & Burrow, M. (2019). *Using waste plastics in road construction*. https://www.xe.com/

Shaikh, A., Khan, N., Shah, F., Shukla, D., & Kale, G. (2017). Use of Plastic Waste in Road Construction. *International Journal of Advance Research and Development*, *2*(5).

Sojobi, A. O., Nwobodo, S. E., & Aladegboye, O. J. (2016). Recycling of polyethylene terephthalate (PET) plastic bottle wastes in bituminous asphaltic concrete. *Cogent Engineering*, *3*(1). https://doi.org/10.1080/23311916.2015.1133480

Sommer, F., Dietze, V., Baum, A., Sauer, J., Gilge, S., Maschowski, C., & Gieré, R. (2018). Tire abrasion as a major source of microplastics in the environment. *Aerosol and Air Quality Research*, *18*(8). https://doi.org/10.4209/aaqr.2018.03.0099

The British standards institution. (2020). *BS EN 12697-29:2020 Bituminous mixtures – Test methods Part 29: Determination of the dimensions of a bituminous specimen*.

The British standards institution. (2012). *BS EN 933-1:2012 Tests for geometrical properties of aggregates Part 1: Determination of particle size distribution — Sieving method*.

The British standards institution. (2017). *BS EN 12697-23:2017 Bituminous mixtures - Test methods Part 23: Determination of the indirect tensile strength of bituminous specimens*.

The British standards institution. (2018). *BS EN 12697-5:2018 Bituminous mixtures - Test methods Part 5: Determination of the maximum density*.

The British standards institution. (2018a). *BS EN 12697-24:2018 Bituminous mixtures - Test methods Part 24: Resistance to fatigue*.

The British standards institution. (2018b). *BS EN 12697-26:2018 Bituminous mixtures - Test methods Part 26: Stiffness*.

The British standards institution. (2019). *BS EN 12697-31:2019 Bituminous mixtures – Test methods Part 31: Specimen preparation by gyratory compactor*.

The British standards institution. (2020a). *BS EN 12697-6:2020 Bituminous mixtures — Test methods Part 6: Determination of bulk density of bituminous specimens*.

The British standards institution. (2020b). *BS EN 12697-28:2020 Bituminous mixtures – Test methods Part 28: Preparation of samples for determining binder content, water content and grading*.

The British standards institution. (2020c). *BS EN 12697-39:2020 Bituminous mixtures — Test methods Part 39: Binder content by ignition*.

Van Dijk, W., & Visser, W. (1977). ENERGY APPROACH TO FATIGUE FOR PAVEMENT DESIGN. *In Proceedings of the Association of Asphalt Paving Technologist, 21-23 February; San Antonio, Texas: 1-40*, *46*.

Vasudevan, R., Ramalinga Chandra Sekar, A., Sundarakannan, B., & Velkennedy, R. (2012). A technique to dispose waste plastics in an ecofriendly way - Application in construction of flexible pavements. *Construction and Building Materials*, *28*(1). https://doi.org/10.1016/j.conbuildmat.2011.08.031

Vasudevan, R., Velkennedy, R., Sekar, A. R. C., & Sundarakannan, B. (2010). Utilization of Waste Polymers for Flexible Pavement and Easy Disposal of Waste Polymers. *International Journal of Pavement Research and Technology*, *3*(1).

Willis, R., Yin, F., & Moraes, R. (2020). Recycled Plastics in Asphalt Part A: State of the Knowledge. *National Asphalt Pavement Association (NAPA)*.

World Bank, Pawan Patil, Natalya Stankevich, Nina Tsydenova, & Zoie Diana. (2023). *Plastic Waste in Road Construction - A Path Worth Paving?: Application of Dry Process in South Asia*. https://doi.org/10.1596/39839

Wright, S. L., & Kelly, F. J. (2017). Plastic and Human Health: A Micro Issue? *Environmental Science and Technology*, *51*(12), 6634–6647. https://doi.org/10.1021/ACS.EST.7B00423/SUPPL_FILE/ES7B00423_SI_001.PDF

Wu, S., Tahri, O., Shen, S., Zhang, W., & Muhunthan, B. (2021). Environmental impact evaluation and long-term rutting resistance performance of warm mix asphalt technologies. *Journal of Cleaner Production*, *278*, 123938. https://doi.org/10.1016/J.JCLEPRO.2020.123938

Yin, F., Moraes, R., & Anand, A. (2020). Recycled Plastics in Asphalt Part B: Literature Review. *National Asphalt Pavement Association (NAPA)*.

Annex

Annex I. Binder content by Ignition test results

LEGEND	
W_t	Mass of sample basket and catch pan
$W_{t+m,\ BI}$	Mass of sample basket + catch pan + mixture, Before Ignition
$W_{t+a,\ AI}$	Mass of sample basket + catch pan + mixture, After Ignition
$W_{m,BI}$	Mass of mixture, Before Ignition
$W_{a,AI}$	Mass of aggregates, After Ignition
CF	Calibration Factor
B_m	Corrected binder content of bituminous mixture

Ignition test (Carbolite)

Usura 24 % RAP

1st sample		
W_t	2847	g
$W_{t+m,\ BI}$	4253,4	g
$W_{t+a,\ AI}$	4164,2	g
$W_{m,BI}$	1406,4	g
$W_{a,AI}$	1317,2	g
CF	/	%
B_m	6,34	%

Average
6,36

2nd sample		
W_t	2854,3	g
$W_{t+m,\ BI}$	4257,5	g
$W_{t+a,\ AI}$	4168,1	g
$W_{m,BI}$	1403,2	g
$W_{a,AI}$	1313,8	g
CF	/	%
B_m	6,38	%

Table 36 Ignition test U24

Ignition test (Carbolite)

Usura 24 % RAP + 0,5 % PS

1st sample		
W_t	2854,8	g
$W_{t+m,\ BI}$	4254	g
$W_{t+a,\ AI}$	4163,3	g
$W_{m,BI}$	1399,2	g
$W_{a,AI}$	1308,5	g
CF	/	%
B_m	6,48	%

Average
6,51

2nd sample		
W_t	2847,1	g
$W_{t+m,\ BI}$	4247,6	g
$W_{t+a,\ AI}$	4155,9	g
$W_{m,BI}$	1400,5	g
$W_{a,AI}$	1308,8	g
CF	/	%
B_m	6,55	%

Table 37 Ignition test U24PS0,5

Ignition test (Carbolite)				Usura 24 % RAP + 1 % PS			
1st sample					2st sample		
W_t	2854,9	g			W_t	2847,1	g
$W_{t+m,\ BI}$	4258,9	g			$W_{t+m,\ BI}$	4265,8	g
$W_{t+a,\ AI}$	4169,7	g			$W_{t+a,\ AI}$	4171,1	g
$W_{m,BI}$	1404,0	g			$W_{m,BI}$	1418,7	g
$W_{a,AI}$	1314,8	g			$W_{a,AI}$	1324	g
CF	/	%	Average		CF	/	%
B_m	6,39	%	6,39		B_m	6,68	%

Table 38 Ignition test U24PS1

In red: rejected test sample due to large variation in binder content (test precision and repeatability)

Annex II. Particle size distribution (Sieve analysis)

UR24							
Sieve size (mm)	Sieve Mass (g)	Sieve + Agg (g)	Retained (g)	Retained (g) + Filler	Cumulative R (g)	Cumulative R (%)	Passing (%)
16	1302,1	1302,1	0,0	0,0	0,0	0,0	100,0
12,5	1183,7	1215,7	32,0	32,0	32,0	2,4	97,6
8	1070,4	1187,3	116,9	116,9	148,9	11,4	88,6
6,3	1053,4	1148,2	94,8	94,8	243,7	18,6	81,4
4	1107,8	1358,7	250,9	250,9	494,6	37,8	62,2
2	974,8	1239,5	264,7	264,7	759,3	58,0	42,0
0,5	784,0	1080,9	296,9	296,9	1056,2	80,6	19,4
0,25	726,5	793,0	66,5	66,5	1122,7	85,7	14,3
0,063	773,0	850,7	77,7	77,7	1200,4	91,6	8,4
Pan	724,5	728,9	4,4	109,7	1310,1	100,0	0,0
Total	9700,2	10905,0	1204,8	1310,1			

Table 39 U24 Sieve analysis

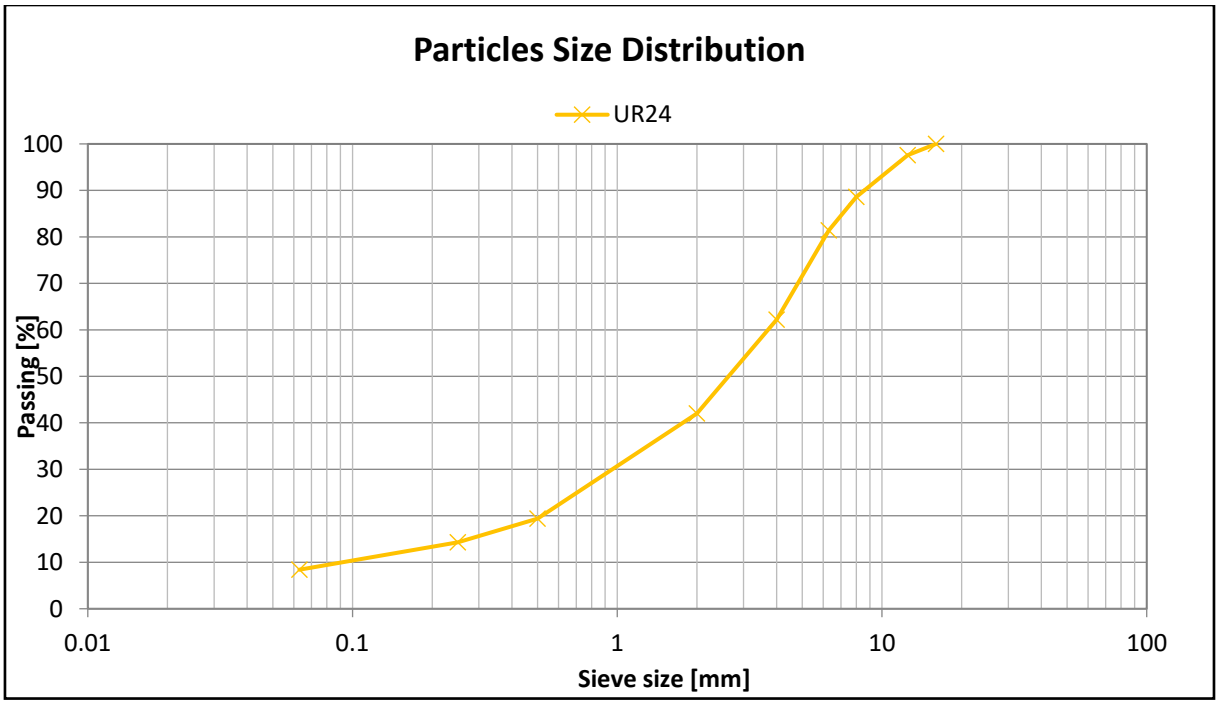

Figure 107 U24 Particle size distribution

UR24PS0,5							
Sieve size (mm)	**Sieve Mass (g)**	**Sieve + Agg (g)**	**Retained (g)**	**Retained (g) + Filler**	**Cumulative R (g)**	**Cumulative R (%)**	**Passing (%)**
16	1302,1	1302,1	0,0	0,0	0,0	0,0	100,0
12,5	1183,8	1207,7	23,9	23,9	23,9	1,8	98,2
8	1070,5	1198,1	127,6	127,6	151,5	11,6	88,4
6,3	1053,3	1166,8	113,5	113,5	265,0	20,3	79,7
4	1107,9	1356,3	248,4	248,4	513,4	39,3	60,7
2	974,8	1234,4	259,6	259,6	773,0	59,1	40,9
0,5	784,1	1070,9	286,8	286,8	1059,8	81,1	18,9
0,25	726,6	795,2	68,6	68,6	1128,4	86,3	13,7
0,063	773,0	847,9	74,9	74,9	1203,3	92,0	8,0
Pan	724,6	726,8	2,2	104,1	1307,4	100,0	0,0
Total	9700,7	10906,2	1205,5	1307,4			

Table 40 U24PS0,5 Sieve analysis

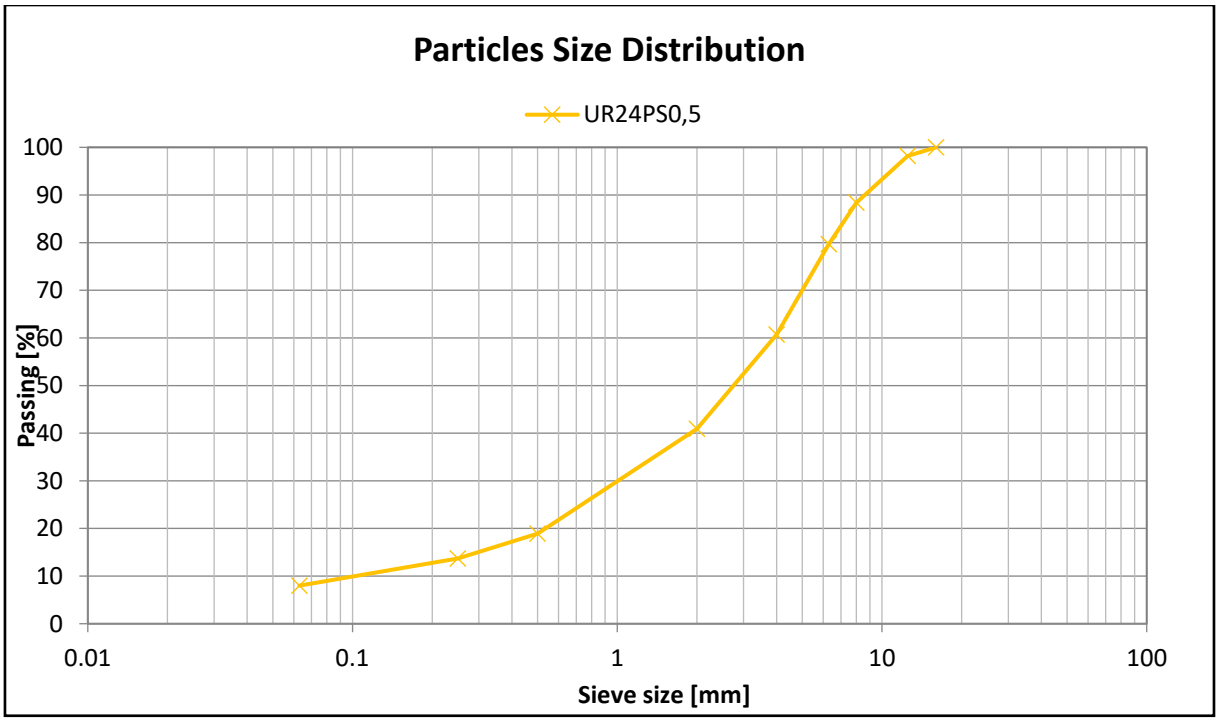

Figure 108 U24PS0,5 Particle size distribution

UR24PS1							
Sieve size (mm)	**Sieve Mass (g)**	**Sieve + Agg (g)**	**Retained (g)**	**Retained (g) + Filler**	**Cumulative R (g)**	**Cumulative R (%)**	**Passing (%)**
16	1302,1	1311,8	9,7	9,7	9,7	0,7	99,3
12,5	1183,8	1186,9	3,1	3,1	12,8	1,0	99,0
8	1070,5	1232,8	162,3	162,3	175,1	13,3	86,7
6,3	1053,3	1163,5	110,2	110,2	285,3	21,6	78,4
4	1107,9	1379,9	272,0	272,0	557,3	42,2	57,8
2	974,8	1219,2	244,4	244,4	801,7	60,7	39,3
0,5	784,1	1059,6	275,5	275,5	1077,2	81,6	18,4
0,25	726,7	795,0	68,3	68,3	1145,5	86,7	13,3
0,063	773,0	845,0	72,0	72,0	1217,5	92,2	7,8
Pan	724,6	726,2	1,6	103,2	1320,7	100,0	0,0
Total	9700,8	10919,9	1219,1	1320,7			

Table 41 U24PS1 Sieve analysis

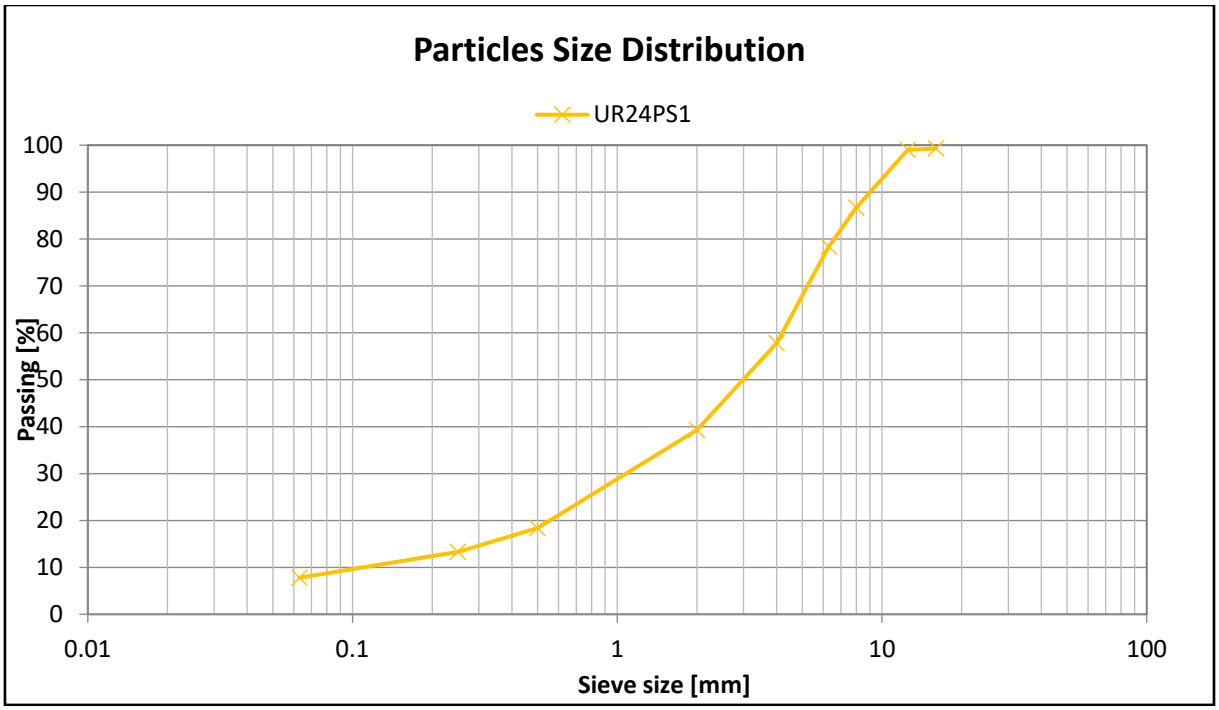

Figure 109 U24PS1 Particle size distribution

U24 – Result validation	
Before washing	
Pan weight (g)	408,7
Pan + Aggregate wt. (g)	1719,2
Aggregate wt. (g)	1310,5
After washing and drying	
Pan weight (g)	408,7
Pan + Aggregate wt. (g)	1613,9
Aggregate wt. (g)	1205,2
Filler weight (g)	105,3
Rn ~ M_1 [%]	0,033189512
f ~ M_1 [%]	0,030522701

Table 42 U24 Sieve analysis result validation

U24PS0,5 - Result Validation	
Before washing	
Pan weight (g)	409
Pan + Aggregate wt. (g)	1716,4
Aggregate wt. (g)	1307,4
After washing and drying	
Pan weight (g)	409
Pan + Aggregate wt. (g)	1614,5
Aggregate wt. (g)	1205,5
Filler weight (g)	101,9
Rn ~ M_1 [%]	0,00
f ~ M_1 [%]	0,00

Table 43 U24PS0,5 Sieve analysis result validation

U24PS1 - Result validation	
Before washing	
Pan weight (g)	408,8
Pan + Aggregate wt. (g)	1729,9
Aggregate wt. (g)	1321,1
After washing and drying	
Pan weight (g)	408,8
Pan + Aggregate wt. (g)	1628,3
Aggregate wt. (g)	1219,5
Filler weight (g)	101,6
Rn ~ M_1 [%]	0,032800328
f ~ M_1 [%]	0,030277799

Table 44 U24PS1 Sieve analysis result validation

Annex III. TMD test results

LEGEND	
T	Water temperature
ρ_w	Water density
m_1	Mass of pyknometer + cap
m_2	Mass of pyknometer + cap + mixture
m_3	Mass of pyknometer + cap + mixture + water
V_p	Volume of the pyknometer
ρ_{mm}	Theoretical maximum density

TMD 1

Usura 24 % RAP

Pyknometer Q+A		
T	28,2	°C
ρ_w	0,996	Mg/m^3
m_1	917,2	g
m_2	1620	g
m_3	2685,8	g
V_p	0,0013479212	m^3
ρ_{mm}	2,527	Mg/m^3

Pyknometer P+15		
T	28,3	°C
ρ_w	0,996	Mg/m^3
m_1	937,2	g
m_2	1809,5	g
m_3	2795,8	g
V_p	0,0013337455	m^3
ρ_{mm}	2,538	Mg/m^3

AVERAGE	ρ_{mm}	2,533	Mg/m^3

TMD 2

Pyknometer P+15		
T	29,1	°C
ρ_w	0,996	Mg/m^3
m_1	917,2	g
m_2	1710,6	g
m_3	2742,2	g
V_p	0,0013479212	m^3
ρ_{mm}	2,542	Mg/m^3

Pyknometer Q+A		
T	29,5	°C
ρ_w	0,996	Mg/m^3
m_1	937,2	g
m_2	1739,7	g
m_3	2750,9	g
V_p	0,0013337455	m^3
ρ_{mm}	2,521	Mg/m^3

In red: rejected test sample due to large variation in TMD (test precision and repeatability)

AVERAGE	ρ_{mm}	2,531	Mg/m^3

Table 45 U24 TMD tests

TMD 1	Usura 24 % RAP + 0,5 % PS

Pyknometer Q+A		
T	20,8	°C
ρ_w	0,998	Mg/m^3
m_1	917,2	g
m_2	1680,9	g
m_3	2726,3	g
V_p	0,0013479212	m^3
ρ_{mm}	2,541	Mg/m^3

Pyknometer P+15		
T	21,1	°C
ρ_w	0,998	Mg/m^3
m_1	937,1	g
m_2	1754,7	g
m_3	2763,8	g
V_p	0,0013337455	m^3
ρ_{mm}	2,534	Mg/m^3

AVERAGE	ρ_{mm}	2,537	Mg/m^3

TMD 2

Pyknometer Q+A		
T	20,4	°C
ρ_w	0,998	Mg/m^3
m_1	917,2	g
m_2	1695,9	g
m_3	2734,3	g
V_p	0,0013479212	m^3
ρ_{mm}	2,531	Mg/m^3

Pyknometer P+15		
T	20	°C
ρ_w	0,998	Mg/m^3
m_1	937,1	g
m_2	1750,9	g
m_3	2762,5	g
V_p	0,0013337455	m^3
ρ_{mm}	2,540	Mg/m^3

AVERAGE	ρ_{mm}	2,536	Mg/m^3

Table 46 U24PS0,5 TMD tests

TMD 1	Usura 24 % RAP + 1 % PS

Pyknometer Q+A		
T	15,9	°C
ρ_w	0,999	Mg/m^3
m_1	917,2	g
m_2	1704,9	g
m_3	2739,6	g
V_p	0,0013479212	m^3
ρ_{mm}	2,523	Mg/m^3

Pyknometer P+15		
T	14,6	°C
ρ_w	0,999	Mg/m^3
m_1	937,1	g
m_2	1733,4	g
m_3	2750,9	g
V_p	0,0013337455	m^3
ρ_{mm}	2,524	Mg/m^3

AVERAGE	ρ_{mm}	2,524	Mg/m^3

TMD 2	Usura 24 % RAP + 1 % PS

Pyknometer Q+A		
T	13,3	°C
ρ_w	0,999	Mg/m^3
m_1	917,2	g
m_2	1634,7	g
m_3	2698,3	g
V_p	0,0013479212	m^3
ρ_{mm}	2,529	Mg/m^3

Pyknometer P+15		
T	12,3	°C
ρ_w	1,000	Mg/m^3
m_1	937,1	g
m_2	1765	g
m_3	2771	g
V_p	0,0013337455	m^3
ρ_{mm}	2,530	Mg/m^3

AVERAGE	ρ_{mm}	2,529	Mg/m^3

Table 47 U24PS1 TMD tests

Annex IV.Specimen gyratory compaction results

Trial Specimen	M_1 [g]	M_2 [g]	M_3 [g]	T [°C]	ρ_w [Mg/m³]	P_{ssd} [Mg/m³]	ρ_{tmd} [Mg/m³]	N_{max}	v_{real} at N_{max} [%]	Final H [mm]
U24T1	1186,5	719,9	1187,5	24,6	0,9972	2,530	2,533	200	0,10	59,9
U24PS0,5T2	1391,8	837,3	1395,7	24,6	0,9972	2,486	2,537	200	2,03	72,0
U24PS1T2	1386,5	833,8	1388,4	24,0	0,9974	2,493	2,526	200	1,29	71,5

Table 48 Trial Compaction results for all mixtures

U24T1	
D_{mold} [mm]	100
M [g] (weighed after compaction)	1186,5
H_{final} [mm]	59,9

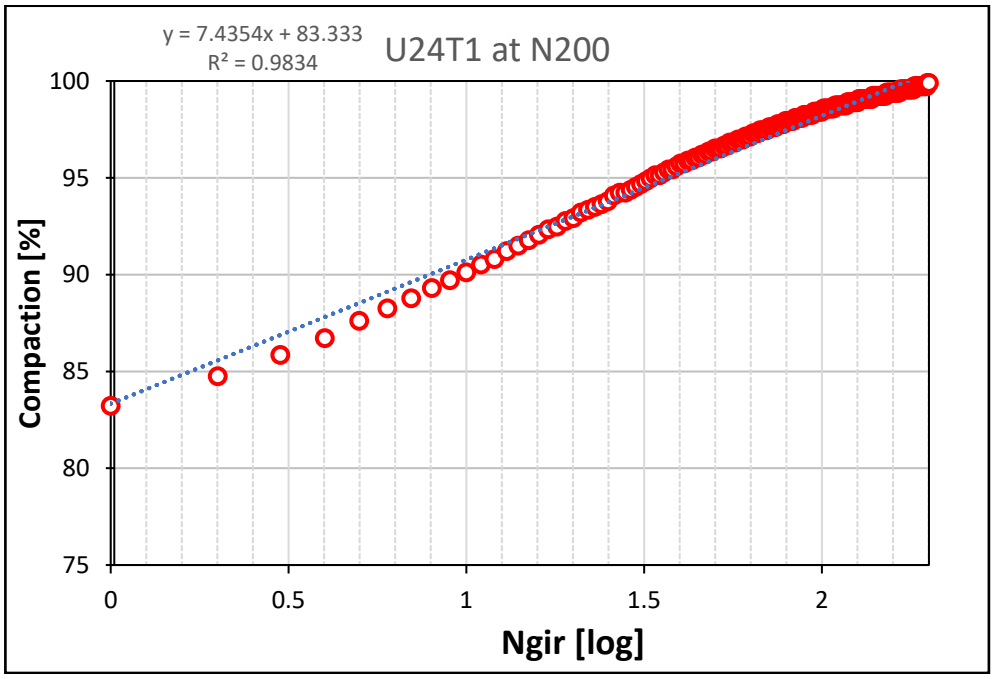

Figure 110 U24T1 trial compaction curve

U24PS0,5T2	
D_{mold} [mm]	100
M [g] (weighed after compaction)	1391,80
H_{final} [mm]	72,0

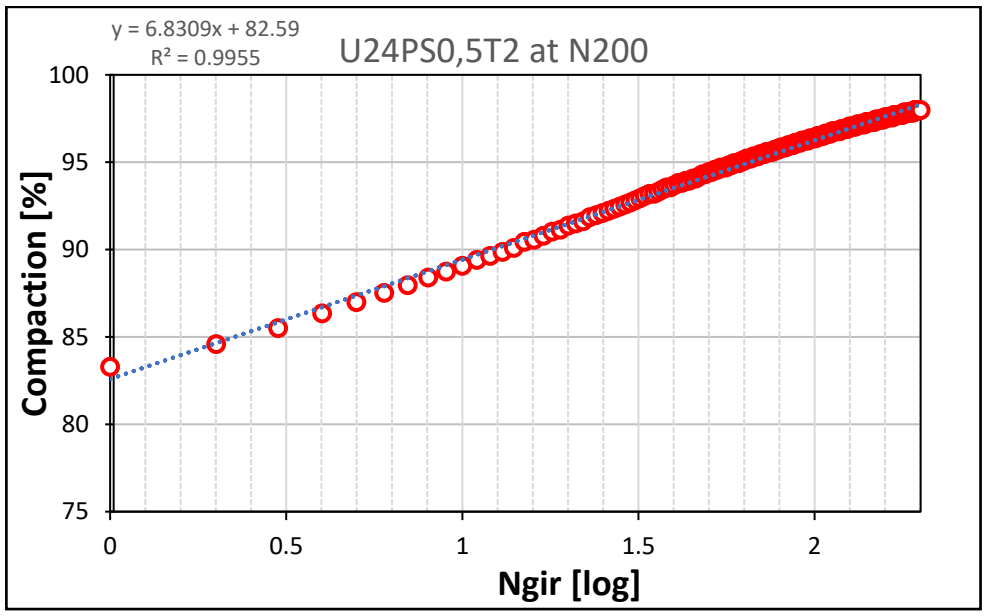

Figure 111 U24PS0,5T2 trial compaction curve

U24PS1T2	
D_{mold} [mm]	100
M [g] (weighed after compaction)	1386,5
H_{final} [mm]	71,5

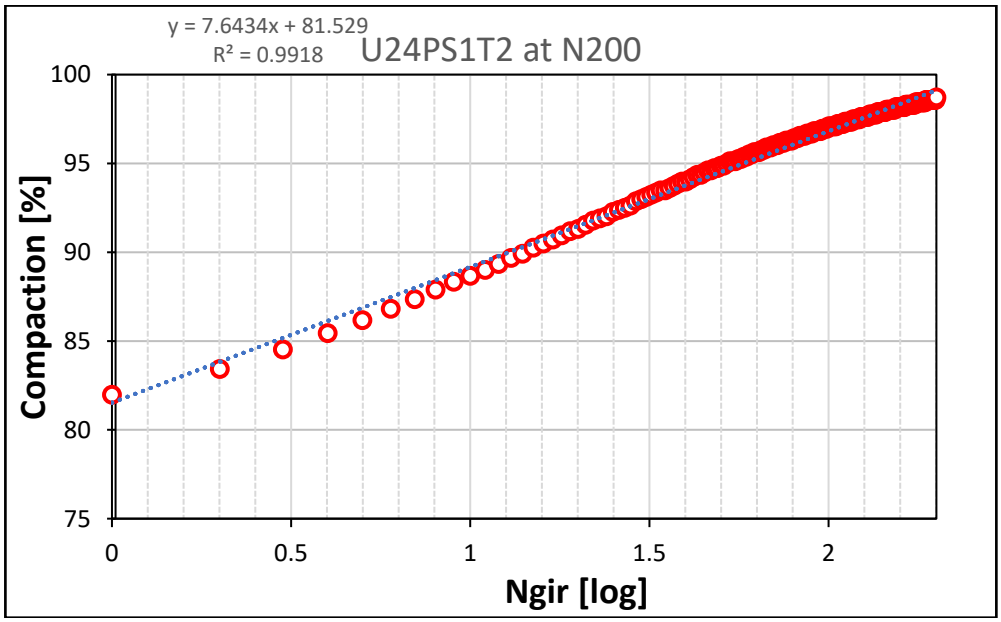

Figure 112 U24PS1 trial compaction curve

Gyratory Shear Compactor Specimen Properties							
U24							
ID	N_{max}	d	Target H	Achieved H	M_{sample}	v	c_x
[-]	[girations]	[mm]	[mm]	[mm]	[g]	[%]	[%]
U24A	100	100	60 ± 2	60,1	1168,9	0,70	99,30
U24B				59,8	1168,8	0,75	99,25
U24C				59,4	1167,6	0,42	99,58
U24D				60,4	1167,5	1,14	98,86
U24E				59,6	1168,4	0,76	99,24
U24F				60,4	1170,0	0,91	99,09
U24G				61,2	1171,8	1,80	98,20
U24H				60,0	1170,5	0,90	99,10
U24I				59,9	1169,7	0,56	99,44
U24J				59,6	1166,0	0,88	99,12
U24K				60,3	1169,7	0,63	99,37
U24L				60,2	1172,1	0,51	99,49
U24M				59,9	1170,0	0,95	99,05
U24N				60,5	1171,5	0,84	99,16
U24O				60,4	1169,8	1,18	98,82
U24P				59,4	1169,1	0,42	99,58
U24Q				60,0	1169,6	0,23	99,77
U24R				60,4	1170,2	0,78	99,22
U24S				59,3	1167,2	0,37	99,63
U24Gbis				60,4	1169,0	0,93	99,07
			Mean	**60,06**	**1169,37**	**0,78**	**99,22**
			Std. Dev.	0,47	1,55	0,35	0,35

Table 49 Specimen compaction results for U24

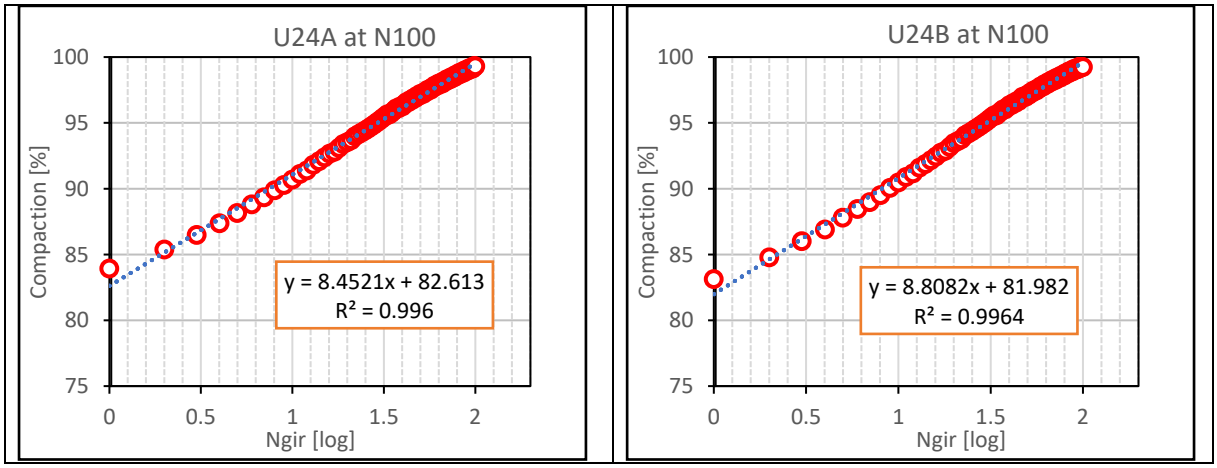

Table 50 Sample compaction curves for U24

Gyratory Shear Compactor Specimen Properties							
U24PS0,5							
ID	N_{max}	d	Target H	Achieved H	M_{sample}	v_{real}	c_x
[-]	[girations]	[mm]	[mm]	[mm]	[g]	[%]	[%]
U24PS0,5A				59,50	1140,80	2,42	97,58
U24PS0,5B				60,20	1140,10	3,43	96,57
U24PS0,5C				60,10	1143,50	3,22	96,78
U24PS0,5D				60,90	1144,20	3,68	96,32
U24PS0,5E				60,90	1142,90	4,43	95,57
U24PS0,5F				60,10	1142,40	3,71	96,29
U24PS0,5G				60,80	1142,70	4,20	95,80
U24PS0,5H				59,70	1142,30	2,98	97,02
U24PS0,5I				60,20	1141,80	3,02	96,98
U24PS0,5J	100	100	60 ± 2	59,80	1140,00	3,04	96,96
U24PS0,5K				60,30	1142,50	3,14	96,86
U24PS0,5L				59,70	1143,50	2,80	97,20
U24PS0,5M				60,70	1142,10	3,75	96,25
U24PS0,5N				60,70	1142,30	3,75	96,25
U24PS0,5O				61,10	1141,50	4,40	95,60
U24PS0,5P				60,90	1142,60	4,28	95,72
U24PS0,5Q				60,20	1142,70	2,69	97,31
U24PS0,5R				59,90	1143,00	2,84	97,16
U24PS0,5S				60,40	1141,20	3,51	96,49
			Mean	**60,32**	**1142,22**	**3,44**	**96,56**
			Std. Dev.	0,48	1,11	0,60	0,60

Table 51 Specimen compaction results for U24PS0,5

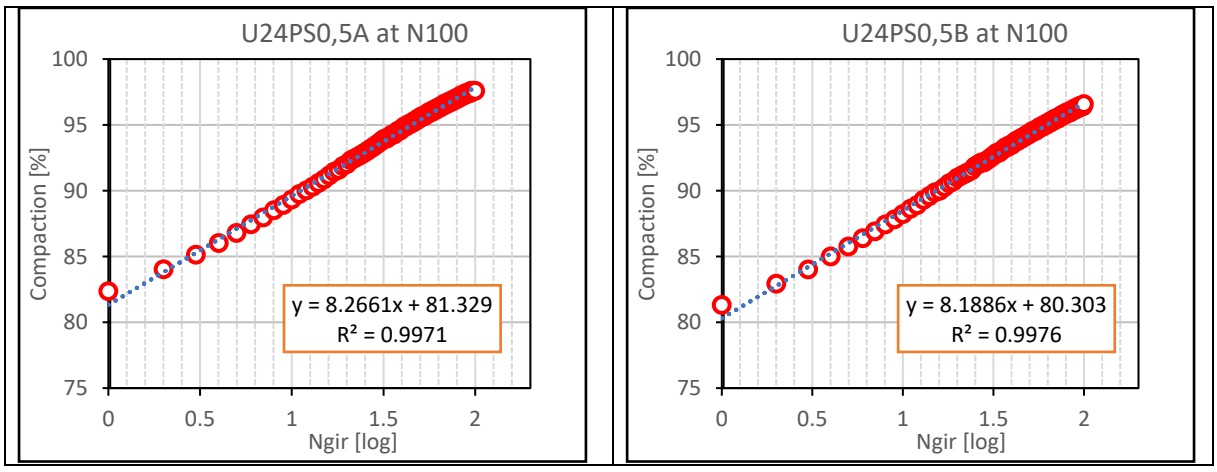

Table 52 Sample compaction curves for U24PS0,5

Gyratory Shear Compactor Specimen Properties							
U24PS1							
ID	N_{max}	d	Target H	Achieved H	M_{sample}	v	c_x
[-]	[girations]	[mm]	[mm]	[mm]	[g]	[%]	[%]
U24PS1A	100	100	60 ± 2	60,0	1143,9	3,20	96,80
U24PS1B				60,4	1144,3	2,77	97,23
U24PS1C				60,0	1145,1	2,48	97,52
U24PS1D				60,6	1146,9	2,52	97,48
U24PS1E				60,4	1145,5	2,84	97,16
U24PS1F				59,6	1144,8	1,92	98,08
U24PS1G				59,7	1145,2	2,08	97,92
U24PS1H				60,6	1145,1	2,72	97,28
U24PS1I				60,5	1144,4	3,13	96,87
U24PS1J				60,4	1143,6	2,79	97,21
U24PS1K				59,7	1143,6	2,51	97,49
U24PS1L				59,8	1145,7	2,48	97,52
U24PS1M				60,8	1144,6	3,77	96,23
U24PS1N				60,3	1144,2	2,48	97,52
U24PS1O				59,6	1145,4	2,02	97,98
U24PS1P				60,8	1144,9	3,43	96,57
U24PS1Q				59,5	1144,6	2,14	97,86
U24PS1R				60,9	1145,3	3,91	96,09
U24PS1S				60,3	1146,3	2,63	97,37
U24PS1Bbis				60,6	1145,7	3,39	96,61
			Mean	**60,23**	**1144,96**	**2,76**	**97,24**
			Std. Dev.	0,45	0,85	0,56	0,56

Table 53 Specimen compaction results for U24PS1

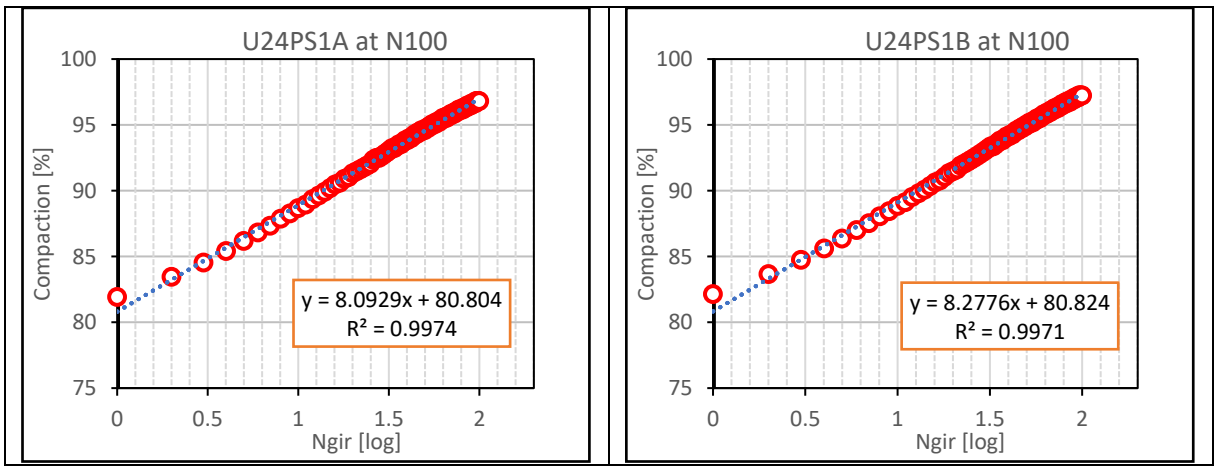

Table 54 Sample compaction curves for U24PS1

Annex V. Compacted specimen geometric expansion

U24									
D = 100 mm	[mm]	[mm]	[mm]	[mm]	[mm]	[mm]	[mm]	[mm]	[mm]
Specimen	H_1	H_2	H_3	H_4	Average	Compactor Height	Difference	Mean Increase	Diameter
U24A	60,2	60,4	60,3	60,0	60,2	60,1	0,12	0,18	100,0
U24B	60,1	60,1	60,1	60,1	60,1	59,8	0,30	0,18	100,1
U24C	59,9	59,8	59,8	59,8	59,8	59,4	0,43	0,18	100,1
U24D	60,4	60,4	60,5	60,4	60,4	60,4	0,03	0,18	100,0
U24E	60,1	60,0	60,0	59,9	60,0	59,6	0,40	0,18	100,2
U24F	60,5	60,5	60,4	60,5	60,5	60,4	0,08	0,18	100,0
U24G	61,4	61,4	61,4	61,4	61,4	61,2	0,20	0,18	NA
U24H	60,2	60,3	60,2	60,2	60,2	60	0,22	0,18	NA
U24I	60,2	60,1	59,9	60,1	60,1	59,9	0,18	0,18	NA
U24J	60,0	59,8	59,8	59,8	59,9	59,6	0,25	0,18	See below
U24K	60,6	60,5	60,4	60,4	60,5	60,3	0,18	0,18	See below
U24L	60,1	60,2	60,1	60,2	60,2	60,2	0,05	0,18	See below
U24M	60,2	60,1	60,2	60,1	60,2	59,9	0,25	0,18	See below
U24N	60,5	60,4	60,5	60,4	60,5	60,5	0,05	0,18	See below
U24O	60,6	60,4	60,6	60,5	60,5	60,4	0,13	0,18	See below
U24P	59,8	59,5	59,6	59,6	59,6	59,4	0,23	0,18	100,4
U24Q	60,0	60,0	60,0	60,0	60,0	60,0	0,00	0,18	100,2
U24R	60,4	60,4	60,4	60,2	60,4	60,4	0,05	0,18	100,3
U24S	59,6	59,7	59,8	59,7	59,7	59,3	0,40	0,18	100,3
U24Gbis	60,4	60,5	60,4	60,5	60,5	60,4	0,05	0,18	100,2
						MEAN	0,18		100,15

Table 55 U24 STA Specimen geometric expansion

AFTER LONG-TERM AGING											
U24											
D = 100 mm	[mm]	[mm]	[mm]	[mm]	[mm]	[mm]	[mm]	[mm]	[mm]	[mm]	[mm]
Specimen LTA	H_1	H_2	H_3	H_4	Average	Compactor Height	Difference	ΔDiff	Average diameter	Mean Increase	Mean Diameter
U24J	60,1	60,0	60,1	60,0	60,1	59,6	0,4	0,20	100,3	0,20	100,24
U24K	60,2	60,4	60,4	60,2	60,3	60,3	0,0	-0,18	100,2	0,20	100,24
U24L	60,3	60,3	60,2	60,2	60,3	60,2	0,0	0,00	100,3	0,20	100,24
U24M	60,3	60,5	60,4	60,2	60,4	59,9	0,4	0,20	100,3	0,20	100,24
U24N	60,5	60,5	60,5	60,5	60,5	60,5	0,0	-0,05	100,2	0,20	100,24
U24O	60,6	60,7	60,6	60,7	60,7	60,4	0,3	0,13	100,3	0,20	100,24
						Mean	0,20				

Table 56 U24 LTA Specimen geometric expansion

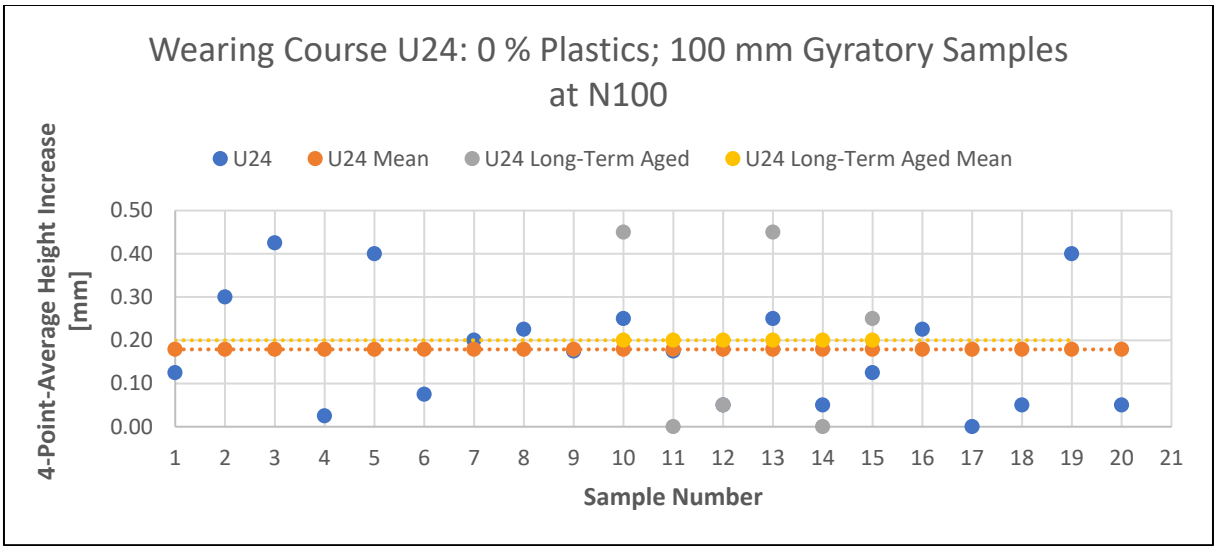

Figure 113 U24 Height increase results

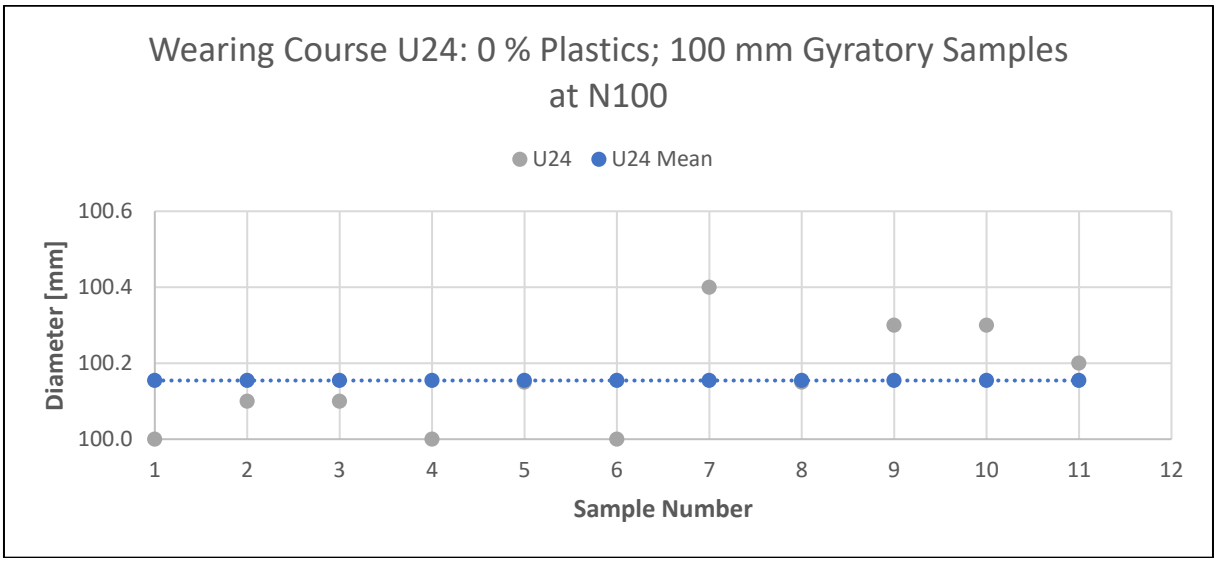

Figure 114 U24 STA diameter increase results

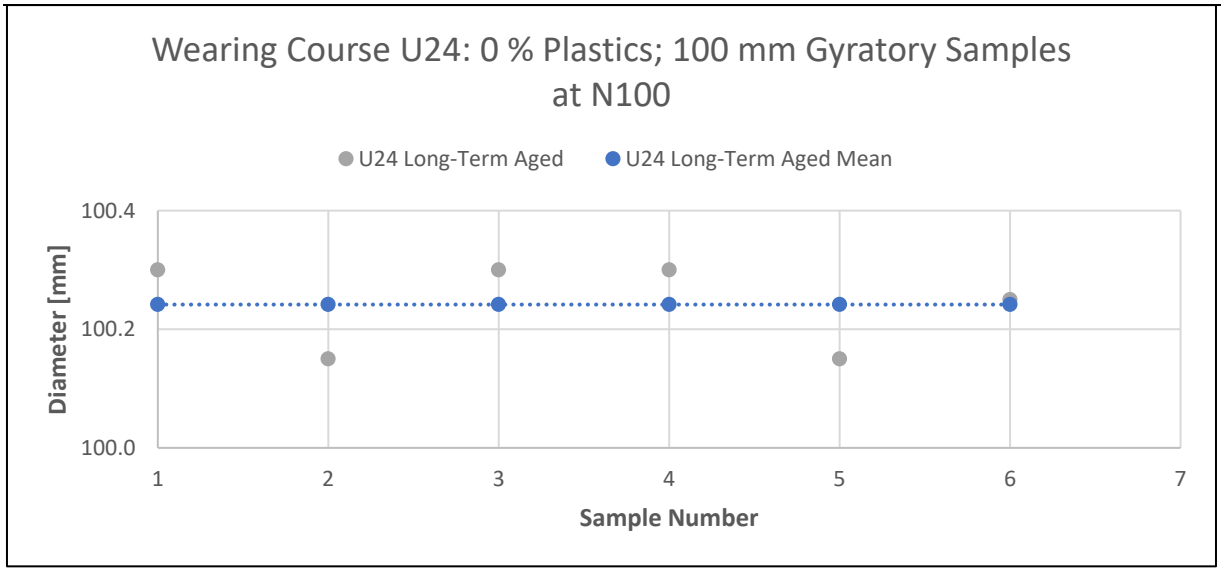

Figure 115 U24 LTA diameter increase

U24PS0,5									
D = 100 mm	[mm]	[mm]	[mm]	[mm]	[mm]	[mm]	[mm]	[mm]	[mm]
Specimen	H_1	H_2	H_3	H_4	Average	Compactor Height	Difference	Mean Increase	Diameter
U24PS0,5A	60,0	60,1	60,0	59,7	60,0	59,5	0,45	0,34	100,3
U24PS0,5B	60,7	60,8	60,5	60,4	60,6	60,2	0,40	0,34	100,0
U24PS0,5C	60,5	60,7	60,6	60,6	60,6	60,1	0,50	0,34	100,2
U24PS0,5D	61,3	61,1	61,1	61,0	61,1	60,9	0,23	0,34	100,0
U24PS0,5E	61,4	61,1	61,1	61,5	61,3	60,9	0,38	0,34	100,2
U24PS0,5F	60,5	60,4	60,4	61,0	60,6	60,1	0,48	0,34	100,2
U24PS0,5G	61,0	61,0	61,0	61,1	61,0	60,8	0,23	0,34	NA
U24PS0,5H	60,1	60,1	60,1	60,2	60,1	59,7	0,42	0,34	NA
U24PS0,5I	60,2	60,5	60,4	60,4	60,4	60,2	0,17	0,34	NA
U24PS0,5J	60,4	60,3	60,4	60,2	60,3	59,8	0,53	0,34	See below
U24PS0,5K	60,7	60,8	60,6	60,7	60,7	60,3	0,40	0,34	See below
U24PS0,5L	60,1	60,2	60,3	60,0	60,2	59,7	0,45	0,34	See below
U24PS0,5 M	60,6	60,6	60,8	60,6	60,7	60,7	0,05	0,34	See below
U24PS0,5N	61,0	60,9	61,2	61,1	61,1	60,7	0,35	0,34	See below
U24PS0,5O	61,6	61,2	61,4	61,4	61,4	61,1	0,30	0,34	See below
U24PS0,5P	61,1	61,1	61,0	61,1	61,1	60,9	0,17	0,34	100,5
U24PS0,5Q	60,4	60,5	60,4	60,3	60,4	60,2	0,20	0,34	100,1
U24PS0,5R	60,4	60,1	60,7	60,6	60,5	59,9	0,55	0,34	100,3
U24PS0,5S	60,5	61,0	60,7	60,6	60,7	60,4	0,30	0,34	100,3
						MEAN	0,34		100,20

Table 57 U24PS0,5 STA Specimen geometric expansion

AFTER LONG-TERM AGING
U24PS0,5

D = 100 mm	[mm]	[mm]	[mm]	[mm]	[mm]	[mm]	[mm]	[mm]	[mm]	[mm]	[mm]
Specimen LTA	H_1	H_2	H_3	H_4	Average	Compactor Height	Difference	ΔDiff	Average diameter	Mean Increase	Mean Diameter
U24PS0,5J	60,4	60,4	60,2	60,1	60,3	59,8	0,48	-0,05	100,3	0,40	100,26
U24PS0,5K	60,9	60,8	60,8	60,7	60,8	60,3	0,50	0,10	100,2	0,40	100,26
U24PS0,5L	60,3	60,1	60,2	60,4	60,3	59,7	0,55	0,10	100,3	0,40	100,26
U24PS0,5M	60,9	60,9	60,7	60,8	60,8	60,7	0,13	0,07	100,2	0,40	100,26
U24PS0,5N	61,3	61,2	61,1	60,9	61,1	60,7	0,42	0,07	100,3	0,40	100,26
U24PS0,5O	61,4	61,4	61,4	61,4	61,4	61,1	0,30	0,00	100,4	0,40	100,26
						Mean	0,40				

Table 58 U24PS0,5 LTA Specimen geometric expansion

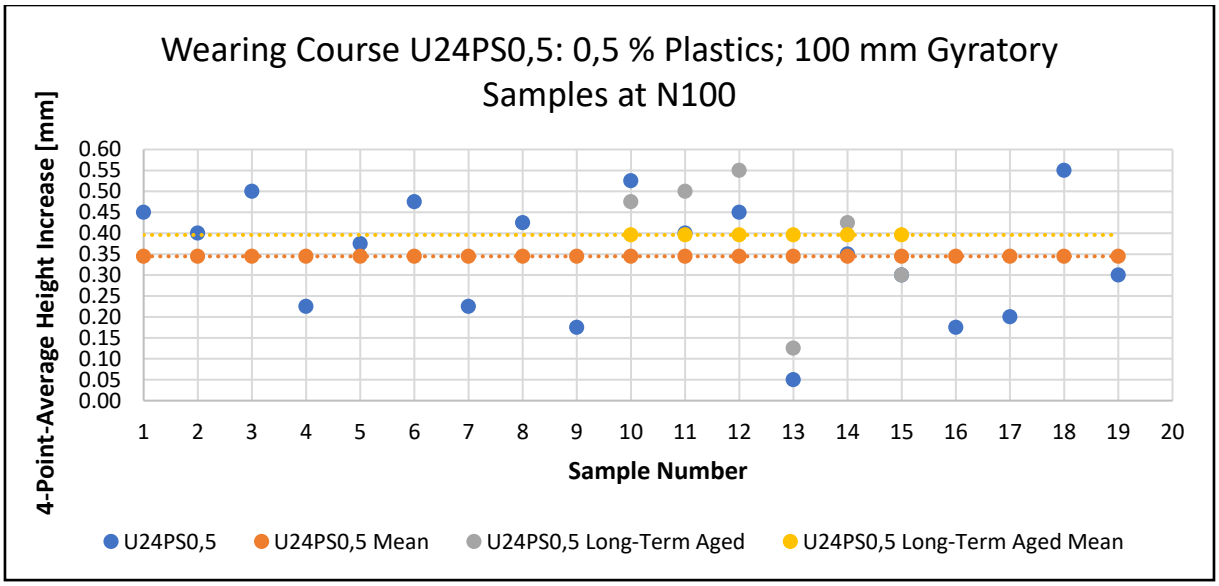

Figure 116 U24PS0,5 Height increase results

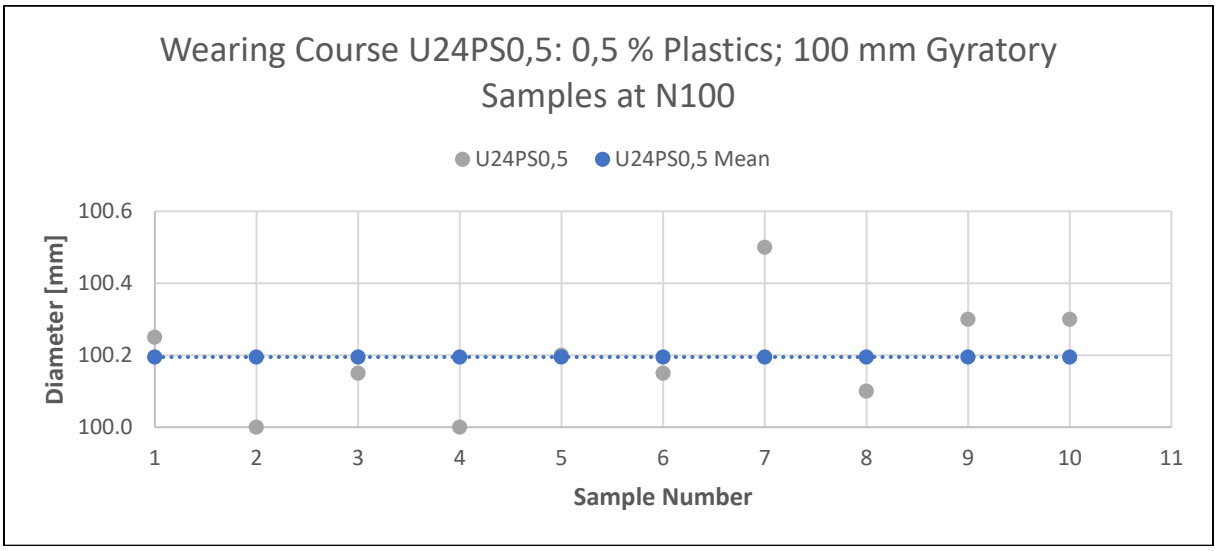

Figure 117 U24PS0,5 STA diameter increase results

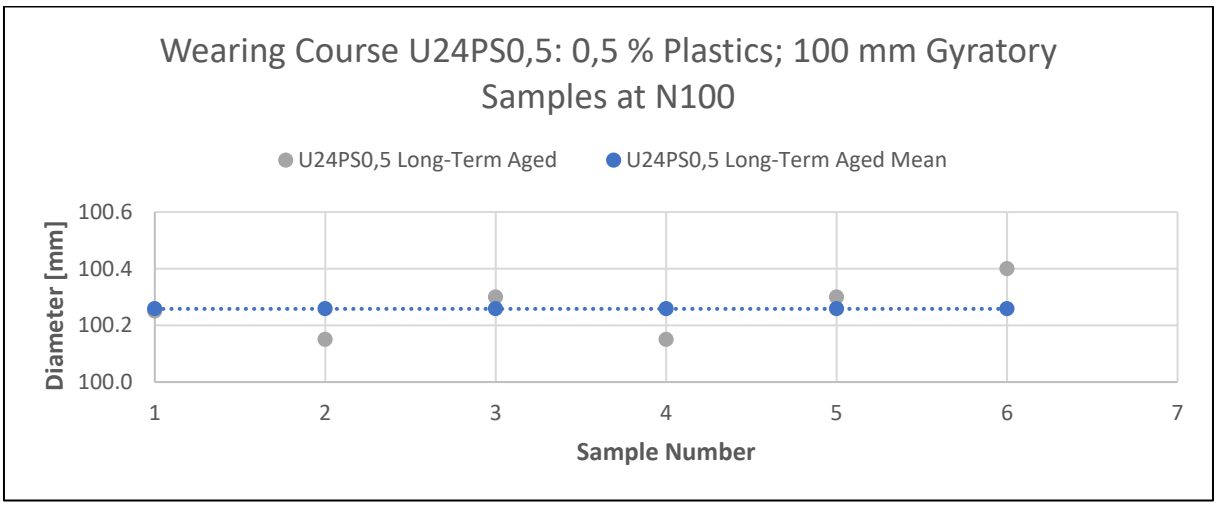

Figure 118 U24PS0,5 LTA diameter increase results

U24PS1									
D = 100 mm	[mm]	[mm]	[mm]	[mm]	[mm]	[mm]	[mm]	[mm]	[mm]
Specimen	H_1	H_2	H_3	H_4	Average	Compactor Height	Difference	Mean Increase	Diameter
U24PS1A	60,6	60,8	60,9	60,9	60,8	60,0	0,80	0,42	100,3
U24PS1B	60,8	60,6	60,6	60,8	60,7	60,4	0,30	0,42	NA
U24PS1C	60,4	60,7	60,6	60,4	60,5	60,0	0,52	0,42	100,1
U24PS1D	60,8	60,9	60,8	60,8	60,8	60,6	0,23	0,42	100,0
U24PS1E	60,7	60,5	60,6	60,8	60,7	60,4	0,25	0,42	100,1
U24PS1F	60,0	60,1	60,0	60,2	60,1	59,6	0,48	0,42	100,1
U24PS1G	60,2	60,0	60,3	60,3	60,2	59,7	0,50	0,42	NA
U24PS1H	60,8	60,8	60,9	60,8	60,8	60,6	0,23	0,42	NA
U24PS1I	61,0	60,8	60,8	60,9	60,9	60,5	0,38	0,42	NA
U24PS1J	60,7	60,8	60,8	60,7	60,8	60,4	0,35	0,42	See below
U24PS1K	60,2	60,3	60,3	60,5	60,3	59,7	0,63	0,42	See below
U24PS1L	60,0	60,3	60,5	60,4	60,3	59,8	0,50	0,42	See below
U24PS1M	61,0	61,2	61,0	61,2	61,1	60,8	0,30	0,42	See below
U24PS1N	60,1	60,3	60,3	60,4	60,3	60,3	0,02	0,42	See below
U24PS1O	60,2	59,9	60,0	60,0	60,0	59,6	0,42	0,42	See below
U24PS1P	61,0	60,9	61,0	61,1	61,0	60,8	0,20	0,42	100,4
U24PS1Q	60,4	60,1	60,0	60,1	60,2	59,5	0,65	0,42	100,3
U24PS1R	61,2	61,5	61,5	61,2	61,4	60,9	0,45	0,42	100,6
U24PS1S	60,8	60,7	60,8	61,0	60,8	60,3	0,53	0,42	100,3
U24PS1Bbis	60,9	61,2	61,4	61,5	61,3	60,6	0,65	0,42	100,3
						MEAN	0,42		100,22

Table 59 U24PS1 STA Specimen geometric expansion

AFTER LONG-TERM AGING
U24PS1

D = 100 mm	[mm]	[mm]	[mm]	[mm]	[mm]	[mm]	[mm]	[mm]	[mm]	[mm]	[mm]
Specimen LTA	H_1	H_2	H_3	H_4	Average	Compactor Height	Difference	ΔDiff	Average diameter	Mean Increase	Mean Diameter
U24PS1J	60,6	60,7	60,8	60,9	60,8	60,4	0,35	0,00	100,4	0,51	100,40
U24PS1K	60,2	60,4	60,1	60,5	60,3	59,7	0,60	-0,03	100,3	0,51	100,40
U24PS1L	60,3	60,3	60,8	60,6	60,5	59,8	0,70	0,20	100,5	0,51	100,40
U24PS1M	61,5	61,2	61,3	61,2	61,3	60,8	0,50	0,20	100,4	0,51	100,40
U24PS1N	60,6	60,7	60,6	60,8	60,7	60,3	0,38	0,35	100,4	0,51	100,40
U24PS1O	60,0	60,3	60,2	60,0	60,1	59,6	0,52	0,10	100,5	0,51	100,40
						Mean	0,51				

Table 60 U24PS1 LTA Specimen geometric expansion

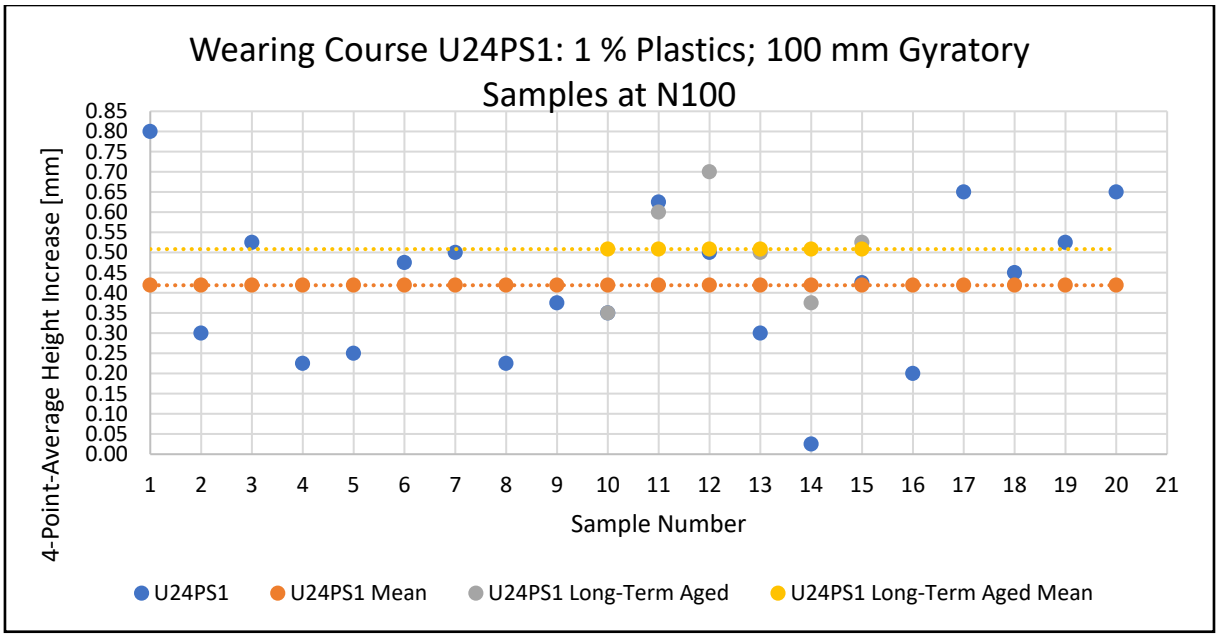

Figure 119 U24PS1 Height increase results

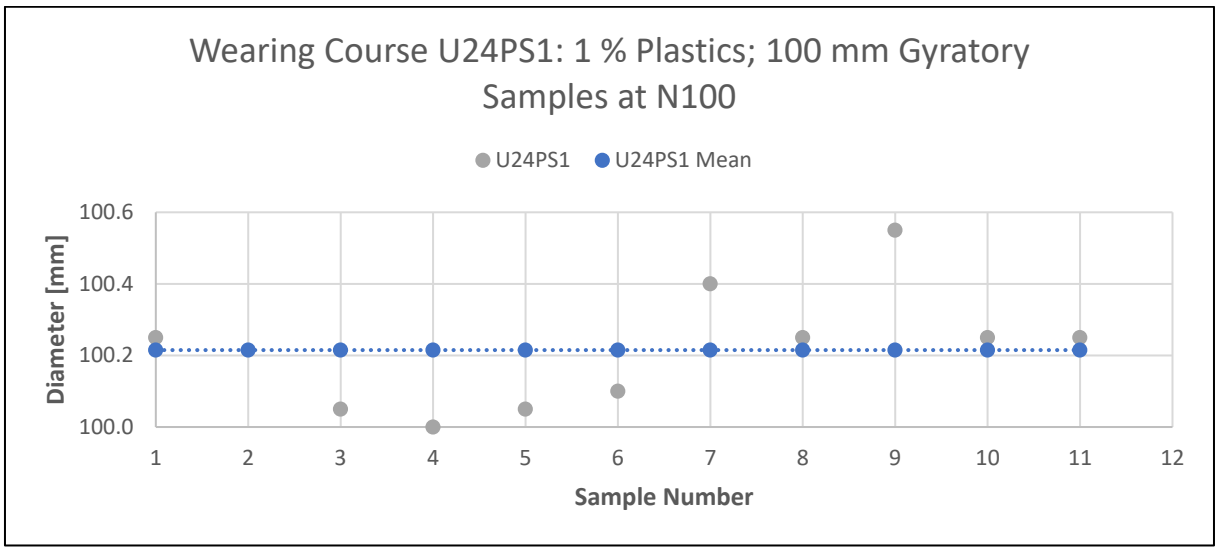

Figure 120 U24PS1 STA diameter increase results

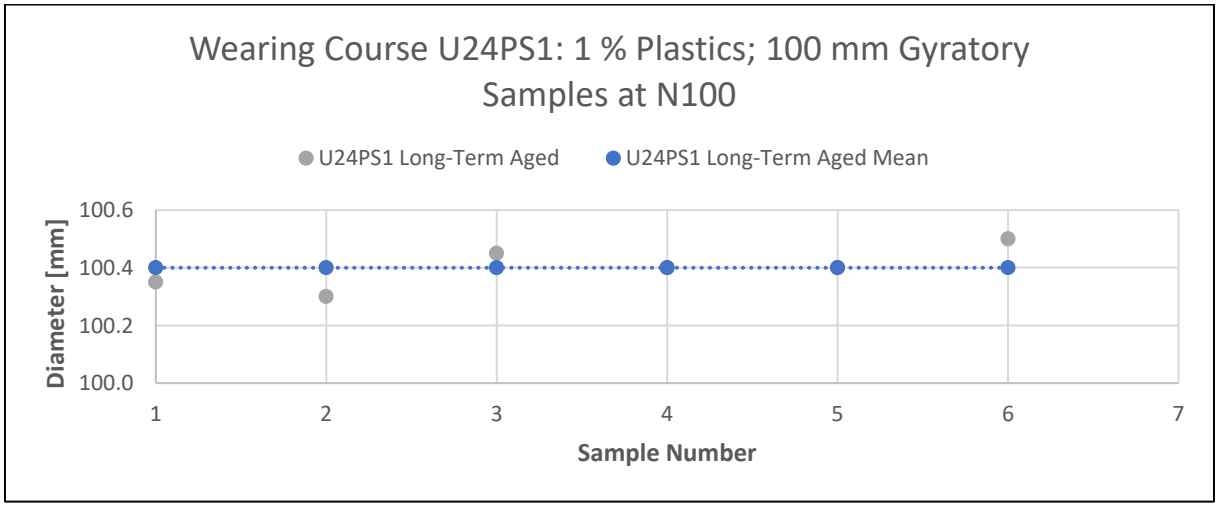

Figure 121 U24PS1 LTA diameter increase results

Annex VI.ITSM IT-CY Stiffness Modulus test results

ITSM IT-CY	Stiffness Modulus [Mpa] Test Temperature [°C]				v_{real}
Specimen	10	20	25	30	[%]
U24A	13830	7398	NA	3062	0,70
U24B	15958	7778	NA	3031	0,75
U24C	15296	7503	NA	3306	0,42
U24D	15897	7496	NA	3052	1,14
U24E	16495	7761	NA	3327	0,76
U24F	17004	7605	NA	3308	0,91
U24G	15065	NA	NA	NA	1,80
U24Gbis	NA	NA	3647	NA	0,93
U24H	17168	NA	5450	NA	0,90
U24I	18285	NA	5851	NA	0,56
U24P	NA	7963	NA	NA	0,42
U24Q	NA	NA	5828	NA	0,23
U24R	NA	NA	5591	NA	0,78
U24S	NA	NA	5033	NA	0,37
MEAN STA	***16111***	***7643***	***5233***	***3181***	***0,76***
Standard Deviation STA	***1314***	***199***	***833***	***146***	***0,39***
U24J LTA	16765	7972	NA	3468	0,88
U24K LTA	17261	8730	NA	3687	0,63
U24L LTA	17306	9941	NA	3914	0,51
U24M LTA	18488	9579	NA	4260	0,95
U24N LTA	17794	8784	NA	4089	0,84
U24O LTA	16078	8674	NA	3579	1,18
MEAN LTA	***17282***	***8947***	***NA***	***3833***	***0,83***
Standard Deviation LTA	***829***	***705***	***NA***	***308***	***0,23***

Table 61 U24 Stiffness Modulus results at 10, 20, 25, 30 degrees Celsius

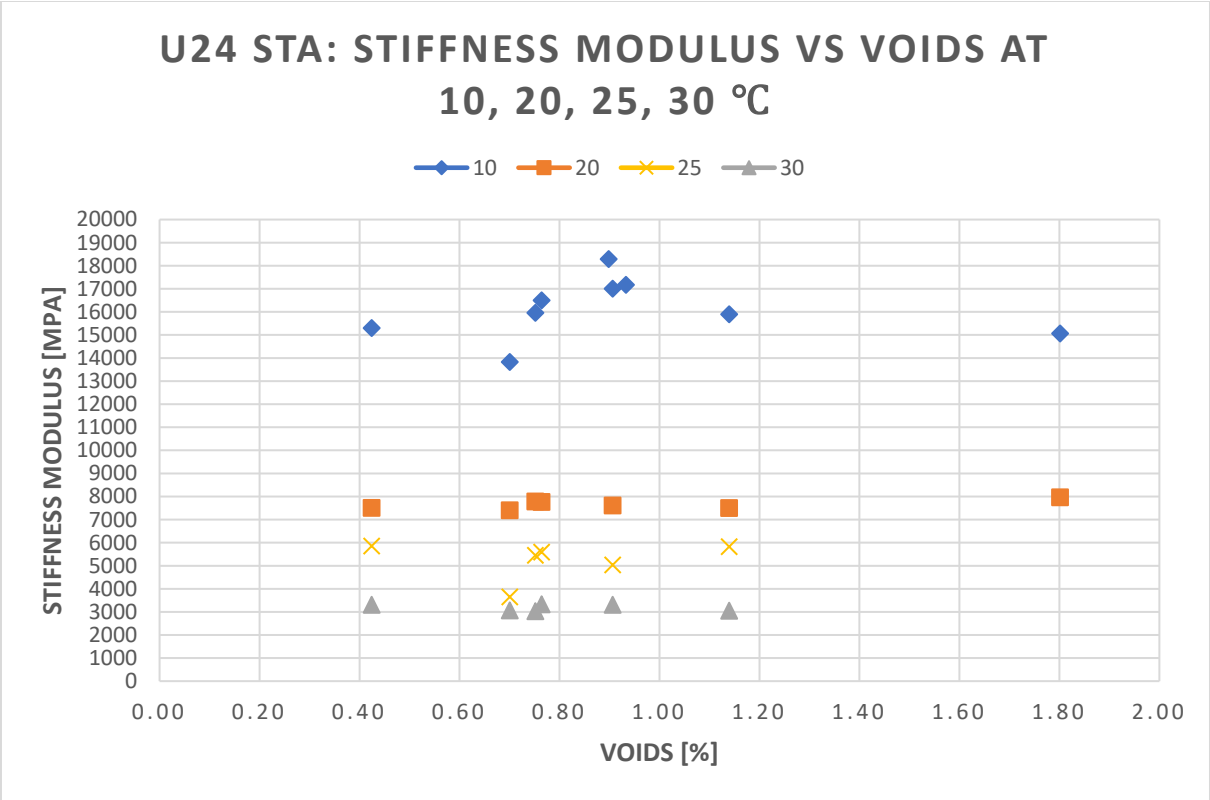

Figure 122 U24 STA Stiffness modulus [MPa] vs void content [%] at 10, 20, 25, 30 degrees Celsius

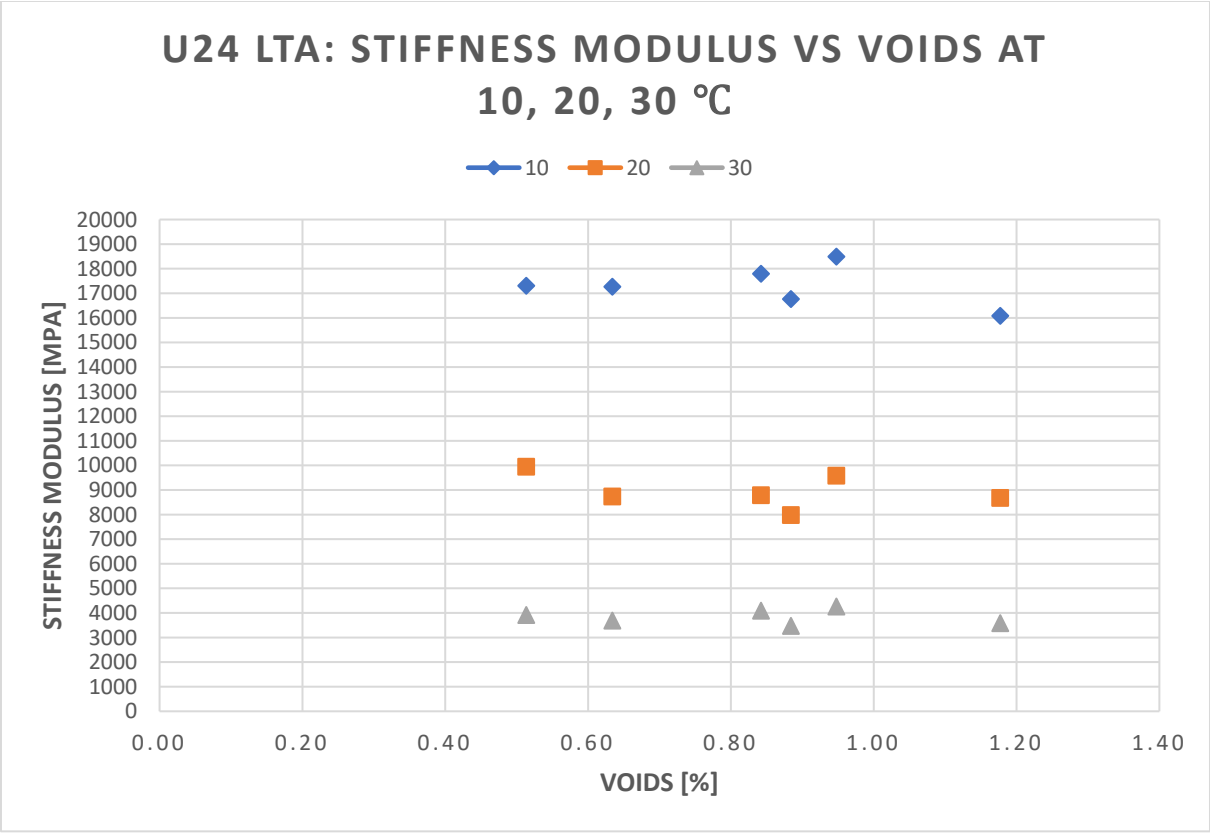

Figure 123 U24 LTA Stiffness modulus [MPa] vs void content [%] at 10, 20, 25, 30 degrees Celsius

ITSM IT-CY	Stiffness Modulus [Mpa] Test Temperature [°C]				v_{real}
Specimen	10	20	25	30	[%]
U24PS0,5A	15502	7926	NA	3627	2,42
U24PS0,5B	17468	8483	NA	3939	3,43
U24PS0,5C	16456	8231	NA	3710	3,22
U24PS0,5D	15712	7793	NA	3587	3,68
U24PS0,5E	14764	7581	NA	3469	4,43
U24PS0,5F	16739	8229	NA	3744	3,71
U24PS0,5G	15761	NA	5701	NA	4,20
U24PS0,5H	16799	NA	6508	NA	2,98
U24PS0,5I	16318	NA	5957	NA	3,02
U24PS0,5Q	NA	NA	6615	NA	2,69
U24PS0,5R	NA	NA	6825	NA	2,84
U24PS0,5S	NA	NA	5690	NA	3,51
U24PS0,5P	NA	7491	NA	NA	4,28
Mean STA	***16169***	***7962***	***6216***	***3679***	***3,42***
Standard Deviation STA	***815***	***368***	***495***	***160***	***0,63***
U24J LTA	17173	9075	NA	4457	3,04
U24K LTA	16044	9460	NA	4223	3,14
U24L LTA	19218	9435	NA	5139	2,80
U24M LTA	19269	9712	NA	4904	3,75
U24N LTA	16520	9439	NA	4217	3,75
U24O LTA	17344	9318	NA	4167	4,40
Mean LTA	***17594***	***9406***	***NA***	***4518***	***3,48***
Standard Deviation LTA	***1359***	***208***	***NA***	***410***	***0,59***

Table 62 U24PS0,5 Stiffness Modulus results at 10, 20, 25, 30 degrees Celsius

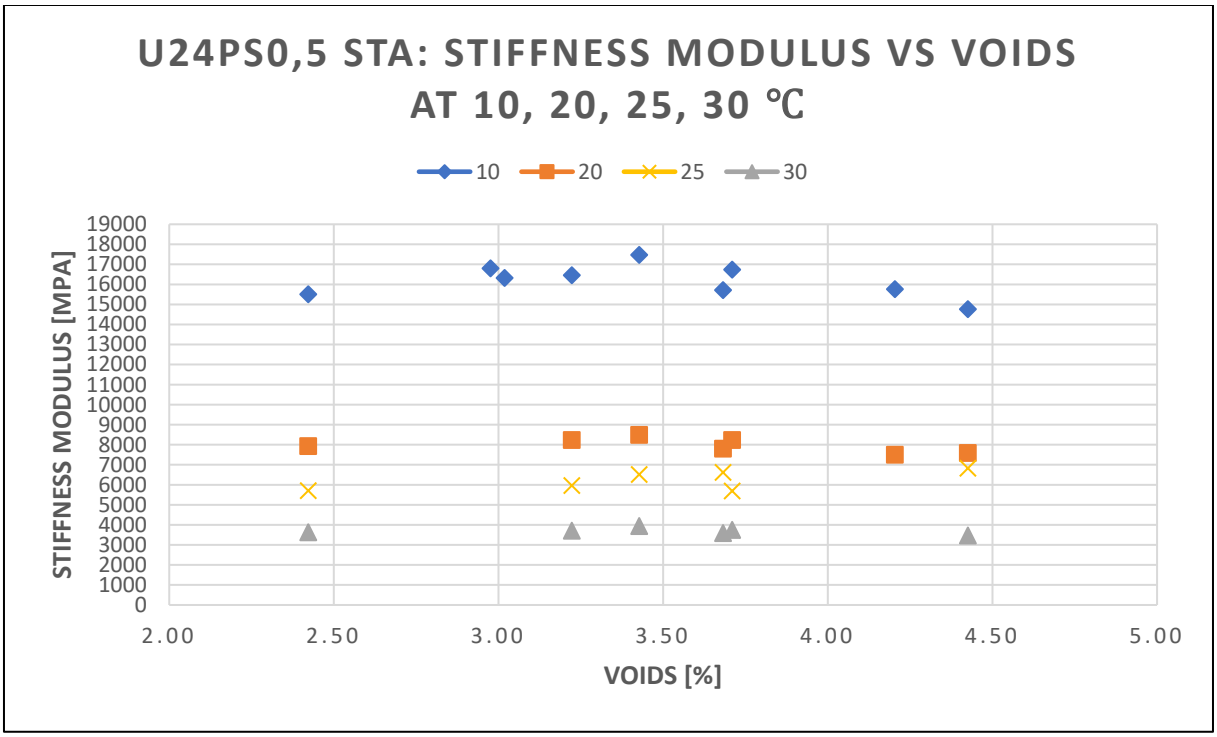

Figure 124 U24PS0,5 STA Stiffness modulus [MPa] vs void content [%] at 10, 20, 25, 30 degrees Celsius

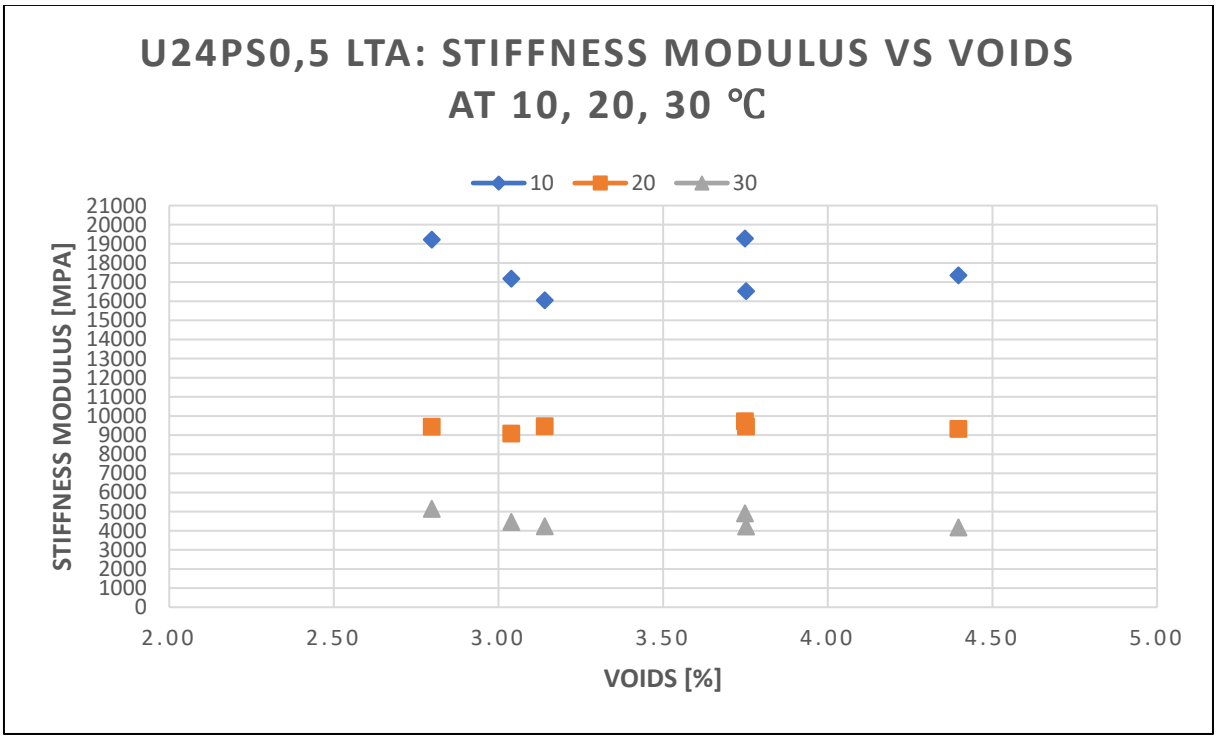

Figure 125 U24PS0,5 LTA Stiffness modulus [MPa] vs void content [%] at 10, 20, 25, 30 degrees Celsius

ITSM IT-CY	Stiffness Modulus [Mpa] Test Temperature [°C]				v_{real}
Specimen	10	20	25	30	[%]
U24PS1A	16299	7115	NA	3095	3,20
U24PS1B	15082	7311	NA	NA	2,77
U24PS1Bbis	NA	7881	NA	NA	3,39
U24PS1C	14884	6959	NA	2729	2,48
U24PS1D	15004	7093	NA	3098	2,52
U24PS1E	14162	6389	NA	2805	2,84
U24PS1F	16350	7409	NA	3316	1,92
U24PS1G	17160	NA	5817	NA	2,08
U24PS1H	15152	NA	4817	NA	2,72
U24PS1I	16432	NA	5800	NA	3,13
U24PS1P	NA	NA	4915	NA	3,43
U24PS1Q	NA	NA	5527	NA	2,14
U24PS1R	NA	8109	NA	NA	3,91
U24PS1S	NA	NA	5143	NA	2,63
MEAN STA	***15614***	***7283***	***5337***	***3009***	***2,80***
Standard Deviation STA	***973***	***538***	***440***	***240***	***0,57***
U24PS1J LTA	17475	7906	NA	4128	2,79
U24PS1K LTA	16519	7932	NA	3836	2,51
U24PS1L LTA	17593	9359	NA	3918	2,48
U24PS1M LTA	15207	8558	NA	3802	3,77
U24PS1N LTA	15420	9109	NA	4357	2,48
U24PS1O LTA	18336	8917	NA	3736	2,02
MEAN LTA	***16758***	***8630***	***NA***	***3963***	***2,67***
Standard Deviation LTA	***1261***	***610***	***NA***	***236***	***0,59***

Table 63 U24PS1 Stiffness Modulus results at 10, 20, 25, 30 degrees Celsius

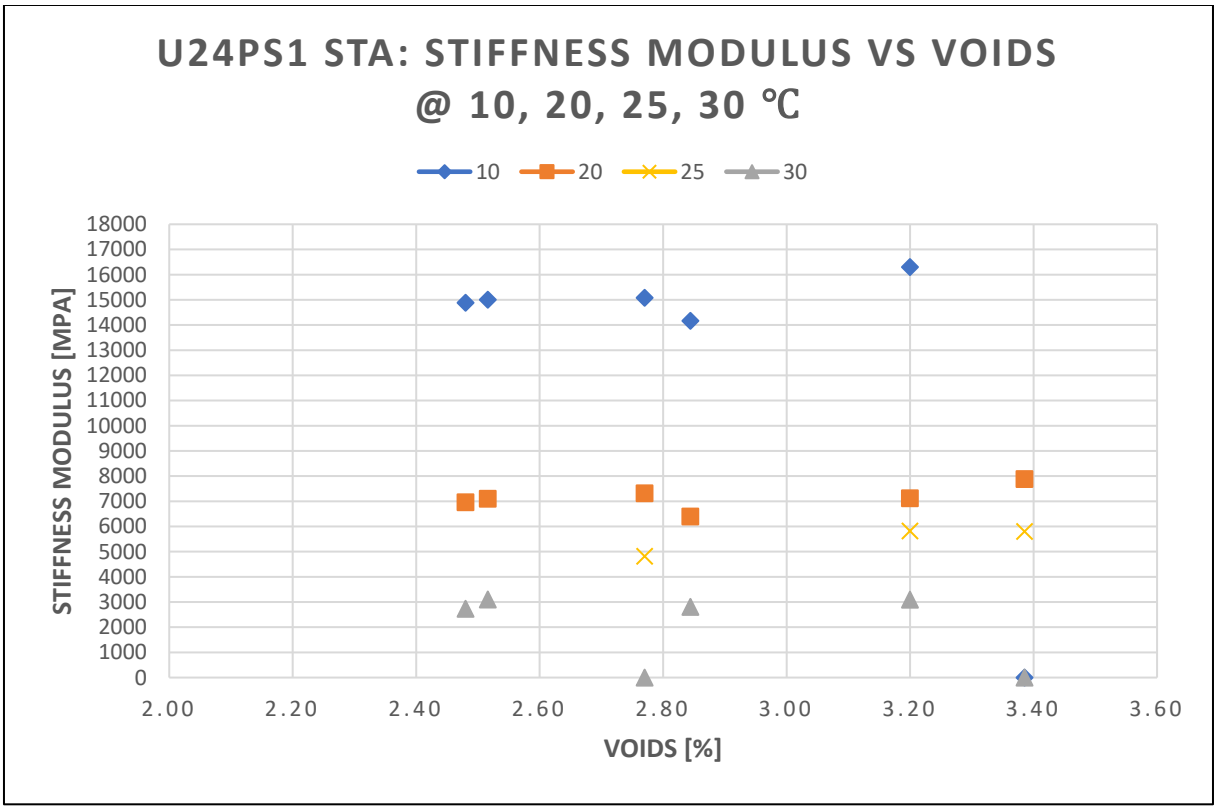

Figure 126 U24PS1 STA Stiffness modulus [MPa] vs void content [%] at 10, 20, 25, 30 degrees Celsius

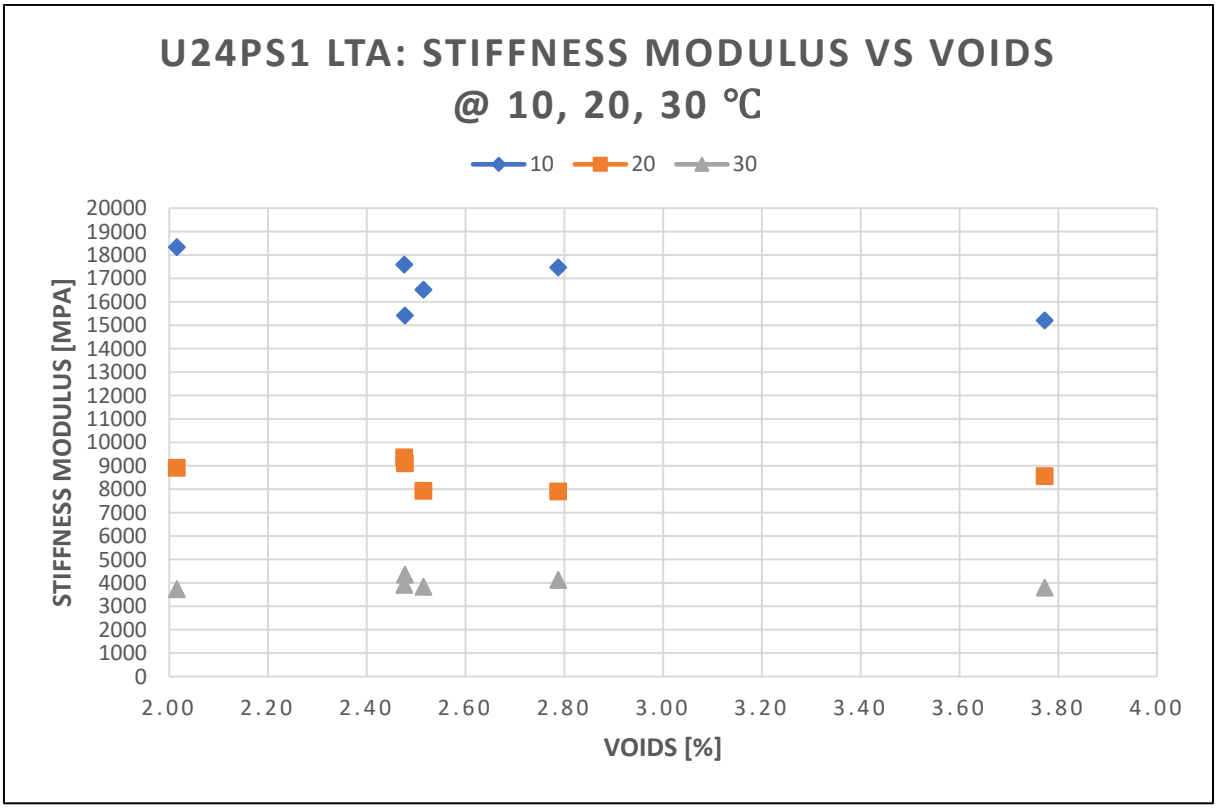

Figure 127 U24PS1 LTA Stiffness modulus [MPa] vs void content [%] at 10, 20, 25, 30 degrees Celsius

Annex VII. ITS test results

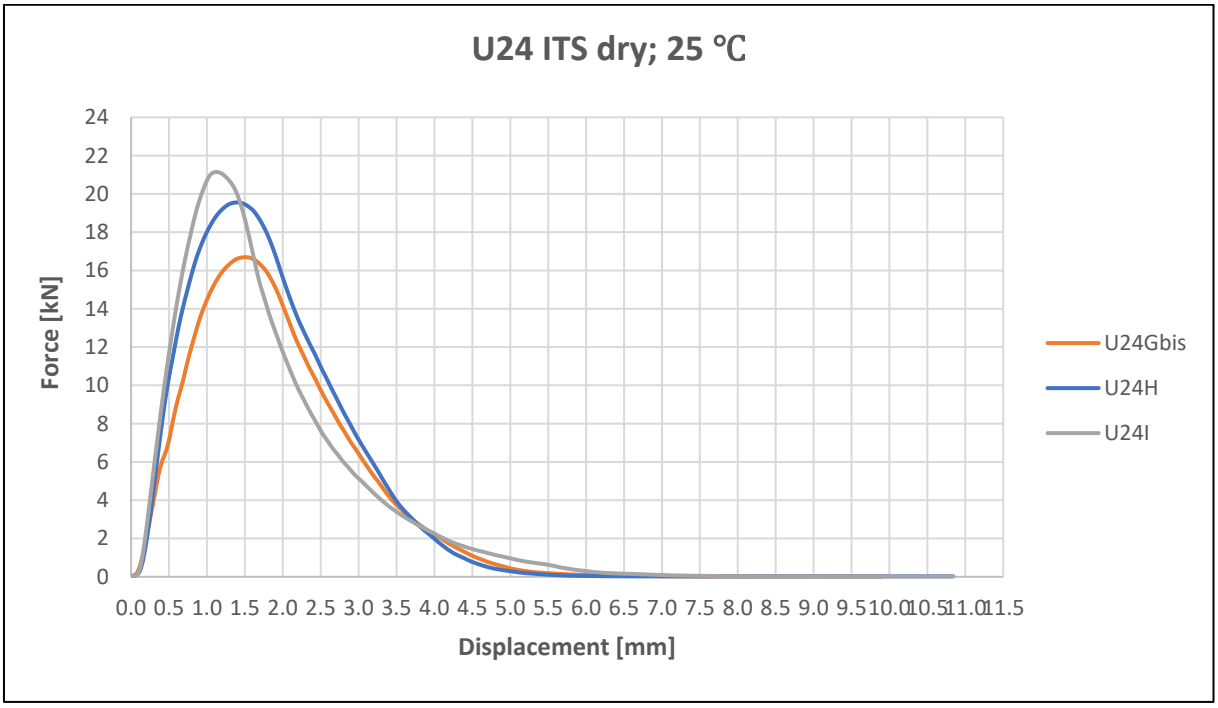

Figure 128 U24 ITS dry tests at 25 degrees Celsius: force [kN] vs displaement [mm]

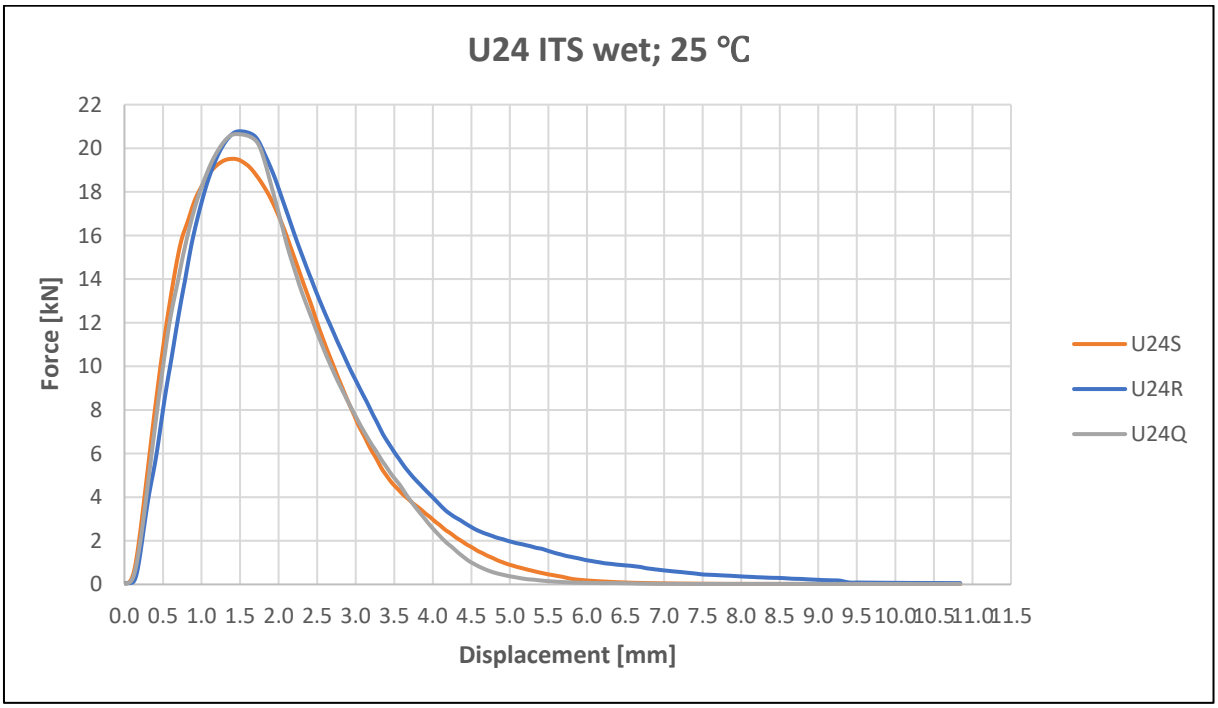

Figure 129 U24 ITS wet tests at 25 degrees Celsius: force [kN] vs displaement [mm]

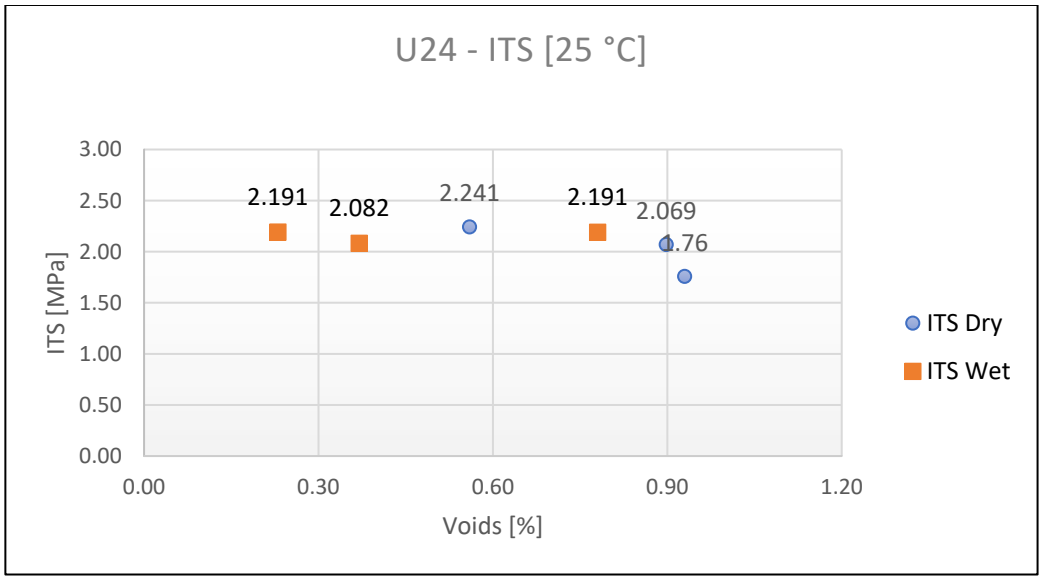

Figure 130 U24 ITS [MPa] vs void content [%]

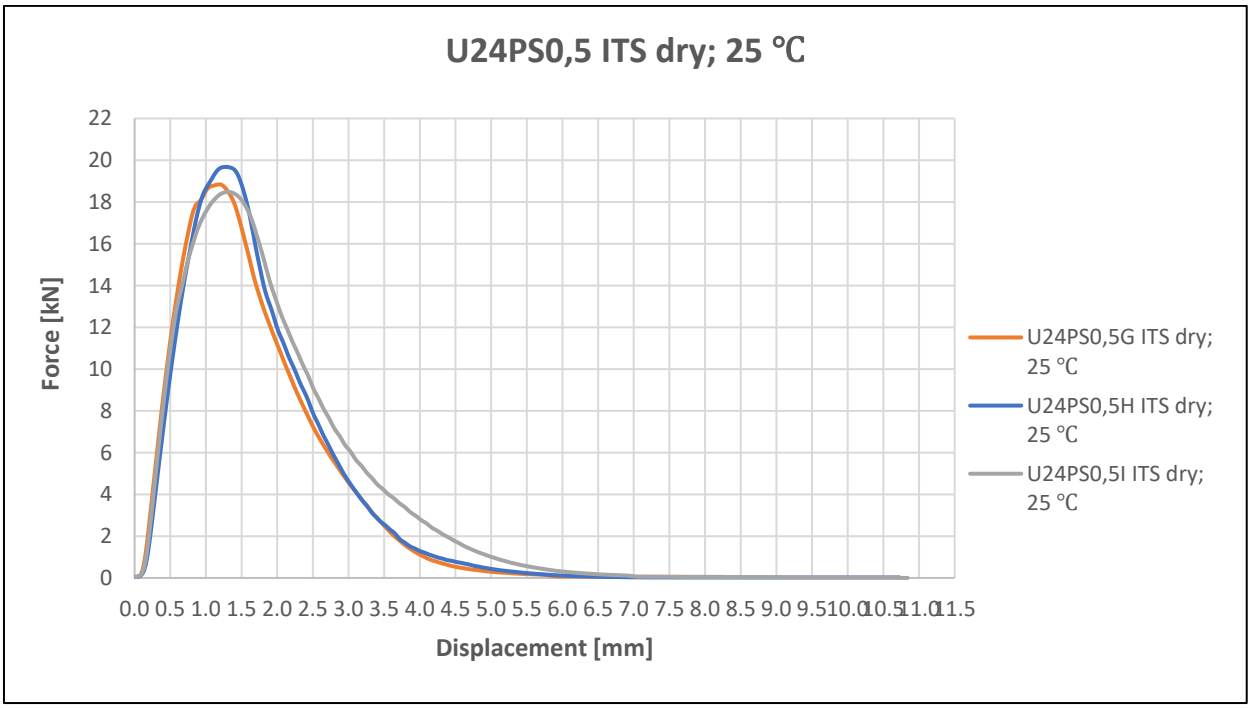

Figure 131 U24PS0,5 ITS dry tests at 25 degrees Celsius: force [kN] vs displaement [mm]

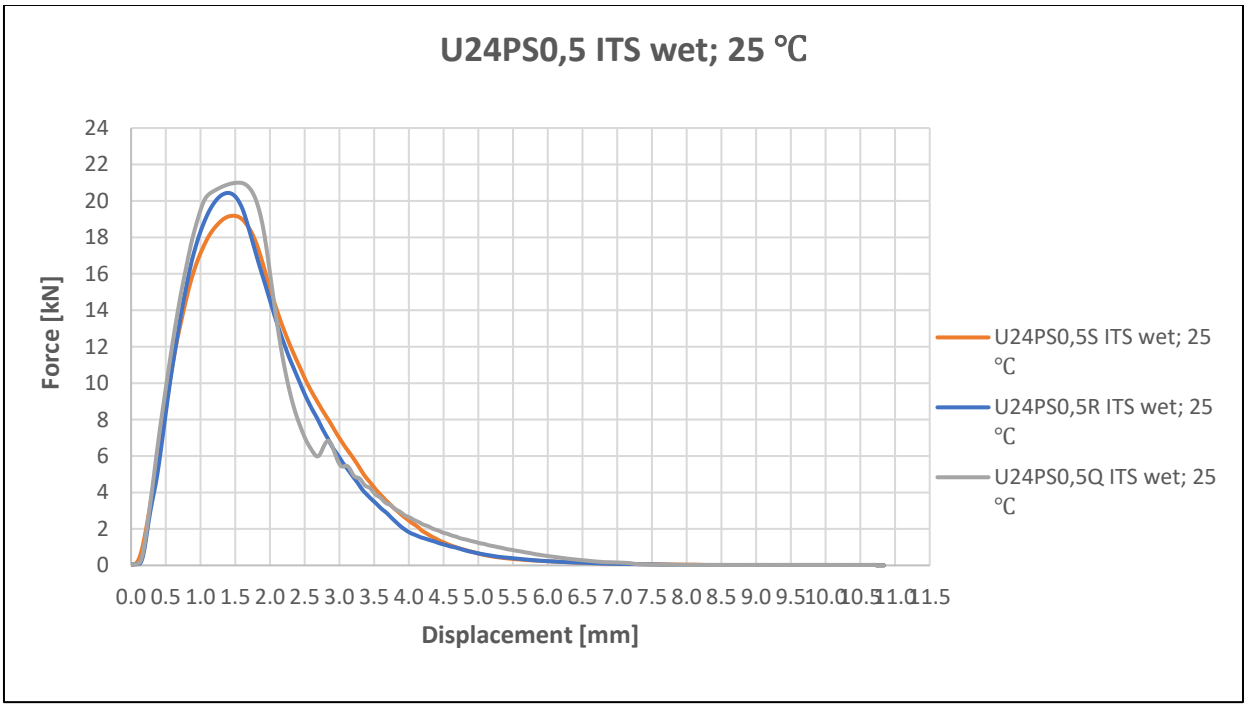

Figure 132 U24PS0,5 ITS wet tests at 25 degrees Celsius: force [kN] vs displaement [mm]

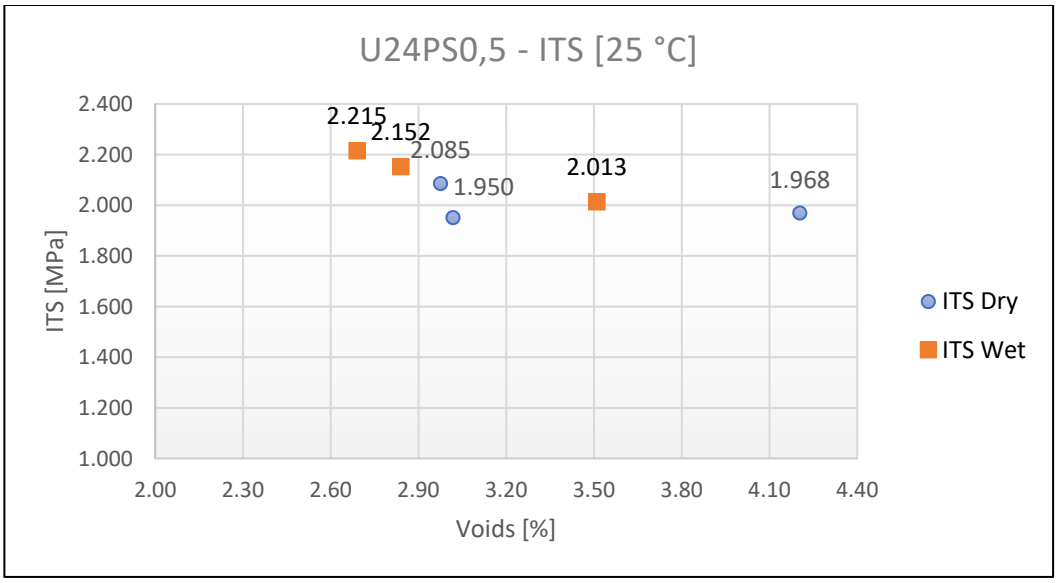

Figure 133 U24PS0,5 ITS [MPa] vs void content [%]

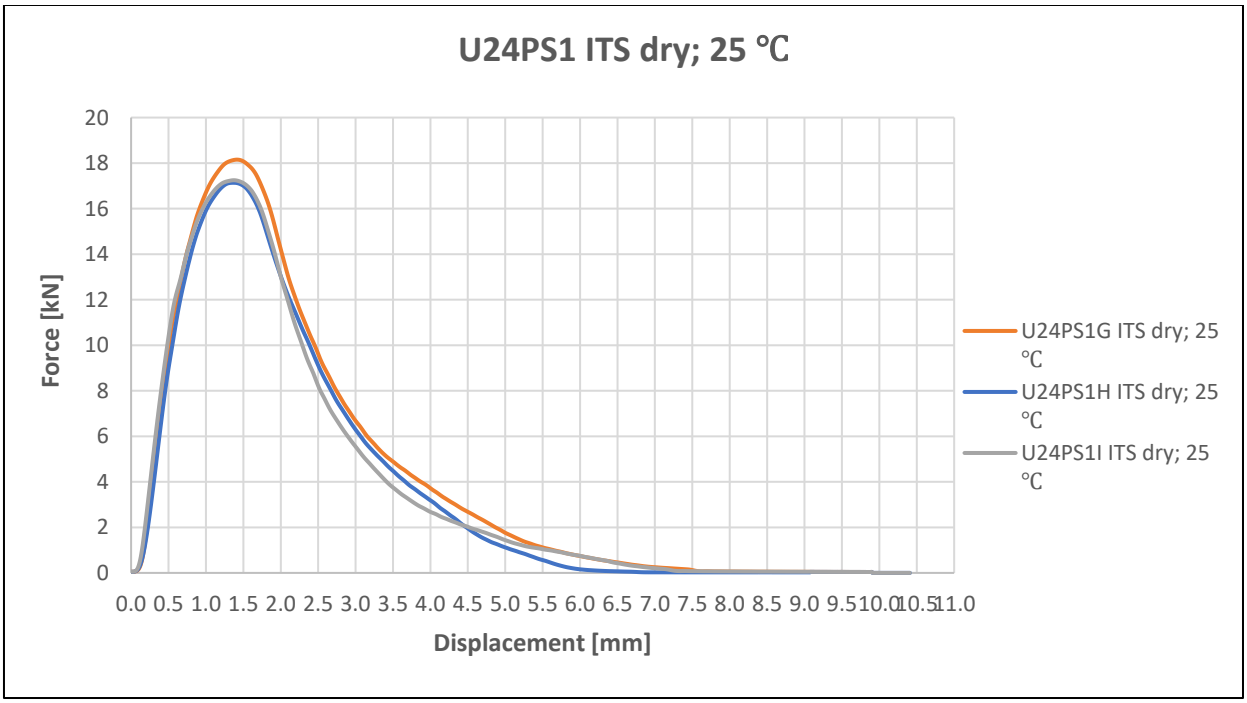

Figure 134 U24PS1 ITS dry tests at 25 degrees Celsius: force [kN] vs displaement [mm]

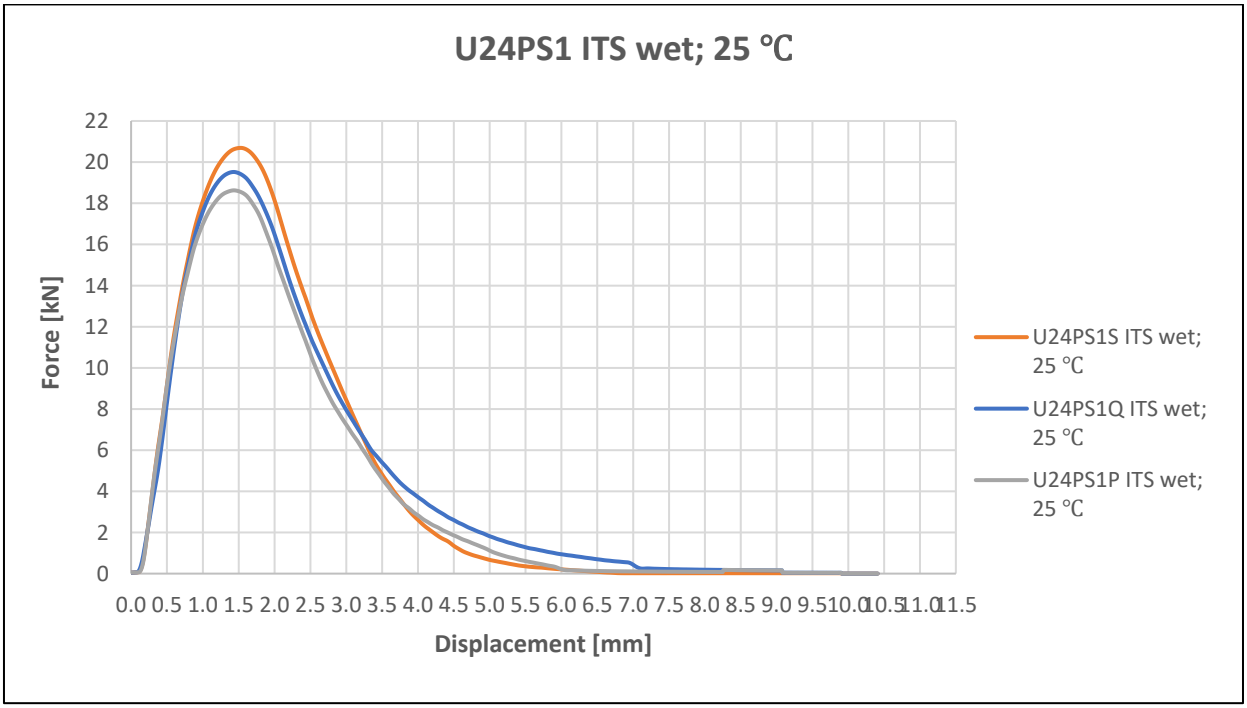

Figure 135 U24PS1 ITS wet tests at 25 degrees Celsius: force [kN] vs displaement [mm]

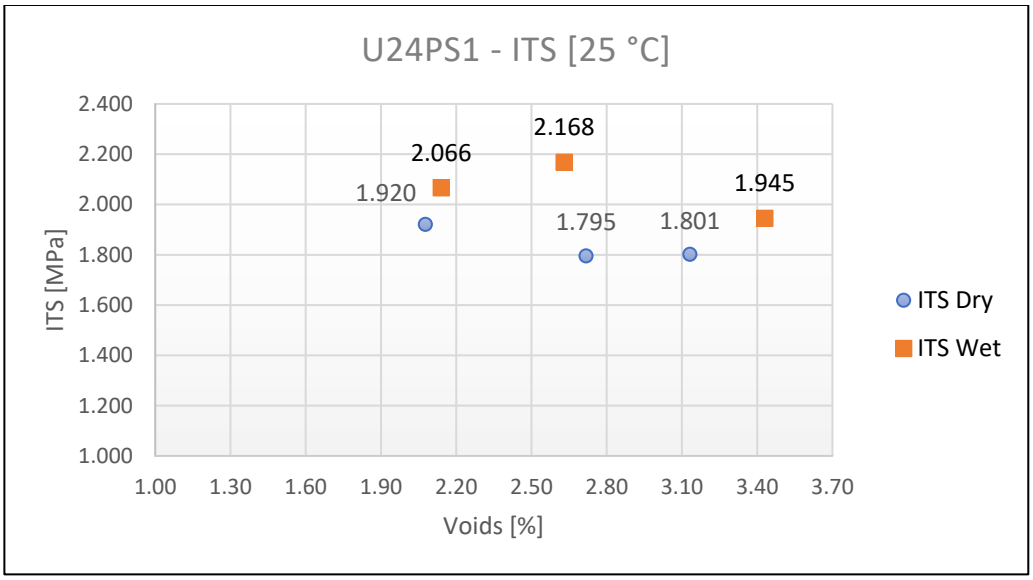

Figure 136 U24PS1 ITS [MPa] vs void content [%]

Annex VIII. CIT-CY Fatigue performance test results

Fatigue CIT-CY	Mean stress level [kPa] applied to specimens		
	1	2	3
STA	175	270	440
LTA	215	300	475

Table 64 Stress levels [kPa] applied in CIT-CY fatigue controlled-stress tests

Material	U24 Fatigue Line [20 °C]				
Temperature	20 °C				
d	100 mm				
ID	**E**	**s_0**	**εa**	**$N_{f\ (energy\ ratio)}$**	**$N_{f\ (sample\ break)}$**
	(MPa)	(kPa)	(µm/m)	(-)	(-)
U24A	7398	440	89,14	4540	5840
U24B	7778	(trial)	68,39	13010	16960
U24E	7761	440	90,39	5090	7290
U24C	7503	270	51,79	29750	43100
U24F	7605	175	32,22	496600	591460
U24P	7963	270	49,78	41250	55600
U24D	7496	175	32,87	453550	587970

Material	U24 LTA Fatigue Line [20 °C]				
Temperature	20 °C				
d	100 mm				
ID	**E**	**Stress level**	**εa**	**$N_{f\ (energy\ ratio)}$**	**$N_{f\ (sample\ break)}$**
	(MPa)	[-]	(µm/m)	(-)	(-)
U24N	8784	300	57,59	34420	46440
U24K	8730	475	99,17	2190	2840
U24M	9579	300	53,46	33540	44250
U24L	9941	475	99,23	2480	3340
U24J	7972	215	39,51	96850	126972
U24O	8674	215	41,90	169290	170700

Table 65 U24 sample initial horizontal strain amplitude, and fatigue life (using energy ratio or break criteria)

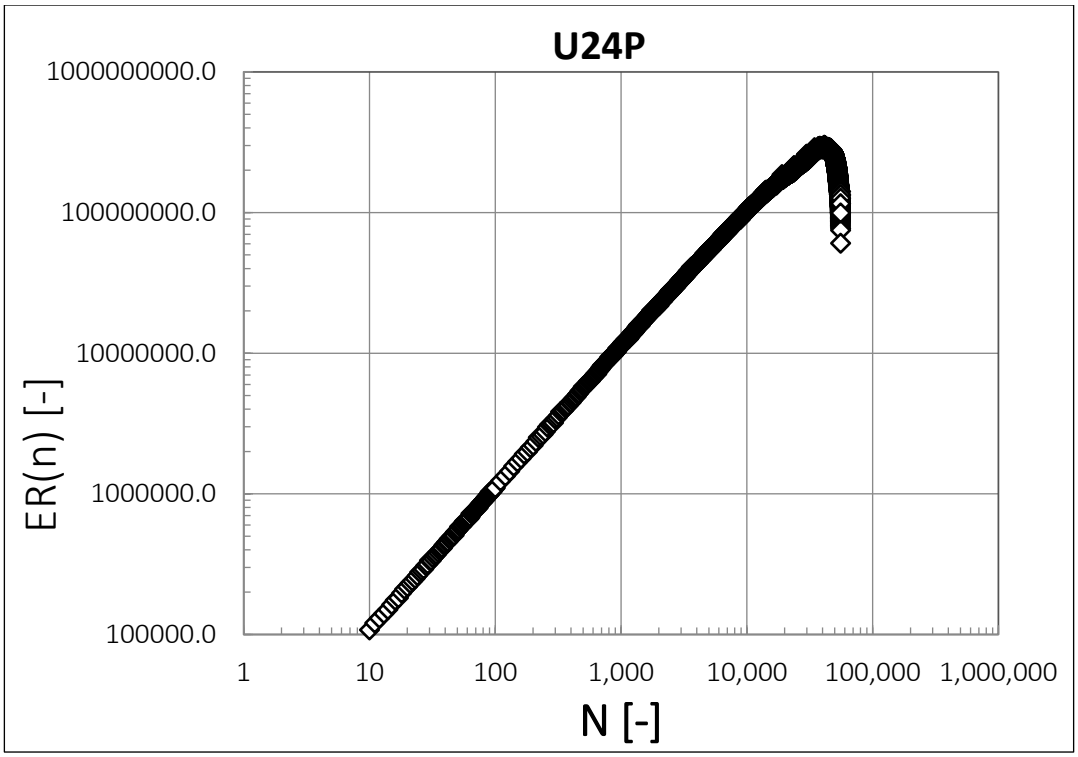

Figure 137 U24P sample energy ratio [-] vs load cycle [-]

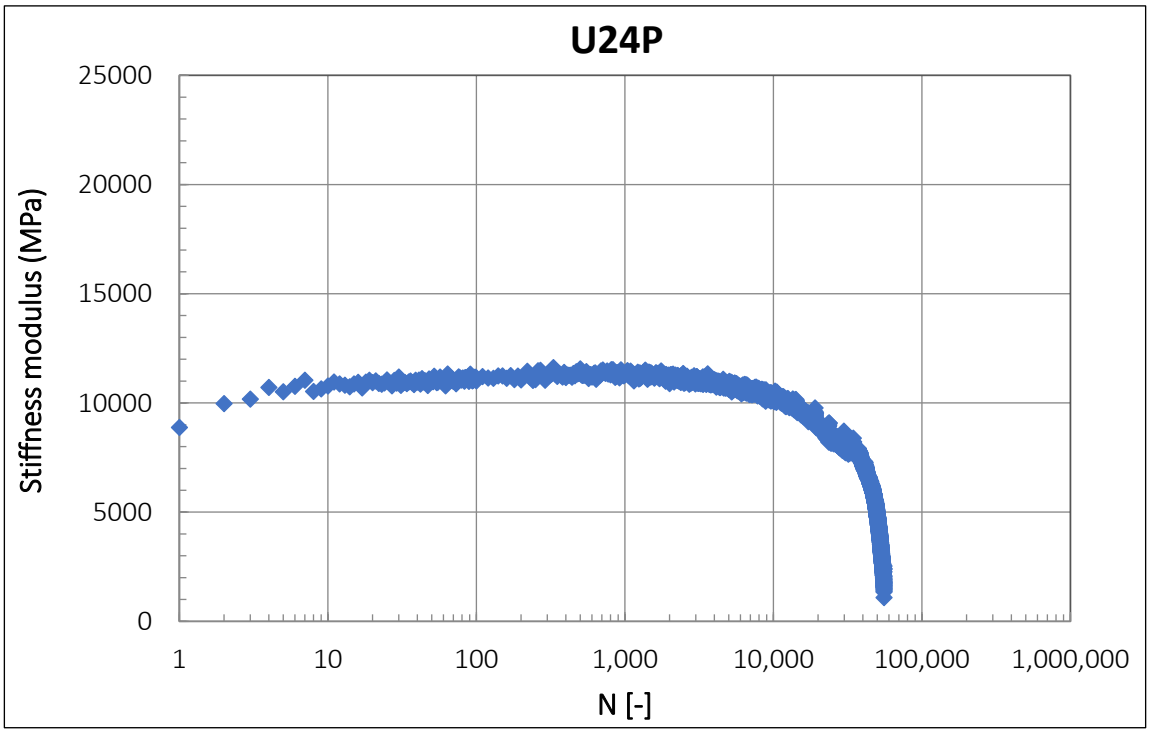

Figure 138 U24P sample stiffness modulus [MPa] vs load cycle [-]

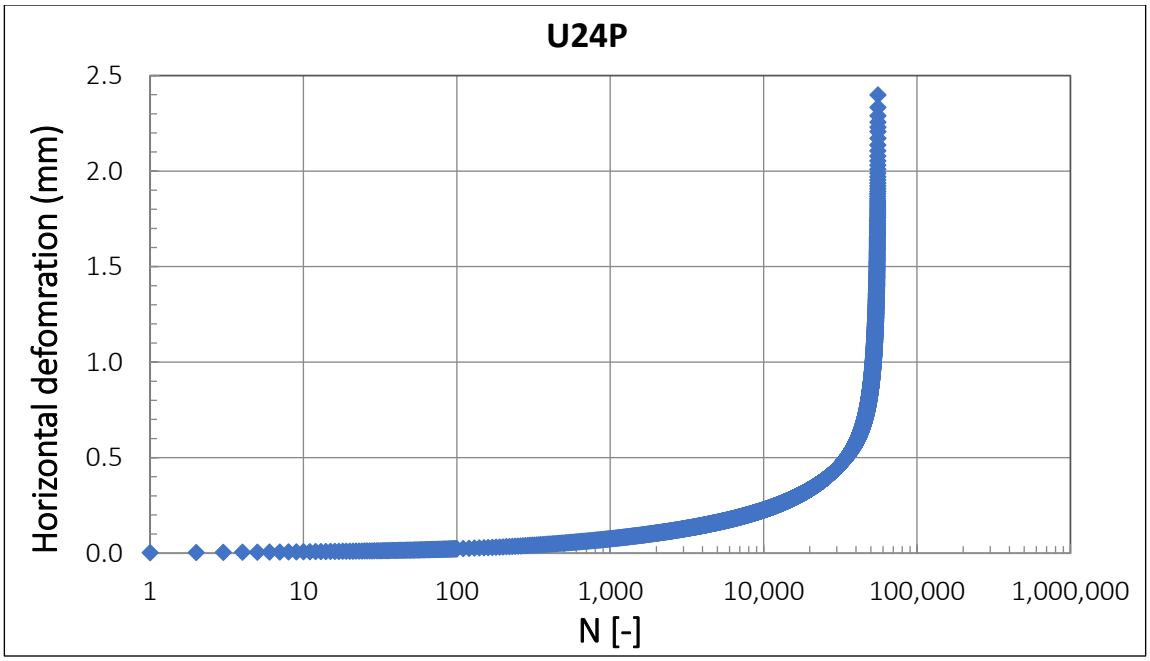

Figure 139 U24P sample average horizontal deformation [mm] vs load cycle [-]

Material	U24PS0,5 Fatigue Line [20 °C]				
Temperature	20 °C				
d	100 mm				
ID	**E**	**s_0**	**ε_a**	**$N_{f\ (energy\ ratio)}$**	**$N_{f\ (sample\ break)}$**
	(MPa)	(kPa)	(µm/m)	(-)	(-)
U24PS0,5D	7793	270	53,90	50190	64390
U24PS0,5F	8229	270	52,25	38380	51540
U24PS0,5A	7926	440	91,02	4350	6260
U24PS0,5C	8231	440	84,80	3450	4410
U24PS0,5B	8483	(Trial)	84,84	3660	5280
U24PS0,5P	7491	175	40,56	102700	136750
U24PS0,5E	7581	175	36,61	160520	222970

Material	U24PS0,5 LTA Fatigue Line [20 °C]				
Temperature	20 °C				
d	100 mm				
ID	**E**	**s_0**	**ε_a**	**$N_{f\ (energy\ ratio)}$**	**$N_{f\ (sample\ break)}$**
	(MPa)	(kPa)	(µm/m)	(-)	(-)
U24PS0,5K	9460	300	59,10	24490	33750
U24PS0,5M	9712	300	50,92	26030	37880
U24PS0,5J	9075	475	85,46	2530	3788
U24PS0,5L	9435	475	77,85	2910	4520
U24PS0,5O	9318	215	36,73	188360	261050
U24PS0,5N	9439	215	35,63	182580	266730

Table 66 U24PS0,5 sample initial horizontal strain amplitude, and fatigue life (using energy ratio or break criteria)

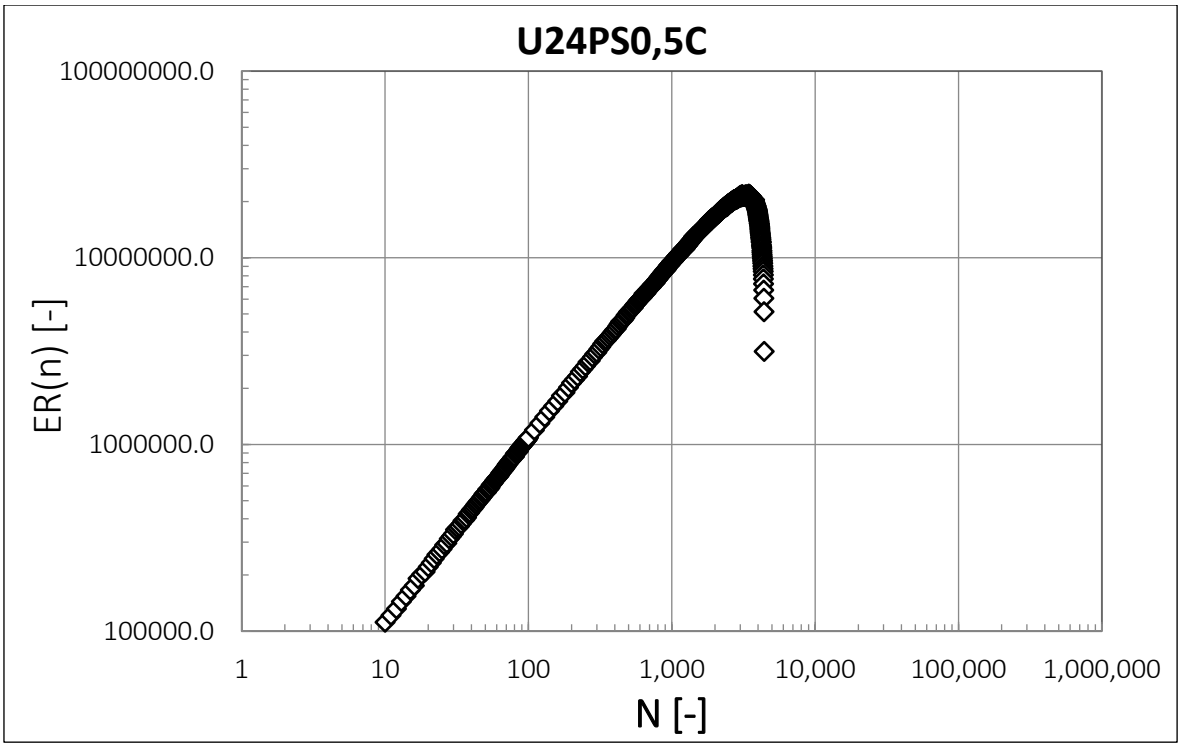

Figure 140 U24PS0,5C sample energy ratio [-] vs load cycle [-]

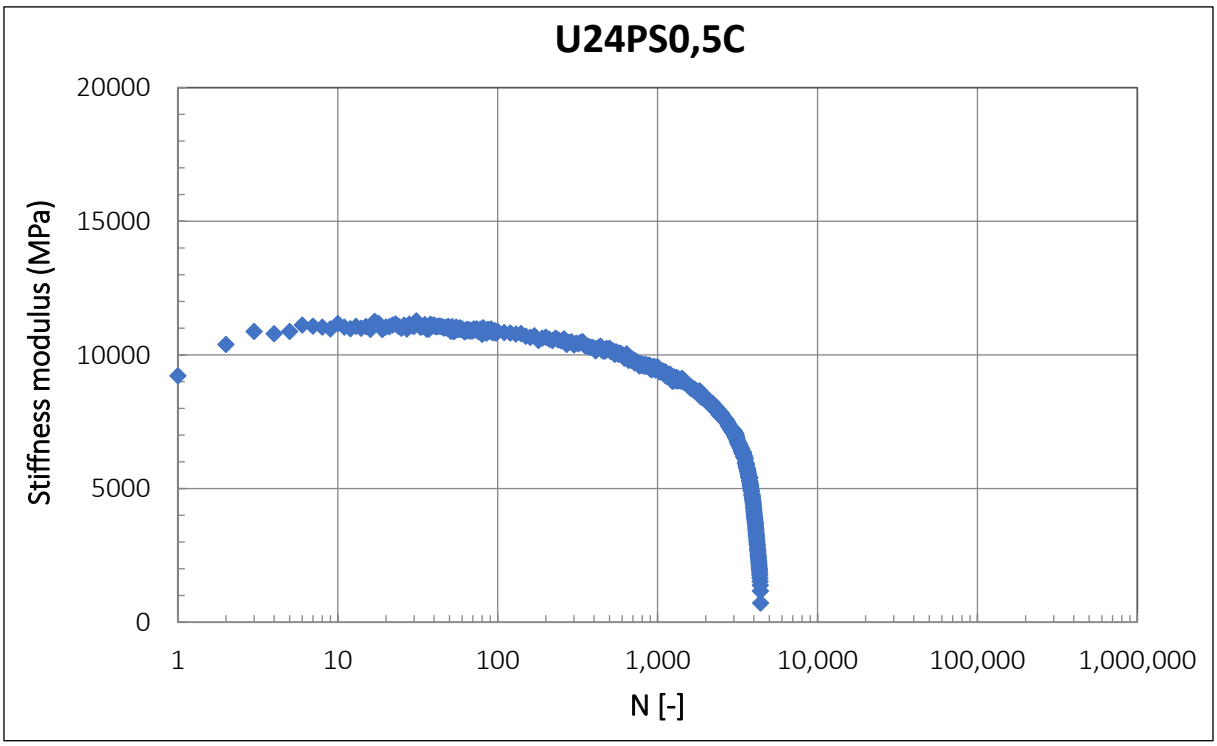

Figure 141 U24PS0,5C sample stiffness modulus [MPa] vs load cycle [-]

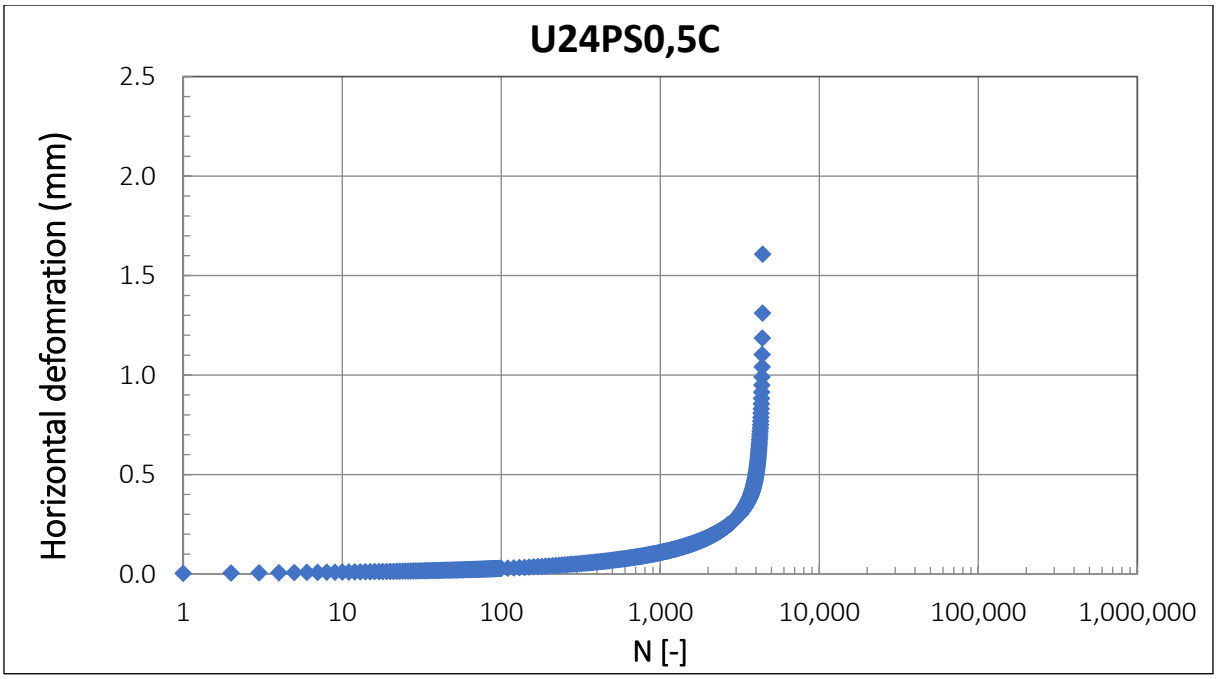

Figure 142 U24PS0,5C sample average horizontal deformation [mm] vs load cycle [-]

Material	U24PS1 Fatigue Line [20 °C]				
Temperature	20 °C				
d	100 mm				
ID	**E**	**s_0**	**ε6**	**$N_{f(energy\ ratio)}$**	**$N_{f(sample\ break)}$**
	(MPa)	(kPa)	(μm/m)	(-)	(-)
U24PS1D	7093	270	52,39	24310	33350
U24PS1C	6959	270	52,73	27800	37050
U24PS1A	7115	440	98,73	2560	3367
U24PS1F	7409	440	86,03	4100	5500
U24PS1E	6389	175	31,34	190890	259520
U24PS1R	8109	175	32,34	258280	335634

Material	U24PS1 LTA Fatigue Line [20 °C]				
Temperature	20 °C				
d	100 mm				
ID	**E**	**s_0**	**ε6**	**$N_{f(energy\ ratio)}$**	**$N_{f(sample\ break)}$**
	(MPa)	(kPa)	(μm/m)	(-)	(-)
U24PS1M	8558	300	60,45	18840	25280
U24PS1N	9109	475	87,84	3930	5105
U24PS1O	8917	475	87,66	3200	4240
U24PS1L	9359	215	39,24	122650	178811
U24PS1K	7932	215	40,05	117930	161620

Table 67 U24PS1 sample initial horizontal strain amplitude, and fatigue life (using energy ratio or break criteria)

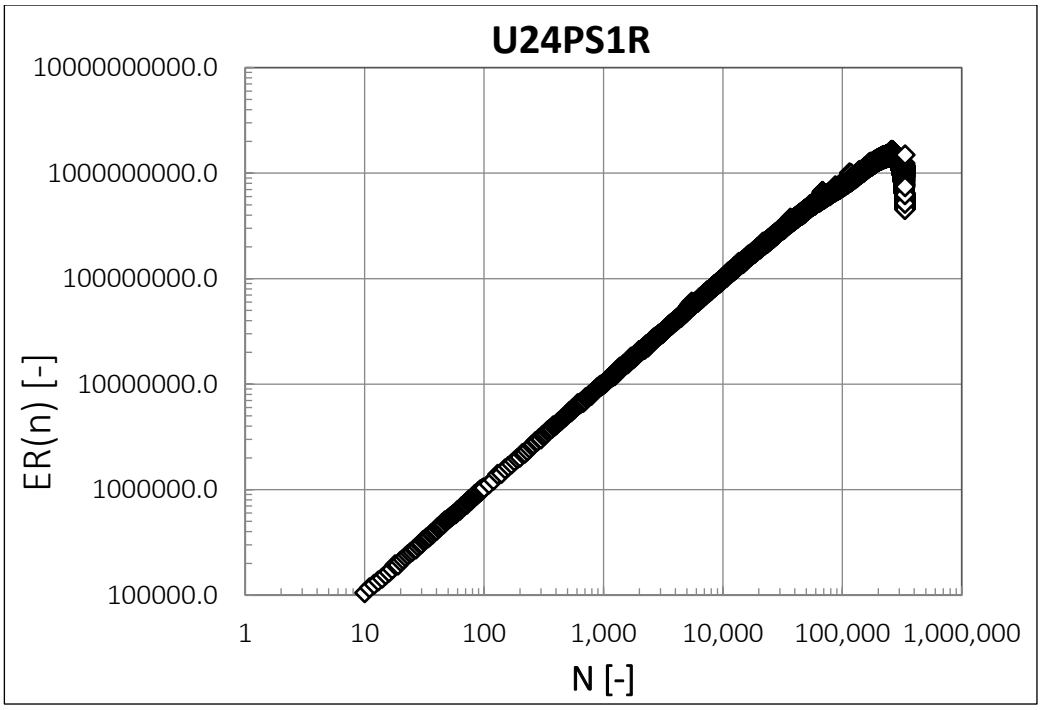

Figure 143 U24PS1R sample energy ratio [-] vs load cycle [-]

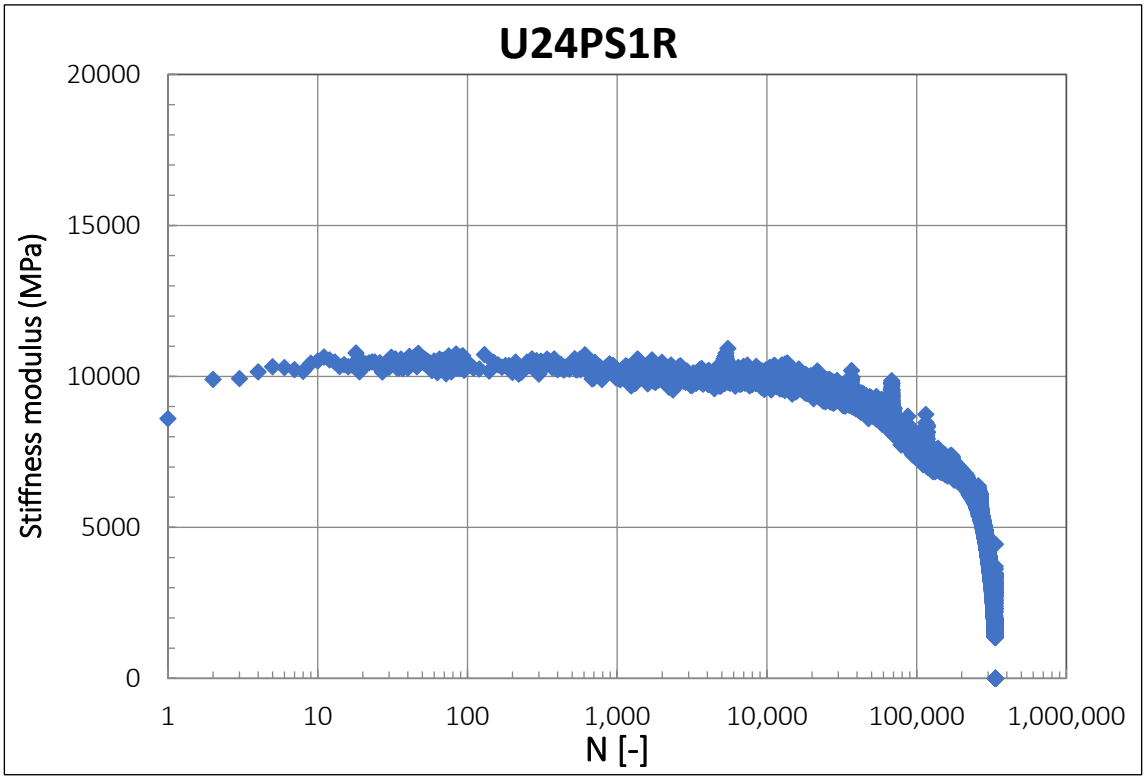

Figure 144 U24PS1R sample stiffness modulus [MPa] vs load cycle [-]

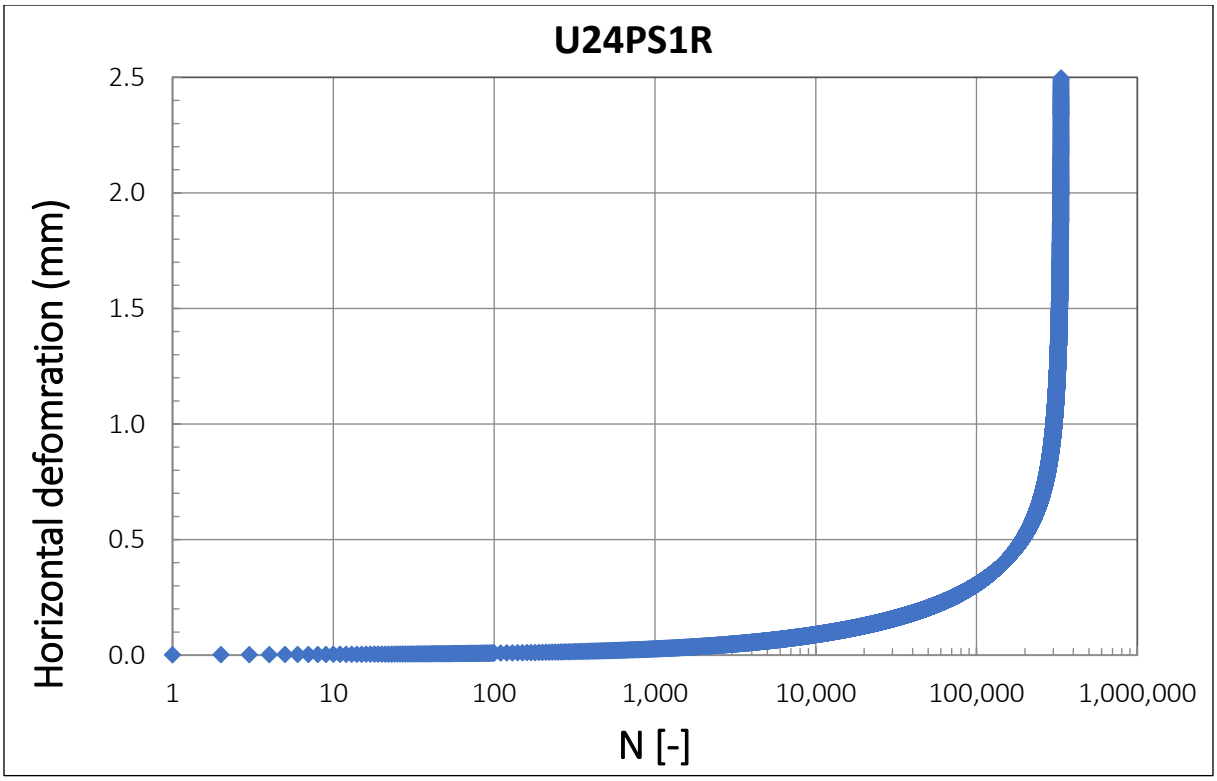

Figure 145 U24PS1R sample average horizontal deformation [mm] vs load cycle [-]

Fatigue CIT-CY	Stress level [kPa] applied to specimens (2 repetitions per level)			
	1	2	3	Trial level
U24	175	270	440	350
Mean εa_0 (µm/m)	32,6	50,8	89,8	68,4
Mean $N_{f\ fracture}$	589751	49350	6565	16960
U24 LTA	215	300	475	
Mean εa_0 (µm/m)	40,7	55,6	99,2	/
Mean $N_{f\ fracture}$	148836	45345	3090	/

Fatigue CIT-CY	Stress level [kPa] applied to specimens (2 repetitions per level)			
	1	2	3	Trial level
U24PS0,5	175	270	440	430
Mean εa_0 (µm/m)	38,6	53,1	87,9	84,8
Mean $N_{f\ fracture}$	179500	57972	5335	5280
U24PS0,5 LTA	215	300	475	
Mean εa_0 (µm/m)	36,15	55	81,7	/
Mean $N_{f\ fracture}$	263890	35815	4154	/

Fatigue CIT-CY	Stress level [kPa] applied to specimens (2 repetitions per level)			
	1	2	3	Trial level
U24PS1	175	270	440	440
Mean εa_0 (µm/m)	31,8	52,6	92,35	105,7*
Mean $N_{f\ fracture}$	297577	35200	4434	2970
U24PS1 LTA	215	300	475	
Mean εa_0 (µm/m)	39,7	60,4	87,8	/
Mean $N_{f\ fracture}$	166216	25280	4673	/

**Rejected test sample due to exceedance of the initial horizontal strain amplitude permitted by norms*

Table 68 U24, U24PS0,5, U24PS1 STA & LTA failure cycles and initial horizontal strain amplitude (using sample break criteria)

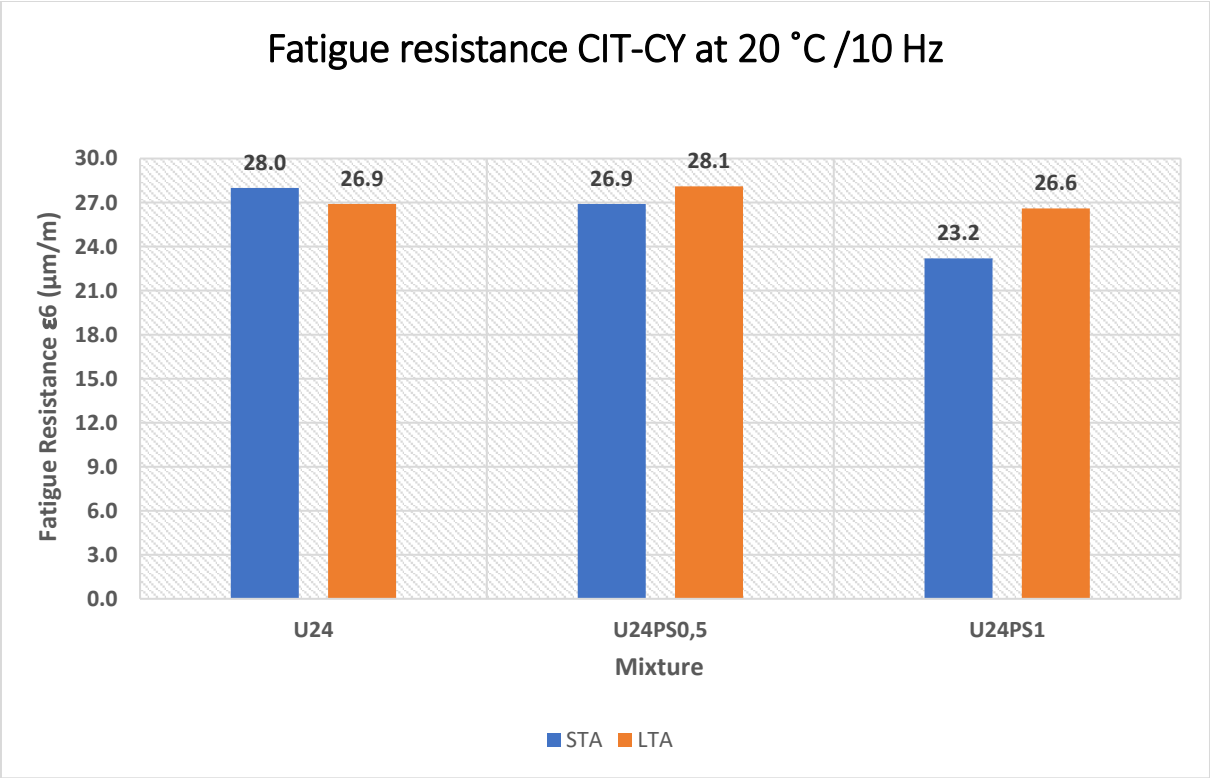

Figure 146 Fatigue resistance ε6 (µm/m) results for tested specimens, using sample break criterion for failure cycles

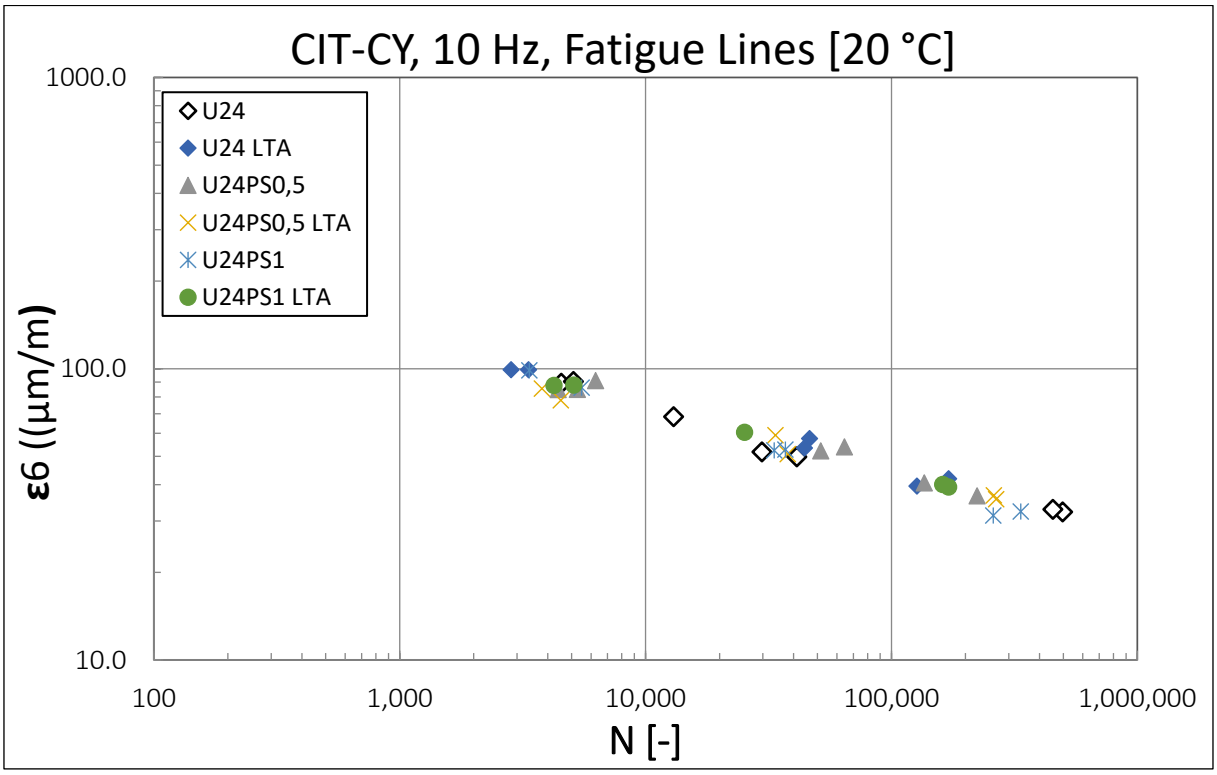

Figure 147 Fatigue lines of all mixture specimens, using sample break criterion for failure cycles

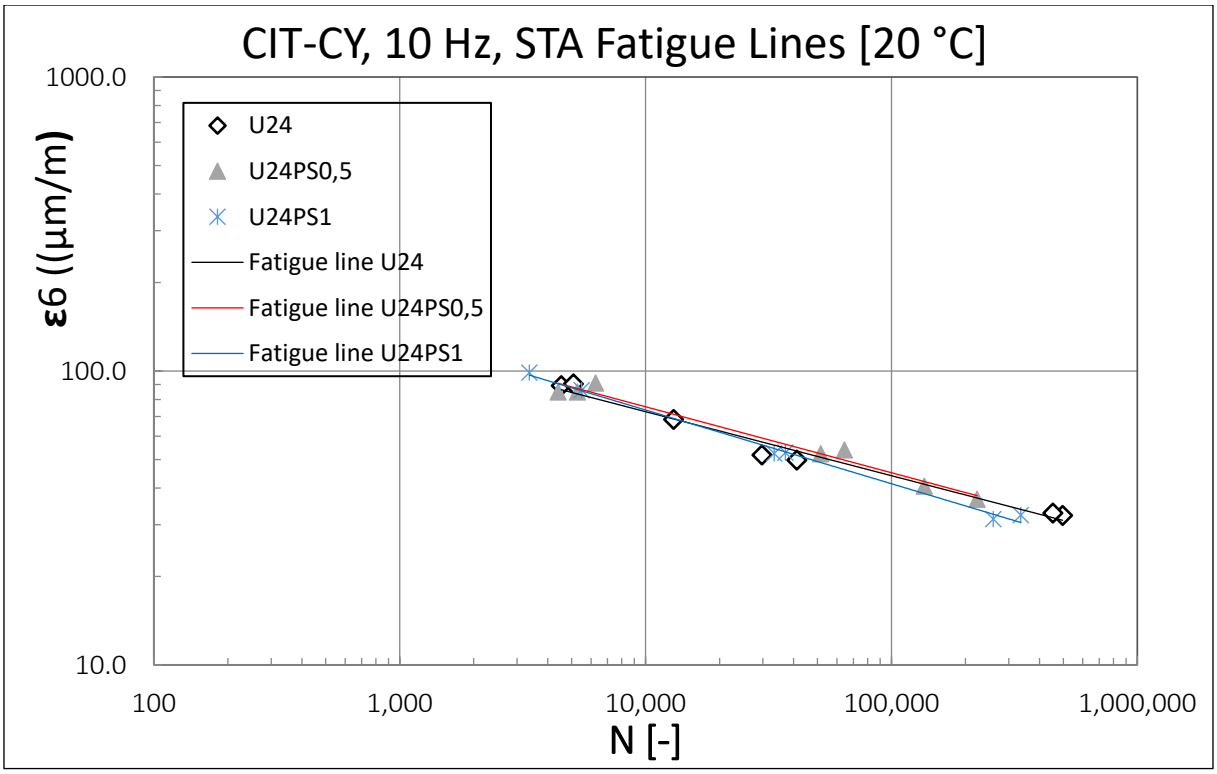

Figure 148 Fatigue lines of all mixture STA specimens, using sample break criterion for failure cycles

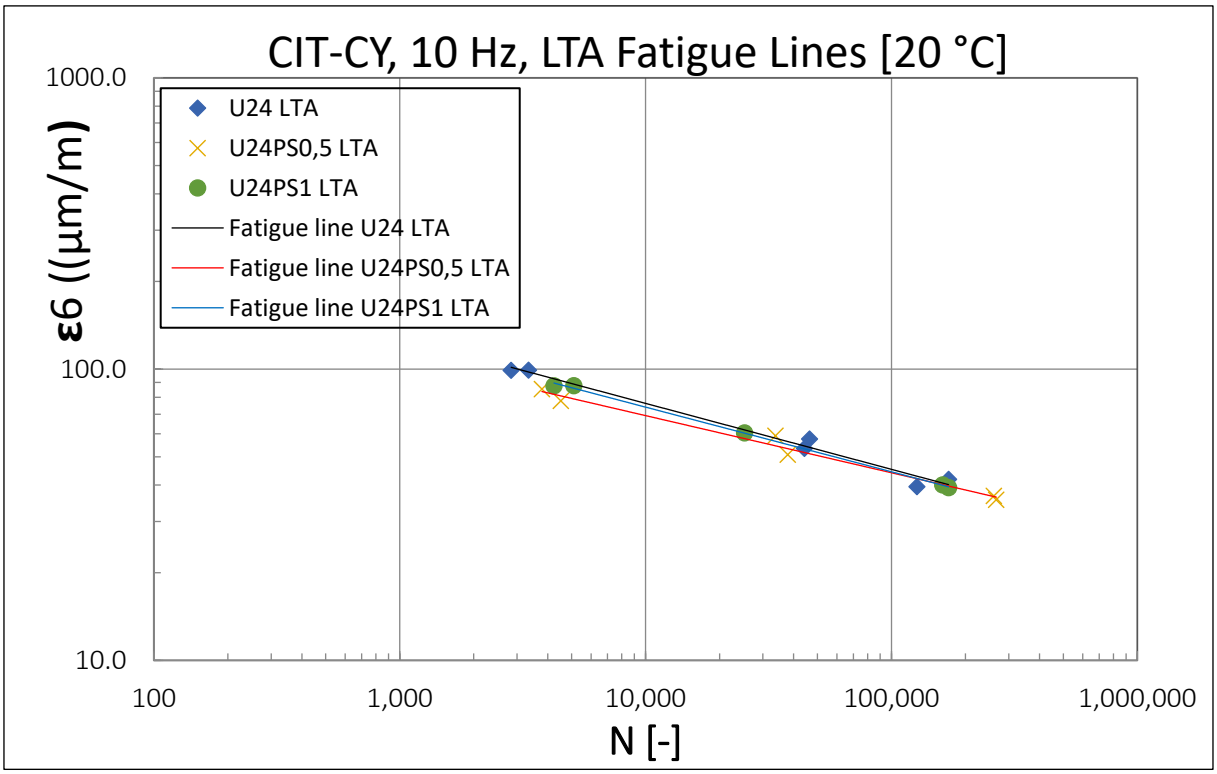

Figure 149 Fatigue lines of all mixture LTA specimens, using sample break criterion for failure cycles

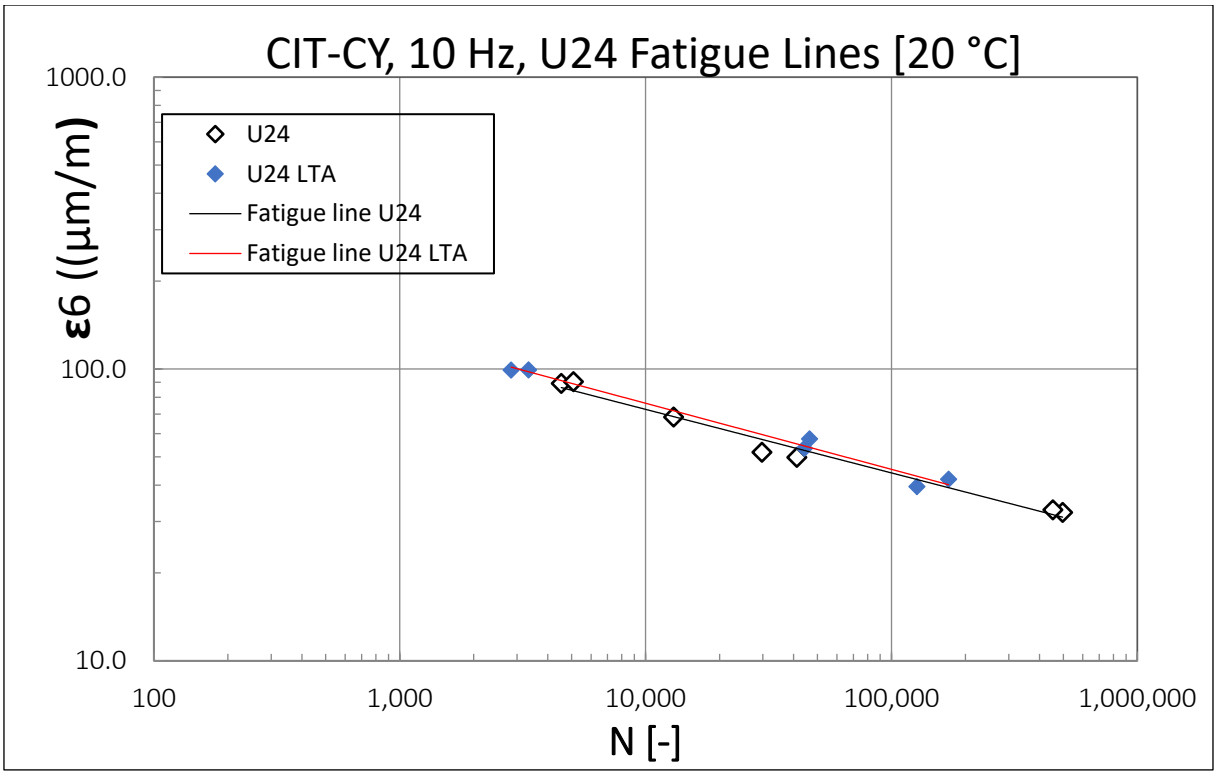

Figure 150 Fatigue lines of U24 specimens, using sample break criterion for failure cycles

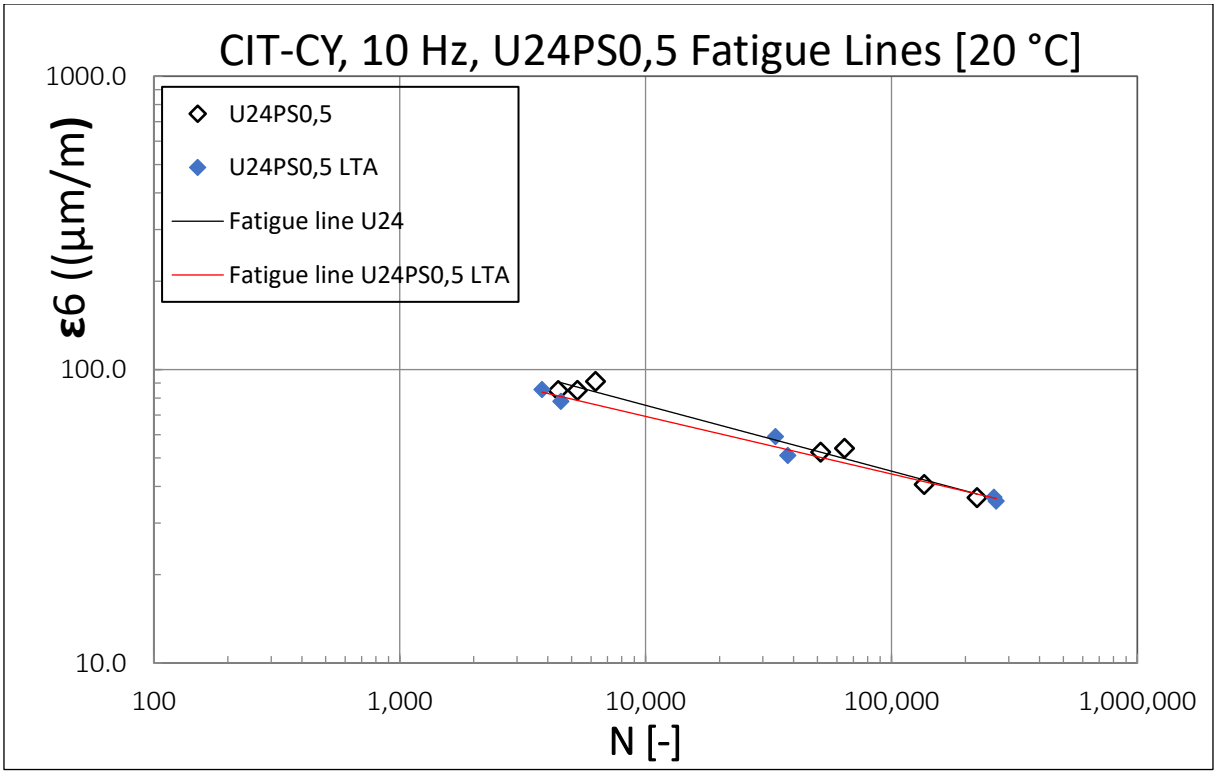

Figure 151 Fatigue lines of U24PS0,5 specimens, using sample break criterion for failure cycles

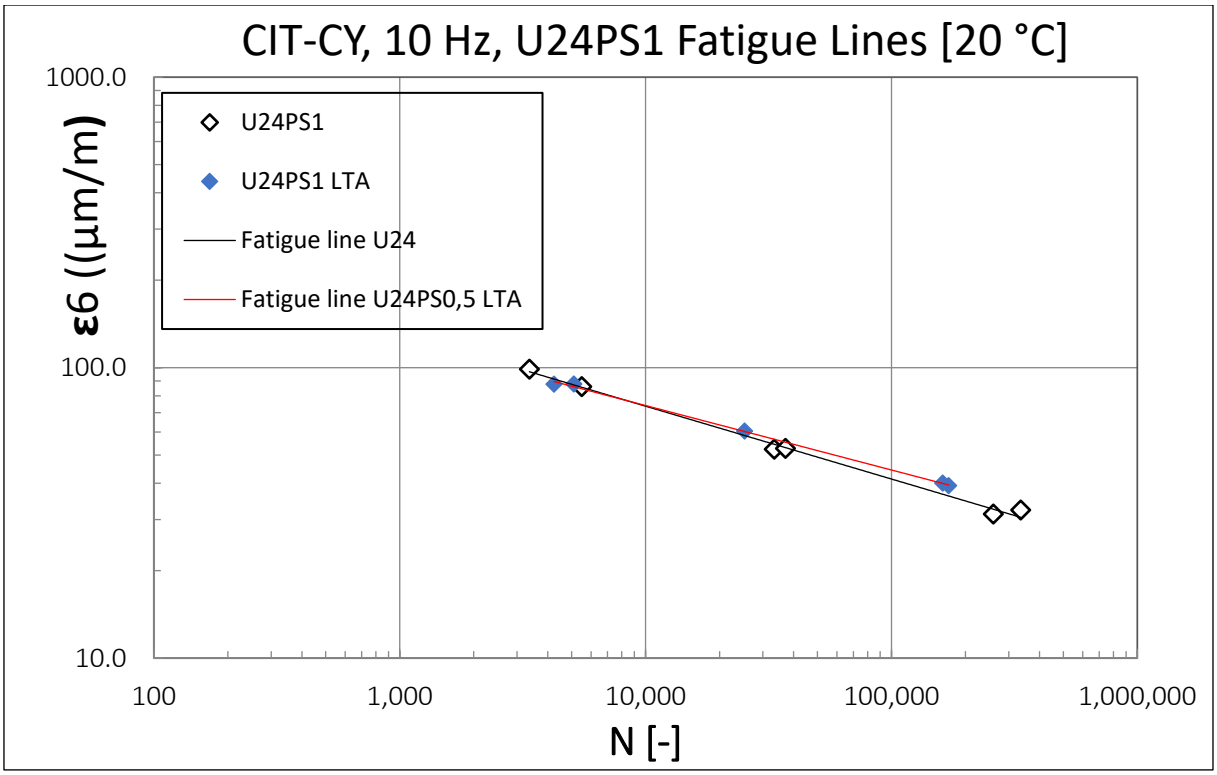

Figure 152 Fatigue lines of U24PS1 specimens, using sample break criterion for failure cycles